Cumulant theory of the unitary Bose gas

Cumulant theory of the unitary Bose gas: Prethermal and Efimovian dynamics

V. E. Colussi,[1,*] H. Kurkjian,[2] M. Van Regemortel,[2,3] S. Musolino,[1] J. van de Kraats,[1] M. Wouters,[2] and S. J. J. M. F. Kokkelmans[1]

[1]*Eindhoven University of Technology, PO Box 513, 5600 MB Eindhoven, Netherlands*
[2]*TQC, Universiteit Antwerpen, Universiteitsplein 1, B-2610 Antwerp, Belgium*
[3]*Joint Quantum Institute, National Institute of Standards and Technology and the University of Maryland, Gaithersburg, Maryland 20899, USA*

(Received 20 July 2020; accepted 28 October 2020; published 11 December 2020)

We study the quench of a degenerate ultracold Bose gas to the unitary regime, where interactions are as strong as allowed by quantum mechanics. We lay the foundation of a cumulant theory able to simultaneously capture the three-body Efimov effect and ergodic evolution. After an initial period of rapid quantum depletion, a universal prethermal stage is established, characterized by a kinetic temperature and an emergent Bogoliubov dispersion law, while the microscopic degrees of freedom remain far from equilibrium. Integrability is then broken by higher-order interaction terms in the many-body Hamiltonian, leading to a momentum-dependent departure from power law to decaying exponential behavior of the occupation numbers at large momentum. We also find signatures of the Efimov effect in the many-body dynamics and make a precise identification between the observed beating phenomenon and the binding energy of an Efimov trimer. Throughout the paper, our predictions for a uniform gas are quantitatively compared with experimental results for quenched unitary Bose gases in uniform potentials.

DOI: 10.1103/PhysRevA.102.063314

I. INTRODUCTION

Precision control of interatomic interactions in dilute ultracold quantum gases has made possible remarkable progress in our understanding of strongly correlated many-body systems. Here, strongly interacting quantum fluids can be studied in the laboratory, with a great flexibility in the way in which the system is manipulated and probed. Ultracold quantum gases are typically dilute with respect to the range of the specific interatomic interaction and sensitive only to the two-body s-wave scattering length a, which sets the effective interaction strength [1]. Experiments have typically focused on measuring equilibrium or near-equilibrium properties, such as the equation of state or elementary excitations. This picture is realized in two-component Fermi gases [2–4] even in the unitary regime $n|a|^3 \gg 1$, where n is the atomic density, [5–10]. Here, system properties behave universally, scaling continuously as powers of the remaining density (Fermi) scales $k_n = (6\pi^2 n)^{1/3}$, $E_n = \hbar^2 k_n^2/2m$, and $t_n = \hbar/E_n$ and can be related to other strongly interacting Fermi systems such as the inner crust of neutron stars [11–15].

In ultracold quantum gases where multibody effects are not suppressed by the Pauli exclusion principle, an infinite number of three-body bound Efimov states form whose finite size and discrete scaling leads to a spectacular departure from this universal paradigm [16–21]. This includes three-component Fermi gases, whose rich phase diagram is predicted to contain a trimer phase at low densities reminiscent of quantum chromodynamics [22,23]. It also includes (single-component) Bose gases, where quasiequilibrated states have recently been achieved through fast ramps onto the unitary regime before loss-induced heating dominates [24–27]. Here, the conversion of correlation dynamics into a mixture of free atoms, Feshbach dimers, and Efimov trimers was observed in an ultracold Bose gas of ^{85}Rb by sweeping the unitary gas back onto the weakly interacting regime [25]. Within a three-body model, this conversion was shown to be dominated by the Efimov trimer with a size comparable to the interparticle spacing [28], which also leads to an enhanced growth of triplet correlations at early times after the quench [29,30]. Extending these early-time, few-body studies to Fermi timescales requires that the Efimov effect be woven into a many-body framework, which remains an outstanding theoretical challenge.

At the same time, performing a deep quench leaves these strongly interacting systems in a highly excited state. Here, different quantities can effectively prethermalize, equilibrating before the system has relaxed to the true thermal equilibrium [31]. Experimentally, signs of a universal prethermal state characterized by Bogoliubov scalings (phonons and free particles at low and high momenta, respectively) were observed in a quenched ultracold Bose gas of ^{39}K [27]. Whether this prethermal steady state is due to integrable dephasing dynamics, as in the weakly interacting regime [32], or to ergodic mechanisms is unclear. State-of-the-art integrable theories of the postquench evolution [33–36] are by definition unable to capture the relaxation dynamics which must occur in this ergodic system. Additionally, the usual perturbative inclusion of such processes using Boltzmannian approaches [37] is not justified in this regime where the distinctness of collisions is blurred and all rates are on the order of the Fermi scale. The challenge of constructing a many-body framework,

*Corresponding author: colussiv@gmail.com

both ergodic and strongly interacting, therefore remains central.

In this paper, we establish the foundations of a general approach able to capture both the Efimov effect and ergodicity in far-from-equilibrium, strongly interacting ultracold Bose gases. Using the method of cumulants, we track the sequential growth of genuine few-body correlations systematically encoded in the cumulants of the quenched many-body system [29,30,38–44]. Containing only two-body correlations, the cumulant theory at the doublet level is equivalent to the time-dependent Hartree-Fock-Bogoliubov (HFB) and Nozières-Saint James (NSJ) variational approaches studied in Refs. [33–35,44–46]. Here, we show how a universal prethermal stage emerges from the integrable dynamics, providing a framework for the conceptual and quantitative understanding of the universal Bogoliubov scalings observed experimentally. We find that the next truncation level that includes higher-order correlations while respecting the underlying conservation laws is the cumulant theory at the quadruplet level. Although we provide explicit expressions for the cumulant equations of motion in the quadruplet model, its full simulation remains numerically intractable. Therefore, we simulate the cumulant theory truncated at the triplet level, which already contains the Efimov effect, as demonstrated in a study of the embedded few-body problem in Ref. [44]. Within the triplet model, we explore the various manifestations of Efimov physics in the many-body observables, including the instantaneous chemical potential, quantum depletion, pairing field, and two- and three-body contacts. This analysis is performed at times before the violation of energy conservation muddies the long-time dynamics and any physical connections with thermalization.

The organization of this paper is as follows. In Sec. II, we outline the many-body model, calibrated to reproduce finite-range corrections near resonance and reformulated in the symmetry-breaking picture to describe Bose-condensation in the system. In Sec. III, the method of cumulants is introduced and explicit expressions for the cumulant equations of motion are derived, connected with the underlying few-body physics, and the interplay between their truncation and conservation laws is detailed. In Sec. IV, the prethermal stage that emerges in the doublet model is analyzed and compared with experiments. In Sec. V, the departure from the prethermal stage and Efimovian dynamics are analyzed in the triplet model, and we conclude in Sec. VI. The more formal and technical discussions in this paper can be found in the Appendices. In Appendix A, details of the calibrated, finite-range potential are given along with the resulting Efimov spectrum. In Appendix B, the cumulant equations are given in a form more suitable for simulation and their numerical implementation is discussed. In Appendix C, we provide the formal, explicit expressions for the quadruplet equations of motion and discuss their solution. In Appendix D, we connect the cumulant theory outlined in this paper with alternative approaches found in the literature.

II. MANY-BODY MODEL

In this paper, we study a quenched uniform gas of degenerate bosons in a cubic volume V. We consider short-range single-channel interactions that capture the broad, entrance-channel dominated Feshbach resonances used experimentally [24–27,47]. First, we introduce the many-body Hamiltonian in Sec. II A and discuss the potential parameters calibrated to match finite-range corrections near resonance, referring the interested reader to Appendix A for more details. In Sec. II B, we move to the symmetry-breaking picture to describe Bose condensation in the system. In Sec. II C, the many-body Hamiltonian is reformulated in preparation for the cumulant expansion in the following section (Sec. III).

A. Hamiltonian

In an ultracold Bose gas, atoms interact through a local s-wave pairwise potential $\langle \mathbf{r}_{\rm in}|\hat{V}|\mathbf{r}_{\rm out}\rangle = V(|\mathbf{r}_{\rm in}|)\delta^{(3)}(\mathbf{r}_{\rm out}-\mathbf{r}_{\rm in})$ with relative coordinates $\mathbf{r}_{\rm in}$ and $\mathbf{r}_{\rm out}$ [48] of the two incoming and outgoing atoms. The corresponding many-body Hamiltonian is given by

$$\hat{H} = \int d^3r \hat{\psi}^\dagger(\mathbf{r})\left(-\frac{\hbar^2}{2m}\Delta_{\mathbf{r}}\right)\hat{\psi}(\mathbf{r}) + \frac{1}{2}\int d^3r d^3r' \hat{\psi}^\dagger(\mathbf{r})\hat{\psi}^\dagger(\mathbf{r}')V(|\mathbf{r}-\mathbf{r}'|)\hat{\psi}(\mathbf{r}')\hat{\psi}(\mathbf{r}), \quad (1)$$

where $\mathbf{r}_{\rm in} = \mathbf{r} - \mathbf{r}'$ is the relative position for incoming particles located at $\mathbf{r}$ and $\mathbf{r}'$. To diagonalize the kinetic energy part of this Hamiltonian, we introduce the Fourier operators $\hat{\psi}(\mathbf{r}) = (1/\sqrt{V})\sum_{\mathbf{k}} \hat{a}_{\mathbf{k}} e^{i\mathbf{k}\cdot\mathbf{r}}$ for a uniform gas occupying a cubic volume V, which can be taken to infinity in the thermodynamic limit. In Fourier space, this Hamiltonian reads

$$\hat{H} = \sum_{\mathbf{k}} \epsilon_{\mathbf{k}} \hat{a}^\dagger_{\mathbf{k}}\hat{a}_{\mathbf{k}} + \frac{1}{2V}\sum_{\mathbf{k},\mathbf{k}',\mathbf{q}} V_{\mathbf{q}} \hat{a}^\dagger_{\mathbf{k}'+\mathbf{q}}\hat{a}^\dagger_{\mathbf{k}-\mathbf{q}}\hat{a}_{\mathbf{k}}\hat{a}_{\mathbf{k}'}, \quad (2)$$

where $\epsilon_{\mathbf{k}} = \hbar^2k^2/2m$ is the one-body kinetic energy and the Fourier components of the local potential are given by

$$\langle \mathbf{k}|\hat{V}|\mathbf{k}'\rangle = \quad V_{\mathbf{k}'-\mathbf{k}} = \int d^3r\, e^{i\mathbf{r}\cdot(\mathbf{k}-\mathbf{k}')}V(|\mathbf{r}|), \quad (3)$$

which depends only on the magnitude of the difference in relative momenta $\mathbf{k}$ and $\mathbf{k}'$.

The physical properties of ultracold Bose gases are typically characterized by a single parameter, the two-body s-wave scattering length a, which sets the effective strength of two-body interactions and can be adjusted precisely by tuning the binding energy of a Feshbach molecule via external magnetic fields [1,47]. On resonance, the cross section becomes independent of the scattering length in the unitarity limit $\sigma = 8\pi/k^2$ [48]. The gas is both dilute with respect to the range of the interatomic interaction parametrized by the van der Waals length $r_{\rm vdW} = (mC_6/\hbar^2)^{1/4}/2$, where m is the atomic mass and C_6 is the dispersion coefficient associated with the van der Waals interaction between neutral ground-state atoms [47], while being simultaneously strongly interacting $|a|/r_{\rm vdW} \gg 1$. The short-range details of the potential are therefore relatively unimportant, and there is freedom in choosing the potential. All formulas in the main text are therefore given in terms of a local potential for concision but the numerical calculations are actually performed with a separable pairwise potential (see Appendix A) with renormalized effective interaction strength $g = U_0\Gamma$ where $U_0 =$

$4\pi\hbar^2 a/m$ and $\Gamma = 1/(1 - 2a\Lambda/\pi)$. To match finite-range effects in the vicinity of the Feshbach resonance, the relative momentum cutoff is calibrated as $\Lambda = 2/\pi\bar{a}$, where $\bar{a} = 4\pi r_{\rm vdW}/\Gamma(1/4)^2 \approx 0.956 r_{\rm vdW}$ is the mean scattering length and $\Gamma(x)$ is the Gamma function [44,49,50]. This gives $g = -\pi^3\hbar^2\bar{a}/m$ for the effective interaction strength at unitarity. Importantly, this calibration has consequences on the three-body level for the spectrum of Efimov states, and we refer the interested reader to Appendix A for more details on the few-body physics contained in this model.

B. Symmetry-breaking picture

The gas is initially condensed in the $k = 0$ mode, which means that the population

$$N_0 \equiv \langle \hat{a}_0^\dagger \hat{a}_0 \rangle \lesssim N \tag{4}$$

is macroscopic. We describe only evolution that preserves this property, which, for very energetic quenches where all particles are eventually ejected out of the condensate, restricts us to short times. We use the symmetry-breaking picture [51] to describe the dynamics of the condensate: the condensate operator $\hat{a}_0$ is replaced by a wave function $\psi_0 = \langle \hat{a}_0 \rangle/\sqrt{V}$ acting as an order parameter. The Gross-Pitaevskii equation (GPE) describing the dynamics of this wave function ψ_0 is obtained by treating $\hat{H}$ as a classical Hamiltonian and ψ_0 and ψ_0^* as canonically conjugated variables,

$$\begin{aligned} i\hbar\partial_t\psi_0 = \left\langle \frac{\partial \hat{H}}{\partial \psi_0^*} \right\rangle &= V_{\mathbf{0}} n \psi_0 + \psi_0 \frac{1}{V}\sum_{\mathbf{k}\neq 0} V_{\mathbf{k}} \langle \hat{a}_{\mathbf{k}}^\dagger \hat{a}_{\mathbf{k}} \rangle \\ &+ \psi_0^* \frac{1}{V}\sum_{\mathbf{k}\neq 0} V_{\mathbf{k}} \langle \hat{a}_{-\mathbf{k}} \hat{a}_{\mathbf{k}} \rangle + \frac{1}{V^{3/2}} \sum_{\mathbf{k},\mathbf{q}\neq 0} V_{\mathbf{q}} \langle \hat{a}_{\mathbf{k}+\mathbf{q}}^\dagger \hat{a}_{\mathbf{k}} \hat{a}_{\mathbf{q}} \rangle, \end{aligned} \tag{5}$$

where $n = N/V$ is the total atomic density ($n_0 = N_0/V = |\psi_0|^2$ being the density of condensed particles).

To eliminate the condensate variables and focus on the dynamics of the excited fraction, we decompose the condensate wave function into its modulus and phase,

$$\psi_0 = \sqrt{n_0} e^{i\theta_0}, \tag{6}$$

and introduce the operators unrotated by the condensate phase:

$$\hat{b}_{\mathbf{k}} = e^{-i\theta_0} \hat{a}_{\mathbf{k}}. \tag{7}$$

The dynamics of the $\hat{b}$ operators now incorporates the evolution of θ_0 [52]:

$$\begin{aligned} &i\hbar\partial_t \hat{b}_{\mathbf{k}} = [\hat{b}_{\mathbf{k}}, \hat{H}_b], \\ &\text{with} \quad \hat{H}_b = \hat{H} + \hbar\partial_t\theta_0 \sum_{\mathbf{k}} (\hat{b}_{\mathbf{k}}^\dagger \hat{b}_{\mathbf{k}} - \langle \hat{b}_{\mathbf{k}}^\dagger \hat{b}_{\mathbf{k}} \rangle). \end{aligned} \tag{8}$$

We note that the summation involving $\langle \hat{b}_{\mathbf{k}}^\dagger \hat{b}_{\mathbf{k}} \rangle$ has been trivially added to $\hat{H}_b$ to ensure that $\langle \hat{H}_b \rangle = \langle \hat{H} \rangle$. In $\hat{H}_b$, the number of particles in the condensate is no longer treated as an independent variable and is related to the $\hat{b}$ field and total number of particles by the conservation equation:

$$N_0 = N - \sum_{\mathbf{k}} \langle \hat{b}_{\mathbf{k}}^\dagger \hat{b}_{\mathbf{k}} \rangle. \tag{9}$$

The phase derivative can also be expressed in terms of $\hat{b}$, which finally eliminates the condensate variables from the dynamics:

$$\hbar\frac{d\theta_0}{dt} = -\frac{1}{2n_0}\left(\psi_0^* i\hbar\frac{d\psi_0}{dt} - i\hbar\frac{d\psi_0^*}{dt}\psi_0\right), \tag{10}$$

$$\begin{aligned} &= -\Bigg[V_{\mathbf{0}} n + \frac{1}{V}\sum_{\mathbf{k}} \left[V_{\mathbf{k}} \langle \hat{b}_{\mathbf{k}}^\dagger \hat{b}_{\mathbf{k}} \rangle + V_{\mathbf{k}} \mathrm{Re}\, \langle \hat{b}_{-\mathbf{k}} \hat{b}_{\mathbf{k}} \rangle \right] \\ &+ \frac{1}{\sqrt{n_0 V^3}} \sum_{\mathbf{k}\mathbf{q}} V_{\mathbf{q}} \mathrm{Re}\, \langle \hat{b}_{\mathbf{k}+\mathbf{q}}^\dagger \hat{b}_{\mathbf{k}} \hat{b}_{\mathbf{q}} \rangle \Bigg]. \end{aligned} \tag{11}$$

In Sec. IV, we use the interpretation of this equation as a second Josephson relation $\hbar\partial_t\theta_0 = -\mu(t)$ to generalize the notion of an instantaneous chemical potential to our out-of-equilibrium system [53,54].

C. Expansion of the Hamiltonian

We start by expanding the many-body Hamiltonian $\hat{H}_b$ in powers of the noncondensed field $\hat{b}$:

$$\hat{H}_b = E_0(t) + \hat{H}_2 + \hat{H}_3 + \hat{H}_4, \tag{12}$$

$$E_0 = \frac{V_{\mathbf{0}} N_0^2}{2V} - \hbar\partial_t\theta_0 (N - N_0), \tag{13}$$

$$\begin{aligned} \hat{H}_2 = \sum_{\mathbf{k}} &([\epsilon_{\mathbf{k}} + (V_{\mathbf{k}} + V_{\mathbf{0}}) n_0 + \hbar\partial_t\theta_0] \hat{b}_{\mathbf{k}}^\dagger \hat{b}_{\mathbf{k}} \\ &+ \frac{V_{\mathbf{k}} n_0}{2} [\hat{b}_{-\mathbf{k}} \hat{b}_{\mathbf{k}} + \hat{b}_{\mathbf{k}}^\dagger \hat{b}_{-\mathbf{k}}^\dagger]), \end{aligned} \tag{14}$$

$$\hat{H}_3 = \sqrt{\frac{n_0}{V}} \sum_{\mathbf{k},\mathbf{q}} V_{\mathbf{q}} (\hat{b}_{\mathbf{k}+\mathbf{q}}^\dagger \hat{b}_{\mathbf{k}} \hat{b}_{\mathbf{q}} + \text{H.c.}), \tag{15}$$

$$\hat{H}_4 = \frac{1}{2V} \sum_{\mathbf{k},\mathbf{k}',\mathbf{q}} V_{\mathbf{q}} b_{\mathbf{k}'+\mathbf{q}}^\dagger \hat{b}_{\mathbf{k}-\mathbf{q}}^\dagger \hat{b}_{\mathbf{k}} \hat{b}_{\mathbf{k}'}. \tag{16}$$

The usual Bogoliubov approach ($\hat{H}_3 = \hat{H}_4 = 0$) reduces the many-body Hamiltonian to quadratic form and is justified by an expansion in powers of na^3 [1,32]. This approach describes two-body processes at the level of the Born approximation, which will not give the correct unitarity limit $\sigma(k) = 8\pi/k^2$ of the s-wave partial cross section [48]. To overcome this and produce a theory that reproduces the HFB equations at lowest order [55], we rewrite the many-body Hamiltonian by adding and subtracting the partial contraction [56] of $\hat{H}_4$ defined as

$$\delta\hat{H}_2 = \frac{1}{2}\sum_{\mathbf{k}} [\delta\Delta_{\mathbf{k}}^* \hat{b}_{-\mathbf{k}} \hat{b}_{\mathbf{k}} + \text{c.c.}] + \sum_{\mathbf{k}} \delta\epsilon_{\mathbf{k}} \hat{b}_{\mathbf{k}}^\dagger \hat{b}_{\mathbf{k}}, \tag{17}$$

with

$$\Delta_{\mathbf{k}} = \frac{1}{V}\sum_{\mathbf{q}} V_{\mathbf{q}} \langle \hat{b}_{-\mathbf{k}-\mathbf{q}} \hat{b}_{\mathbf{k}+\mathbf{q}} \rangle, \tag{18}$$

$$\delta\epsilon_{\mathbf{k}} = \frac{1}{V}\sum_{\mathbf{q}} (V_{\mathbf{0}} + V_{\mathbf{q}}) \langle \hat{b}_{\mathbf{k}+\mathbf{q}}^\dagger \hat{b}_{\mathbf{k}+\mathbf{q}} \rangle. \tag{19}$$

This yields an effective quartic $\hat{H}_4^{\rm eff} = \hat{H}_4 - \delta\hat{H}_2$ and quadratic Hamiltonian,

$$\hat{H}_2^{\rm eff} = \hat{H}_2 + \delta\hat{H}_2 \equiv \sum_{\mathbf{k}} \left(E_{\mathbf{k}} \hat{b}_{\mathbf{k}}^\dagger \hat{b}_{\mathbf{k}} + \left[\frac{\Delta_{\mathbf{k}}^*}{2} \hat{b}_{-\mathbf{k}} \hat{b}_{\mathbf{k}} + \text{H.c.} \right] \right), \tag{20}$$

whose diagonal and anomalous matrix elements are, respectively,

$$E_{\mathbf{k}} = \epsilon_{\mathbf{k}} + (V_{\mathbf{0}} + V_{\mathbf{k}}) n_0 + \delta\epsilon_{\mathbf{k}} + \hbar\partial_t\theta_0, \tag{21}$$

$$\Delta_{\mathbf{k}} = V_{\mathbf{k}} n_0 + \delta\Delta_{\mathbf{k}}. \tag{22}$$

In the following section, we use the cumulant expansion method to construct equations of motion from this reformulated many-body Hamiltonian.

III. EQUATIONS OF MOTION

Prior to the quench, all N bosons in the gas are prepared in a noninteracting uniform Bose condensate at zero temperature such that $n_0 = n$. A sudden projection of the pure condensate into the unitary regime approximates the effect of the rapid interaction quench. The fully condensed initial state is actually a highly excited state in the strong-coupling regime (for comparison, the ground state of superfluid ^{4}He has a condensed fraction of the order of 0.07 [57]), and the gas begins to rapidly quantum deplete such that $N - N_0$ becomes comparable to N. As the gas evolves, correlations begin to develop amongst excitations and the system becomes strongly correlated. Correlations that intrinsically relate larger numbers of excitations, however, develop *sequentially*, beginning from the generation of correlated pairs out of the condensate [29,30,41–43]. We can use this picture to construct a many-body description of this far-from-equilibrium, strongly interacting system by systematically including intrinsically higher-order effects into our theory, using the method of cumulants. In this section, we outline the cumulant theory, beginning in Sec. III A with an introduction to the cumulant hierarchy. In Sec. III B we detail how truncating this hierarchy impacts the underlying conservation laws. In Sec. III C, the cumulant equations of motion are given explicitly, and in Sec. III D we discuss how they may be solved in a way that reveals the underlying few-body physics at each level of the hierarchy.

A. Hierarchy of cumulants

To describe the coupled-correlation dynamics, we introduce the cumulant of a p-body operator as

$$\left\langle \prod_{i=0}^{l} \hat{b}_{\mathbf{k}_i}^\dagger \prod_{j=0}^{m} \hat{b}_{\mathbf{k}'_j} \right\rangle_c = (-1)^m \prod_{i=0}^{l} \frac{\partial}{\partial x_i} \prod_{j=0}^{m} \frac{\partial}{\partial y_j^*} \times \ln \left\langle e^{\sum_{i=0}^{l} x_i \hat{b}_{\mathbf{k}_i}^\dagger} e^{\sum_{j=0}^{m} y_j^* \hat{b}_{\mathbf{k}'_j}} \right\rangle \Big|_{\mathbf{x},\mathbf{y}=0}. \tag{23}$$

We call the cumulant of an p-body operator (here $p = l + m$), a p uplet. In practice, a p uplet is obtained by subtracting from the quantum average value (the "moment" of the p-body operator) all the possible contractions into products of n-body operator average, with $n < p$ [38,39]. This recursive definition of the cumulants is shown in Table I up to the quadruplet level. In the homogeneous system considered here, only the cumulants that conserve the total momentum [that is, verify $\sum_i \mathbf{k}_i = \sum_j \mathbf{k}'_j$, in the notations of Eq. (23)] can become nonzero during the time evolution. This implies in particular that the singlets $\langle \hat{b}_{\mathbf{k}} \rangle_{\mathbf{k}\neq 0}$ remain zero at all times.

TABLE I. Relations between the cumulant $\langle \hat{O} \rangle_c$ and the quantum average value (the moment) $\langle \hat{O} \rangle$ for operators up to the quadruplet level. The one-body operators $\hat{a}$, $\hat{b}$, $\hat{c}$, and $\hat{d} \in \{\hat{b}_{\mathbf{k}}, \hat{b}_{\mathbf{k}}^\dagger, \mathbf{k} \neq 0\}$ are normally ordered. The cancellation of the singlets $\langle \hat{a} \rangle_c = 0$ (used implicitly in the third and fourth lines of the table) is a consequence of the spatial homogeneity of the gas.

Cumulant order	Moment expansion
Singlet	$\langle \hat{a} \rangle_c = \langle \hat{a} \rangle = 0$
Doublet	$\langle \hat{a}\hat{b} \rangle_c = \langle \hat{a}\hat{b} \rangle - \langle \hat{a} \rangle_c \langle \hat{b} \rangle_c = \langle \hat{a}\hat{b} \rangle$
Triplet	$\langle \hat{a}\hat{b}\hat{c} \rangle_c = \langle \hat{a}\hat{b}\hat{c} \rangle$
Quadruplet	$\langle \hat{a}\hat{b}\hat{c}\hat{d} \rangle_c = \langle \hat{a}\hat{b}\hat{c}\hat{d} \rangle - \langle \hat{a}\hat{b} \rangle_c \langle \hat{c}\hat{d} \rangle_c - \langle \hat{a}\hat{c} \rangle_c \langle \hat{b}\hat{d} \rangle_c - \langle \hat{a}\hat{d} \rangle_c \langle \hat{b}\hat{c} \rangle_c$
...	...

Due to the cubic and quartic parts of the many-body Hamiltonian ($\hat{H}_3$ and $\hat{H}_4^{\rm eff}$, respectively) the doublet dynamics couple to triplets and quadruplets. Therefore, the depletion of the condensate into opposite momentum pairs in turn will sequentially generate higher-order few-body correlations, beginning at the three- and four-body levels. At the next level of the hierarchy, the triplets couple to doublets, quadruplets, and quintuplets, and this trend is repeated to all orders. In practice, this hierarchy must be truncated, which limits the range of validity of the model to times before higher-order few-body correlations become non-negligible [42]. We address truncation of the cumulant hierarchy in the following section.

B. Truncation scheme and conservation laws

When the time evolution of the many-body system is described only approximately, namely, in a truncated cumulant expansion, it is unclear whether the same constants of motion associated with the many-body Hamiltonian arise [55]. Therefore, it is not guaranteed *a priori* that truncation at a given level of cumulants results in a theory which respects all of the underlying conservation laws. With that caveat, we note that all of the truncation schemes studied in this paper conserve the average number of atoms by construction [see Eq. (9)]. We discuss now in detail the interplay between truncation order and the conservation of energy.

1. Doublet truncation

The simplest model within the cumulant theory (the doublet model), which corresponds to the HFB theory [55], can be constructed by keeping only the doublets while setting all higher-order cumulants to zero [58]. This yields the equations of motion:

$$i\hbar\partial_t \langle \hat{a}\hat{b} \rangle \underset{\text{doub}}{\simeq} \left\langle \left[\hat{a}\hat{b}, \hat{H}_2^{\rm eff} \right] \right\rangle, \tag{24}$$

where we have used the abbreviation doub to indicate this particular truncation scheme. The total energy $E \equiv \langle \hat{H} \rangle = \langle \hat{H}_b \rangle$ is here approximated by $E \underset{\text{doub}}{\simeq} \langle \hat{H}_2^{\rm eff} \rangle$, and its time derivative

vanishes, as can by checked by summing over the doublets $\hat{a}\hat{b}$ in Eq. (24) to form the derivative of $\hat{H}_2^{\text{eff}}$. Alternatively, these conclusions are anticipated by the variational derivation [55]. Simulation results for the doublet model are the subject of Sec. IV.

2. Triplet truncation

To go beyond the doublet model, one can first choose to also retain the triplets (the triplet model) in the truncation scheme. This yields the equations of motion

$$i\hbar\partial_t\langle\hat{a}\hat{b}\rangle \underset{\text{tri}}{\simeq} \langle[\hat{a}\hat{b}, \hat{H}_2^{\text{eff}} + \hat{H}_3]\rangle, \tag{25}$$

$$i\hbar\partial_t\langle\hat{a}\hat{b}\hat{c}\rangle \underset{\text{tri}}{\simeq} \langle[\hat{a}\hat{b}\hat{c}, \hat{H}_b]\rangle - \langle[\hat{a}\hat{b}\hat{c}, \hat{H}_3 + \hat{H}_4^{\text{eff}}]\rangle_c, \tag{26}$$

where we have used the abbreviation tri to indicate truncation at the triplet level. From the exact time derivative $i\hbar\partial_t\langle\hat{a}\hat{b}\rangle = \langle[\hat{a}\hat{b}, \hat{H}_b]\rangle$, it also subtracts $\langle[\hat{a}\hat{b}, \hat{H}_4^{\text{eff}}]\rangle$, which is by construction composed only of quadruplets, resulting in Eq. (25). From the exact time derivative $i\hbar\partial_t\langle\hat{a}\hat{b}\hat{c}\rangle = \langle[\hat{a}\hat{b}\hat{c}, \hat{H}_b]\rangle$, it also subtracts the quadruplets and quintuplets contained in $\langle[\hat{a}\hat{b}\hat{c}, \hat{H}_3]\rangle$ and $\langle[\hat{a}\hat{b}\hat{c}, \hat{H}_4^{\text{eff}}]\rangle$, respectively, while the corresponding doublet-doublet and triplet-doublet contributions remain in Eq. (26). Additionally, the triplet truncation of the total energy is $E \underset{\text{tri}}{\simeq} \langle\hat{H}_2^{\text{eff}} + \hat{H}_3\rangle$, and its time derivative does *not* vanish:

$$i\hbar\partial_t E \underset{\text{tri}}{\simeq} \langle[\hat{H}_3, \hat{H}_4^{\text{eff}}]\rangle - \langle[\hat{H}_3, \hat{H}_4^{\text{eff}}]\rangle_c \neq 0. \tag{27}$$

This can be obtained by summing over the doublets and triplets in Eqs. (25) and (26) to form the time derivatives of $\hat{H}_2^{\text{eff}}$ and $\hat{H}_3$, respectively. From the above remarks, the origin of this violation is therefore clear: whereas the cumulant equations of motion [Eqs. (25) and (26)] follow from the full Hamiltonian $\hat{H}_b$, the energy is computed from the truncated Hamiltonian $\hat{H}_2^{\text{eff}} + \hat{H}_3$. Simulation results for the triplet model are the subject of Sec. V, and energy violation results can be found in Appendix B.

3. Quadruplet truncation

Going beyond the doublet model in a way that does not violate energy-conservation therefore requires the addition of quadruplets (the quadruplet model) so the energy is computed from the full Hamiltonian $\hat{H}_b$. This yields the equations of motion

$$i\hbar\partial_t\langle\hat{a}\hat{b}\rangle = \langle[\hat{a}\hat{b}, \hat{H}_b]\rangle, \tag{28}$$

$$i\hbar\partial_t\langle\hat{a}\hat{b}\hat{c}\rangle \underset{\text{quad}}{\simeq} \langle[\hat{a}\hat{b}\hat{c}, \hat{H}_b]\rangle - \langle[\hat{a}\hat{b}\hat{c}, \hat{H}_4^{\text{eff}}]\rangle_c, \tag{29}$$

$$i\hbar\partial_t\langle\hat{a}\hat{b}\hat{c}\hat{d}\rangle \underset{\text{quad}}{\simeq} \langle[\hat{a}\hat{b}\hat{c}\hat{d}, \hat{H}_b]\rangle - \langle[\hat{a}\hat{b}\hat{c}\hat{d}, \hat{H}_3]\rangle_c - \langle[\hat{a}\hat{b}\hat{c}\hat{d}, \hat{H}_4^{\text{eff}}]\rangle_c, \tag{30}$$

where we have used the abbreviation quad to indicate truncation at the quadruplet level [59]. Although the doublet equations of motion are now exact, the quadruplet truncation scheme subtracts $\langle[\hat{a}\hat{b}\hat{c}, \hat{H}_4^{\text{eff}}]\rangle_c$ from the exact time derivative $i\hbar\partial_t\langle\hat{a}\hat{b}\hat{c}\rangle = \langle[\hat{a}\hat{b}\hat{c}, \hat{H}_b]\rangle$ to produce Eq. (29) and subtracts the quintuplets $\langle[\hat{a}\hat{b}\hat{c}\hat{d}, \hat{H}_3]\rangle_c$ and sextuplets $\langle[\hat{a}\hat{b}\hat{c}\hat{d}, \hat{H}_4^{\text{eff}}]\rangle_c$ from the exact time derivative $i\hbar\partial_t\langle\hat{a}\hat{b}\hat{c}\hat{d}\rangle = \langle[\hat{a}\hat{b}\hat{c}\hat{d}, \hat{H}_b]\rangle$ to produce Eq. (30). The quadruplet model trivially conserves the total energy because the full Hamiltonian $\hat{H}_b$ is used to evolve both the energy and cumulants. Although the quadruplet model is not simulated in this paper due to the large resource requirements, with the size of a p-dimensional cumulant array scaling roughly as Λ^{p-1} (see Appendix B), we give the general cumulant equations in the following section.

C. Cumulant equations of motion

We now give the equations of motion for the doublet, triplet, and quadruplet cumulants [Eqs. (28–30)] within the quadruplet model. We use Greek letters α, β, γ … to denote the wave vector indices of the considered cumulants and we keep the bold letters $\mathbf{k}$, $\mathbf{q}$ for the wave vectors which are summed over. The cumulants that compose the closed system of equations of motion are denoted:

$$\begin{aligned} n_\alpha &= \langle\hat{b}_\alpha^\dagger\hat{b}_\alpha\rangle, & c_\alpha &= \langle\hat{b}_{-\alpha}\hat{b}_\alpha\rangle, \\ M_{\alpha,\beta} &= \langle\hat{b}_{\alpha-\beta}^\dagger\hat{b}_\beta^\dagger\hat{b}_\alpha\rangle, & R_{\alpha,\beta} &= \langle\hat{b}_{\beta-\alpha}\hat{b}_\alpha\hat{b}_{-\beta}\rangle, \\ Q_{\alpha,\beta;\gamma} &= \langle\hat{b}_{\alpha+\beta-\gamma}^\dagger\hat{b}_\gamma^\dagger\hat{b}_\alpha\hat{b}_\beta\rangle_c, & P_{\alpha,\beta,\gamma} &= \langle\hat{b}_{\alpha+\beta+\gamma}^\dagger\hat{b}_\alpha\hat{b}_\beta\hat{b}_\gamma\rangle_c, \\ T_{\alpha,\beta,\gamma} &= \langle\hat{b}_{-\alpha-\beta-\gamma}\hat{b}_\alpha\hat{b}_\beta\hat{b}_\gamma\rangle_c. \end{aligned} \tag{31}$$

To obtain compact and readable expressions, one should exploit the invariance of the cumulants under permutation of their indices (for example $M_{\alpha+\beta,\beta}$ is invariant under the exchange of α and β, $P_{\alpha,\beta,\gamma}$ is invariant under the exchange of α, β, and γ). For this purpose, we introduce the symmetrizer $\mathcal{S}_{\alpha_1,\ldots,\alpha_n}$ which sums all the values of a function $f(\alpha_1,\ldots,\alpha_n)$ obtained after permutation of its arguments:

$$\mathcal{S}_{\{\alpha_1,\ldots,\alpha_n\}}[f(\alpha_1,\ldots,\alpha_n)] = \sum_{\sigma\in\mathfrak{S}(n)} f(\alpha_{\sigma(1)},\ldots,\alpha_{\sigma(n)}), \tag{32}$$

where $\mathfrak{S}(n)$ is the set of permutations of $\{1,\ldots n\}$. For the cumulant Q, which obeys the symmetry relation $Q^*_{\alpha,\beta;\gamma} = Q_{\gamma,\alpha+\beta-\gamma;\alpha}$, we will also need the antisymmetrizer:

$$\begin{aligned} &\mathcal{A}_{\{(\alpha,\beta),(\gamma,\delta)\}}[f(\alpha,\beta;\gamma,\delta)] \\ &\quad = f(\alpha,\beta;\gamma,\delta) - [f(\gamma,\delta;\alpha,\beta)]^*. \end{aligned} \tag{33}$$

All the equations of motion we give here can be checked using the computer algebra program available online [60].

Let us first reexpress the coefficients of $\hat{H}_2^{\text{eff}}$ [Eqs. (21) and (22)] and the phase derivative [Eq. (11)] in terms of the doublets and triplets,

$$E_\alpha = \epsilon_\alpha + V_{\mathbf{0}}n + V_\alpha n_0 + \frac{1}{V}\sum_{\mathbf{q}} V_{\mathbf{q}} n_{\alpha+\mathbf{q}} + \hbar\partial_t\theta_0, \tag{34}$$

$$\Delta_\alpha = V_\alpha n_0 + \frac{1}{V}\sum_{\mathbf{q}} V_{\mathbf{q}} c_{\alpha+\mathbf{q}}, \tag{35}$$

$$\hbar\frac{d\theta_0}{dt} = -\left[V_{\mathbf{0}}n + \frac{1}{V}\sum_{\mathbf{q}} V_{\mathbf{q}}(n_{\mathbf{q}} + \text{Re}\, c_{\mathbf{q}}) + \frac{1}{\sqrt{n_0 V^3}}\sum_{\mathbf{k},\mathbf{q}} V_{\mathbf{q}}\text{Re}\, M^*_{\mathbf{k}+\mathbf{q},\mathbf{k}}\right], \tag{36}$$

where E_α and Δ_α are the expressions for the Hartree-Fock Hamiltonian and pairing field, respectively, in the rotating frame [55,61].

For the doublet equations of motion (assuming the invariance of the triplets under parity, $M_{-\alpha,-\beta} = M_{\alpha,\beta}$ and $R_{-\alpha,-\beta} = R_{\alpha,\beta}$), we have

$$i\hbar\partial_t n_\alpha = 2i\mathrm{Im}\left(\Delta_\alpha c_\alpha^* + \sqrt{\frac{n_0}{V}}\sum_{\mathbf{q}}[V_{\mathbf{q}}M^*_{\alpha,\mathbf{q}} - (V_{\mathbf{q}}+V_\alpha)M^*_{\alpha+\mathbf{q},\alpha}] + \frac{1}{V}\sum_{\mathbf{k},\mathbf{q}} V_{\mathbf{q}}Q_{\alpha+\mathbf{q},\mathbf{k};\alpha}\right), \tag{37}$$

$$i\hbar\partial_t c_\alpha = 2E_\alpha c_\alpha + \Delta_\alpha(2n_\alpha+1) + 2\sqrt{\frac{n_0}{V}}\sum_{\mathbf{q}}[V_{\mathbf{q}}R_{\alpha,-\mathbf{q}} + (V_\alpha+V_{\mathbf{q}})M^*_{\mathbf{q},\alpha}] + \frac{2}{V}\sum_{\mathbf{k},\mathbf{q}} V_{\mathbf{q}}P_{\alpha,\mathbf{q}-\alpha,\mathbf{k}}. \tag{38}$$

We note that these doublet equations of motion are equivalent to the Hyperbolic Bloch equations discussed in Ref. [42].

For the triplet equations of motion, we have

$$i\hbar\partial_t M_{\alpha+\beta,\beta} = (E_{\alpha+\beta} - E_\alpha - E_\beta)M_{\alpha+\beta,\beta} - \Delta^*_\alpha M^*_{\beta,\alpha+\beta} - \Delta^*_\beta M^*_{\alpha,\alpha+\beta} + \Delta_{\alpha+\beta}R^*_{\alpha,\alpha+\beta} + \mathcal{M}^{H_3}_{\alpha,\beta} + \mathcal{M}^{H_4}_{\alpha,\beta}, \tag{39}$$

$$i\hbar\partial_t R_{\alpha,\alpha+\beta} = (E_\alpha + E_\beta + E_{\alpha+\beta})R_{\alpha,\alpha+\beta} + \Delta_\alpha M^*_{-\alpha,\beta} + \Delta_\beta M_{-\beta,\alpha} + \Delta_{\alpha+\beta}M^*_{\alpha+\beta,\alpha} + \mathcal{R}^{H_3}_{\alpha,\beta} + \mathcal{R}^{H_4}_{\alpha,\beta}, \tag{40}$$

where we have written separately the contribution of the cubic and quartic Hamiltonians. The former contains both doublet products and quadruplets,

$$\frac{\mathcal{M}^{H_3}_{\alpha,\beta}}{\sqrt{n_0/V}} = \mathcal{S}_{\{\alpha,\beta\}}\Bigg[V_\alpha[n_\alpha n_\beta - n_\gamma(1+n_\alpha+n_\beta)] - c_\gamma c^*_\alpha(V_\gamma+V_\beta) - n_\gamma c^*_\alpha(V_\gamma+V_\alpha) + n_\alpha c^*_\beta(V_\beta+V_\gamma) + \sum_{\mathbf{q}}\left\{\frac{V_\gamma+V_{\mathbf{q}}}{2}P^*_{\alpha,\beta,\mathbf{q}} - (V_\beta+V_{\mathbf{q}})Q_{\gamma,\mathbf{q};\alpha} - V_{\mathbf{q}}\left[P^*_{\alpha,\mathbf{q},\beta-\mathbf{q}} - \frac{1}{2}Q_{\gamma-\mathbf{q},\mathbf{q};\alpha}\right]\right\}\Bigg], \tag{41}$$

$$\frac{\mathcal{R}^{H_3}_{\alpha,\beta}}{\sqrt{n_0/V}} = \mathcal{S}_{\{\alpha,\beta,\gamma'\}}\left[V_\beta\{c_\beta c_{\gamma'} + c_\alpha(1+n_\beta+n_{\gamma'})\} + \sum_{\mathbf{q}}\left\{\frac{V_\alpha+V_{\mathbf{q}}}{2}P_{\alpha+\mathbf{q},\beta,\gamma'} + \frac{V_{\mathbf{q}}}{2}T_{\beta,\gamma',\mathbf{q}}\right\}\right], \tag{42}$$

while the latter contains products of doublets and triplets

$$\mathcal{M}^{H_4}_{\alpha,\beta} = -\frac{\mathcal{S}_{\{\alpha,\beta\}}}{V}\Bigg[\sum_{\mathbf{q}} V_{\mathbf{q}}\frac{1+n_\alpha+n_\beta}{2}M_{\gamma,\alpha-\mathbf{q}} + (V_\alpha+V_{\mathbf{q}})(n_\gamma - n_\beta)M_{\gamma-\mathbf{q},\alpha} + (V_\gamma + V_{\beta+\mathbf{q}})c^*_\beta M^*_{\gamma+\mathbf{q},\gamma} + V_{\mathbf{q}}\{c_\gamma R^*_{\beta,\mathbf{q}-\alpha} - c^*_\beta M^*_{\alpha,\mathbf{q}-\beta}\}\Bigg], \tag{43}$$

$$\mathcal{R}^{H_4}_{\alpha,\beta} = \frac{\mathcal{S}_{\{\alpha,\beta,\gamma'\}}}{V}\left[\sum_{\mathbf{q}}\frac{V_{\mathbf{q}}}{2}(1+n_\alpha+n_\beta)R_{\alpha-\mathbf{q},-\gamma'} + (V_\alpha+V_{\mathbf{q}-\gamma'})c_\beta M^*_{\alpha+\mathbf{q},\alpha}\right]. \tag{44}$$

In these expressions, γ (in $\mathcal{M}^{H_3}$ and $\mathcal{M}^{H_4}$) and γ' (in $\mathcal{R}^{H_3}$ and $\mathcal{R}^{H_4}$), which denote the third wave vector deduced from α and β by momentum conservation, should be replaced, respectively, by $\gamma = \alpha+\beta$ and $\gamma' = -\alpha-\beta$ after the action of the symmetrizer $\mathcal{S}$.

Finally, for the quadruplets, using the notations $\delta = \alpha+\beta-\gamma$, $\delta' = \alpha+\beta+\gamma$, and $\delta'' = -\alpha-\beta-\gamma$ for the fourth wave vector of, respectively, $Q_{\alpha\beta;\gamma}$, $P_{\alpha,\beta,\gamma}$ and $T_{\alpha,\beta,\gamma}$, we have

$$i\hbar\partial_t Q_{\alpha,\beta;\gamma} = (E_\alpha+E_\beta-E_\gamma-E_\delta)Q_{\alpha\beta;\gamma} + \mathcal{S}_{\{\alpha,\beta\}}[\Delta_\alpha P^*_{-\alpha,\gamma,\delta}] - \mathcal{S}_{\{\gamma,\delta\}}[\Delta^*_\gamma P^*_{\alpha,\beta,-\gamma}] + \mathcal{Q}^{H_3}_{\alpha,\beta;\gamma} + \mathcal{Q}^{H_4}_{\alpha,\beta;\gamma}, \tag{45}$$

$$i\hbar\partial_t P_{\alpha,\beta,\gamma} = (E_\alpha+E_\beta+E_\gamma-E_{\delta'})P_{\alpha,\beta,\gamma} + \mathcal{S}_{\{\alpha,\beta,\gamma\}}[\Delta_\alpha Q_{\beta,\gamma;\delta'}] - \Delta^*_{\delta'}T_{\alpha,\beta,\gamma} + \mathcal{P}^{H_3}_{\alpha,\beta,\gamma} + \mathcal{P}^{H_4}_{\alpha,\beta,\gamma}, \tag{46}$$

$$i\hbar\partial_t T_{\alpha,\beta,\gamma} = (E_\alpha+E_\beta+E_\gamma+E_{\delta''})T_{\alpha,\beta,\gamma} + \mathcal{S}_{\{\alpha,\beta,\gamma,\delta''\}}[\Delta_\alpha P_{\beta,\gamma,\delta''}] + \mathcal{T}^{H_3}_{\alpha,\beta,\gamma} + \mathcal{T}^{H_4}_{\alpha,\beta,\gamma}. \tag{47}$$

The lengthy expressions for $\mathcal{Q}^{H_3}_{\alpha,\beta;\gamma}$, $\mathcal{Q}^{H_4}_{\alpha,\beta;\gamma}$, $\mathcal{P}^{H_3}_{\alpha,\beta,\gamma}$, $\mathcal{P}^{H_4}_{\alpha,\beta,\gamma}$, $\mathcal{T}^{H_3}_{\alpha,\beta,\gamma}$, and $\mathcal{T}^{H_4}_{\alpha,\beta,\gamma}$ can be found in Appendix C.

For completeness, the cumulant equations of motion up to the level of triplets can be found given explicitly in Appendix B for a separable potential, which allows for modest simplifications important for numerical implementation. Following this formal discussion of the cumulant equations in the quadruplet model, we now analyze their structure and solution at early times following the quench in the following section.

D. Few-body physics and the early-time structure of the cumulant hierarchy

In this section, we discuss in greater detail the sequential correlation buildup picture using the cumulant equations

of motion outlined in Sec. III C. This discussion also highlights the few-body physics contained at each level of the hierarchy and is therefore crucial to understanding how the Efimov effect is introduced into the many-body model. The sequential buildup of correlations can be understood formally from the structure of the homogeneous and inhomogeneous (drive) terms in the cumulant equations of motion given in Sec. III C. At the lowest level, the correlation buildup begins with the generation of $(\alpha, -\alpha)$ pairs from the drive term $V_\alpha n_0$ in Eq. (38). Consequently, the occupation of momentum modes is reflected in the dynamics of n_α, which remains small compared to unity at early times such that the Bose-enhancement factors $(1 + n_\alpha + n_\beta) \approx 1$ can be ignored and the exponentiation $(n_\alpha)^m$ in the drive terms of the higher-order cumulants vanishes as m tends to infinity. The three-excitation Beliaev-Landau type processes described by M and R cumulants, are the next level to be driven by terms of the form $V_\alpha n_\gamma \sqrt{n_0/V}$ and $V_\beta c_\alpha \sqrt{n_0/V}$ in Eqs. (39) and (40), respectively. At the next level, the quadruplet processes described by Q, P, and T are driven by terms of the form $M_{\gamma+\delta,\gamma}\sqrt{n_0/V}$ and $V_{\gamma-\alpha}n_\gamma n_\delta$, $V_\beta M^*_{\delta',\alpha}\sqrt{n_0/V}$ and $V_{\alpha+\gamma}c_\gamma n_{\delta'}$, and $V_\alpha R_{\gamma,-\delta''}\sqrt{n_0/V}$ and $V_{\alpha+\delta''}c_\gamma c_{\delta''}$ in Eqs. (45)–(47) (see Appendix C), respectively. From these examples, it is clear that the sequential buildup behavior is a general property of the postquench early-time dynamics of cumulants. Indeed, this property serves as the motivation for using cumulants in the present study to describe the buildup of correlations even in the strongly-interacting regime where a natural truncation parameter is lacking.

At early times, these properties of the cumulant hierarchy can be used to generate solutions highlighting the underlying few-body physics in the many-body system. First, the hierarchy is recast into a reduced early-time form by ignoring the $p+1$ and $p+2$ higher-order correlation functions in the equation of motion for cumulants of order p, identical to the truncation scheme in Ref. [39]. At the level of the doublets, the c cumulant equation [Eq. (38)] reduces to

$$i\hbar\partial_t|c_t, c_t\rangle = \hat{H}_{12}(t)|c_t, c_t\rangle + \hat{V}|\psi_{0,t}, \psi_{0,t}\rangle, \tag{48}$$

where $\hat{H}_{12}(t) = \hat{\epsilon}_1 + \hat{\epsilon}_2 - 2\mu(t) + \hat{V}$ is the two-body Hamiltonian in the rotating frame of the condensate, written in terms of the one-body kinetic energy-operator $\hat{\epsilon}|\alpha\rangle = \epsilon_\alpha|\alpha\rangle$ and the pairwise potential $\hat{V}$. The second Josephson relation gives the instantaneous chemical potential $\mu(t) \equiv -\hbar\dot{\theta}_0(t)$. Additionally, the pair matrix has been cast into basis-independent symmetric state $\langle\alpha, \beta|c_t, c_t\rangle = c_\alpha(t)\delta_{\alpha,-\beta}$, which reflects its behavior under unitary transformations [55]. We have also defined the generalized rank (0,2) tensor $|\psi_{0,t}, \psi_{0,t}\rangle = n_0(t)|\mathbf{0}, \mathbf{0}\rangle$, where tensor subscripts in the ket indicate the time. Equation (48) can be solved formally using the two-body evolution operator $\hat{\mathcal{U}}_{12}(t - t_0) = \exp\left[-i\int_{t_0}^t d\tau \hat{H}_{12}(\tau)/\hbar\right]$ as

$$|c_t, c_t\rangle = \hat{\mathcal{U}}_{12}(t - t_0)|c_{t_0}, c_{t_0}\rangle + \frac{1}{i\hbar}\int_{t_0}^t d\tau \hat{\mathcal{U}}_{12}(t - \tau)\hat{V}|\psi_{0,\tau}, \psi_{0,\tau}\rangle, \tag{49}$$

where the initial conditions at $t = t_0$ are encoded in the first term on the right-hand side of the above equality. Analogously, the M-cumulant equation of motion [Eq. (39)] becomes

$$\begin{aligned} i\hbar\partial_t|M_t\rangle\langle M_t, M_t| = {} & \hat{H}_1(t)|M_t\rangle\langle M_t, M_t| \\ & - |M_t\rangle\langle M_t, M_t|\hat{H}_{12}(t) \\ & - |n_t\rangle\langle n_t, \psi_{0,t}|(1 + \hat{P}_{12})\hat{V}, \end{aligned} \tag{50}$$

where $\hat{H}_1(t) = \hat{\epsilon} - \mu(t)$ is the one-body Hamiltonian in the rotating frame of the condensate, and $\hat{P}_{12}$ is the cyclic permutation operator. We have defined rank (1,2) tensors $\langle\alpha|M_t\rangle\langle M_t, M_t|\beta, \gamma\rangle = M_{\alpha,\beta}(t)\delta_{\alpha,\beta+\gamma}\sqrt{V}$ and $\langle\alpha, \beta|\psi_{0,t}, n_t\rangle\langle n_t|\gamma\rangle = \delta_{\gamma,\alpha}\delta_\beta n_\alpha(t)\sqrt{n_0(t)}$. Equation (50) can be solved formally as

$$\begin{aligned} |M_t\rangle\langle M_t, M_t| = {} & \hat{\mathcal{U}}_1(t - t_0)|M_{t_0}\rangle\langle M_{t_0}, M_{t_0}|\hat{\mathcal{U}}_{12}(t_0 - t) \\ & - \frac{1}{i\hbar}\int_{t_0}^t d\tau \hat{\mathcal{U}}_1(t - \tau)|n_\tau\rangle\langle n_\tau, \psi_{0,\tau}|(1 + \hat{P}_{12}) \\ & \times \hat{V}\hat{\mathcal{U}}_{12}(\tau - t), \end{aligned} \tag{51}$$

where $\hat{\mathcal{U}}_1(t - t_0) = \exp\left[-i\int_{t_0}^t d\tau \hat{H}_1(\tau)/\hbar\right]$ is the one-body evolution operator. We have chosen to write the cumulant equations of motion in basis-independent form to facilitate and emphasize the generality of the discussion that follows.

From the formal integral relations [Eqs. (49) and (51)], it is possible to solve for the dynamics of the energies $\mu(t)$, $E_\alpha(t)$, and $\Delta_\alpha(t)$. Approximating the quench as a sudden projection of a pure, noninteracting condensate onto unitarity, the initial conditions in Eqs. (49) and (51) are neglected. Inserting the formal solutions into Eq. (36), we find the time-dependent expression for the chemical potential

$$N_0(t)\mu(t) = \mathrm{Tr}\left[\mathrm{Re}\left[\int_{t_0}^t d\tau \hat{\mathcal{T}}_+(t - \tau)|\psi_{0,\tau}, \psi_{0,\tau}\rangle\langle\psi_{0,t}, \psi_{0,t}| + \hat{\mathcal{T}}_+(t - \tau)(1 + \hat{P}_{12})|n_\tau, \psi_{0,\tau}\rangle\langle\psi_{0,t}, n_\tau|\hat{\mathcal{U}}_1(\tau - t)\right]\right], \tag{52}$$

$$\begin{aligned} \mu(t) = {} & \mathrm{Re}\int_{t_0}^t d\tau \mathcal{T}_+(\mathbf{0}, \mathbf{0}, t - \tau)n_0(\tau) + \mathrm{Re}\int_{t_0}^t d\tau \int d^3q \Big[\mathcal{T}_+\Big(\frac{\mathbf{q}}{2}, \frac{\mathbf{q}}{2}, t - \tau\Big) \\ & + \mathcal{T}_+\Big(\frac{\mathbf{q}}{2}, -\frac{\mathbf{q}}{2}, t - \tau\Big)\Big]\sqrt{\frac{n_0(\tau)}{n_0(t)}}n_\mathbf{q}(\tau)\mathcal{U}_1(\mathbf{q}, \tau - t), \end{aligned} \tag{53}$$

where $\hat{\mathcal{U}}_1(t)|\mathbf{k}\rangle = \mathcal{U}_1(\mathbf{k}, t)|\mathbf{k}\rangle$, and we have defined the retarded two-body T operator in the rotating frame of the condensate [62]

$$\hat{\mathcal{T}}_+(t) = \delta(t)\hat{V} + \frac{1}{i\hbar}\theta(t)\hat{V}\hat{\mathcal{U}}_{12}(t)\hat{V}, \tag{54}$$

with $\theta(t)$ the Heaviside function and $\langle \mathbf{k}+\mathbf{q}, \mathbf{k}-\mathbf{q}|\hat{\mathcal{T}}_+(t)|\mathbf{k}'+\mathbf{p}, \mathbf{k}'-\mathbf{p}\rangle = \delta_{\mathbf{k},\mathbf{k}'}\mathcal{T}_+(\mathbf{q},\mathbf{p},t)$. From Eq. (52), we see that as $t-t_0 \to 0^+$, $\hat{\mathcal{T}}_+(0) = \delta(0)\hat{V}$ and therefore $\mu(t) = V_{\mathbf{0}}n_0$, which is the first Born approximation for the chemical potential of a pure condensate. Analogously, inserting the formal solutions into Eq. (35), we find an expression for the time-dependent pairing field,

$$|\Delta,\Delta\rangle = \int_{t_0}^{t} d\tau \hat{\mathcal{T}}_+(t-\tau)|\psi_{0,\tau},\psi_{0,\tau}\rangle, \tag{55}$$

$$\Delta_{\mathbf{k}}(t) = \int_{t_0}^{t} d\tau \mathcal{T}_+(\mathbf{k},\mathbf{0},t-\tau)n_0(\tau), \tag{56}$$

which has been written in basis-independent form $\langle\alpha,\beta|\Delta,\Delta\rangle = \Delta_\alpha\delta_{\alpha,-\beta}$. As $t-t_0\to 0^+$, the first Born appoximation $\Delta_\alpha(t) = V_\alpha n_0$ is recovered. As time evolves, the memory kernels in Eqs. (52) and (56) are integrated over larger intervals of time. Here, the unitarity limit of the s-wave cross section $\sigma \propto 1/k^2$ translates into the universal behavior $\hat{\mathcal{T}}_+(t) \propto \exp[-2i\theta_0(t)]/\sqrt{t}$ reflecting the gradual decay of resonant collisions. The energy $E_\alpha(t)$, however, contains the Hartree-Fock mean-field energy $E_\alpha^{(\mathrm{HF})} = (V_{\mathbf{0}}+V_\alpha)n_0 + \delta\epsilon_\alpha$ that remains at the level of the first Born approximation regardless of the system dynamics. To estimate the relevance of the Hartree-Fock mean-field energies in the unitary regime, we rescale to the Fermi energy E_n, finding in general $E_\alpha^{(\mathrm{HF})}/E_\mathrm{n} \propto n^{1/3}r_\mathrm{vdW}$ due to the calibration of the effective interaction strength $g \propto r_\mathrm{vdW}$ for the resonance coupling strength (see Appendix A). Therefore, the Hartree-Fock mean-field energies can be neglected in the unitary regime for realistic systems where the criterion $nr_\mathrm{vdW}^3 \ll 1$ is well satisfied.

The presence of few-body operators in the solutions of the cumulant equations of motion reveals how few-body effects are woven into the early-time structure of the hierarchy. To demonstrate this explicitly, we spectrally decompose the evolution operator $\hat{\mathcal{U}}_{12}(t)$ as

$$\hat{\mathcal{U}}_{12}(t) = \sum_i e^{-i\epsilon_i t/\hbar}|\phi_i\rangle\langle\phi_i| + \int d\epsilon\, e^{-i\epsilon t/\hbar}|\phi(\epsilon)\rangle\langle\phi(\epsilon)| \tag{57}$$

into the vacuum bound states $|\phi_i\rangle$ with binding energy ϵ_i and two-body continuum states $|\phi(\epsilon)\rangle$. Qualitatively, the response of the system at a dimer binding energy depends on the overlap between the $|\phi_i\rangle$'s and the driving terms of the memory kernels in Eqs. (49) and (51). At unitarity, the s-wave dimer state is at threshold; however, the system may still respond at any of the infinite number of bound three-body Efimov trimers that exist in vacuum. To understand how the Efimov frequencies enter the cumulant hierarchy, we reduce the equation of motion for the R cumulant [Eq. (40)] to the early-time form

$$i\hbar\partial_t|R_t,R_t,R_t\rangle = \hat{H}_{123}(t)|R_t,R_t,R_t\rangle + (1+\hat{P}_+ + \hat{P}_-) \times \left[(\hat{V}_{12}+\hat{V}_{13})|\psi_{0,t},c_t,c_t\rangle\right], \tag{58}$$

where $\langle\alpha,\beta,\gamma|\hat{V}_{12}|\gamma',\beta',\alpha'\rangle = \delta_{\alpha,\alpha'}\langle\beta,\gamma|\hat{V}|\gamma',\beta'\rangle$, and $\hat{H}_{123}(t) = (1+\hat{P}_+ + \hat{P}_-)\hat{H}_{12}$ is the vacuum three-body Hamiltonian in the rotating frame of the condensate, written in terms of the cyclic and anticyclic permutation operators $\hat{P}_+ \equiv \hat{P}_{123}$ and $\hat{P}_- \equiv \hat{P}_{132}$, respectively, with $\hat{P}_{123}|\alpha,\beta,\gamma\rangle = |\gamma,\alpha,\beta\rangle$. In Refs. [44,63], Eq. (58) was shown to yield generalized three-body T matrices satisfying the Faddeev equations. These T matrices appear in the Gross-Pitaevskii equation as higher-order corrections due to effective three-body scattering, encapsulated in the scattering hypervolume [63–66]. We have also defined the rank (0,3) tensor $\langle\alpha,-\beta,\gamma|R_t,R_t,R_t\rangle = R_{\alpha,\beta}(t)\delta_{\alpha-\beta,-\gamma}\sqrt{V}$, whose formal solution is

$$|R_t,R_t,R_t\rangle = \hat{\mathcal{U}}_{123}(t-t_0)|R_{t_0},R_{t_0},R_{t_0}\rangle + \frac{1}{i\hbar}\int_{t_0}^{t} d\tau\hat{\mathcal{U}}_{123}(t-\tau)(1+\hat{P}_+ + \hat{P}_-)(\hat{V}_{12}+\hat{V}_{13})|\psi_{0,\tau},c_\tau,c_\tau\rangle, \tag{59}$$

where $\hat{\mathcal{U}}_{123}(t-t_0) = \exp\left[-i\int_{t_0}^{t} d\tau\hat{H}_{123}(\tau)/\hbar\right]$ is the three-body evolution operator in the rotating frame of the condensate. The eigendecomposition of the three-body evolution operator is [67]

$$\hat{\mathcal{U}}_{123}(t) = \sum_s \left[\sum_n e^{-iE_{s,n}t/\hbar}|\Phi_{s,n}\rangle\langle\Phi_{s,n}| + \int dE\, e^{-iEt/\hbar}|\Phi_s(E)\rangle\langle\Phi_s(E)|\right], \tag{60}$$

expressed in terms of the vacuum three-body continuum states $|\Phi_s(E)\rangle$ and vacuum three-body bound-states $|\Phi_{n,s}(E)\rangle$ with binding energy $E_{s,n}$. The three-body spectrum can be decomposed into universal channels $s^2 > 0$ that do not support bound states and the Efimovian channel $s = is_0$ with $s_0 \approx 1.006$ that supports an infinite number of trimers. The introduction of additional length scales in the Efimov channel due to the finite size of Efimov trimers can break the universal scaling of system properties with the density [28–30]. In principle, the system can respond at any one of the infinity of Efimov trimer frequencies, determined by the overlap between the Efimov trimer wave functions $|\phi_{is_0,n}\rangle$ and the driving terms in the memory kernel of Eq. (59), which will be studied in Sec. V.

What is the range of validity of the early-time form of the cumulant equations? In Ref. [39], this scheme was designed to include multiple scatterings in the cumulant equations of motion to extend their range of validity. By design, such multiple scatterings are described by the vacuum T-operators—the so-called free dynamics. In Sec. IV, we will see, however, that this picture is spoiled in the presence of strong quantum depletion. In particular, the energy Δ_α, which is negligible and can be ignored at early times, rapidly grows toward the Fermi scale at later times as correlations develop. Consequently, the triplet cumulant dynamics become strongly coupled and therefore can no longer be treated separately as in Eqs. (51) and (59), spoiling the appearance of vacuum operators and energies.

We note that the equations of motion for each of the quadruplets can also be reduced to their early-time forms and solved as integral equations. As in Eqs. (49) and (59), the vacuum one-, two-, three-, and four-body evolution operators also appear in the memory kernels for the Q, P, and T cumulants. However, because the numerical simulation of the full quadruplet cumulant theory outlined in this section remains an outstanding numerical challenge, this mostly formal discussion can be found in Appendix C. Having established the cumulant equations, justified their truncation for quenched systems, and highlighted the underlying few-body physics, we now simulate the doublet model in Sec. IV and the triplet model in Sec. V.

IV. DOUBLET MODEL OF THE QUENCHED UNITARY BOSE GAS

In this section, we study the quenched unitary Bose gas within the doublet model by neglecting all third- and fourth-order cumulants in Sec. III such that only $n_{\mathbf{k}}$ and $c_{\mathbf{k}}$ remain. To mimic the experimental sequence of Refs. [24–27], we make the sudden approximation and model the quench as infinitely fast. An initially pure, noninteracting condensate is then evolved in the unitary regime for a variable amount of time up to $t \sim 2.5t_{\rm n}$, where $n_{\mathbf{k}}$ begins to exceed unity and the exclusion of strongly-driven higher-order cumulants cannot be justified [44,45]. The condensate is depleted by pairwise excitations $(\mathbf{k}, -\mathbf{k})$ described by the c cumulant. In this section, we compare the doublet model results to the experimental data from Refs. [26,27] for quenched unitary Bose gases in a uniform system. The early-time agreement with experiment found in this section motivates an investigation of higher-order effects that will be addressed in Sec. V.

A. Energy and number dynamics

Before comparing against experiment, we study the time dependence of the characteristic energies Δ and $\mu(t)$ [Eqs. (35) and (36), respectively] in the doublet model simulation as a function of the van der Waals diluteness parameter $nr_{\rm vdW}^3$. The dynamics of these energies are shown in Figs. 1(a)–1(c), where we have used the fact that $\Delta_{\mathbf{k}} \equiv \Delta$ is independent of $\mathbf{k}$ within the regime of interest ($|\mathbf{k}| \leqslant \Lambda$). Although not shown, the Hartree-Fock mean-field energies [Eq. (34)] are negligible behaving as finite-range effects which decrease relative to $E_{\rm n}$ as powers of $nr_{\rm vdW}^3$. Such finite-range effects are responsible for the long-time differences between the population dynamics seen in Fig. 1(d). By $nr_{\rm vdW}^3 \approx 10^{-7}$, finite-range contributions to the population dynamics are negligible as the time-dependence is set purely by the Fermi scales characteristic of the universal regime. We compare this with the range of densities $10^{-7} \lesssim nr_{\rm vdW}^3 \lesssim 10^{-9}$ studied experimentally in Refs. [26,27] for quenched unitary Bose gases in a uniform system.

The pairing field and instantaneous chemical potential are also initially nonuniversal, depending on finite-range physics as $\Delta(t = 0^+) = \mu(t = 0^+) = gn$. However, these energies quickly evolve toward the Fermi scale and approach the universal steady state $\mu(t) \approx \Delta \approx -0.5E_{\rm n}$. We understand the universality of the μ and Δ steady states from their evolution

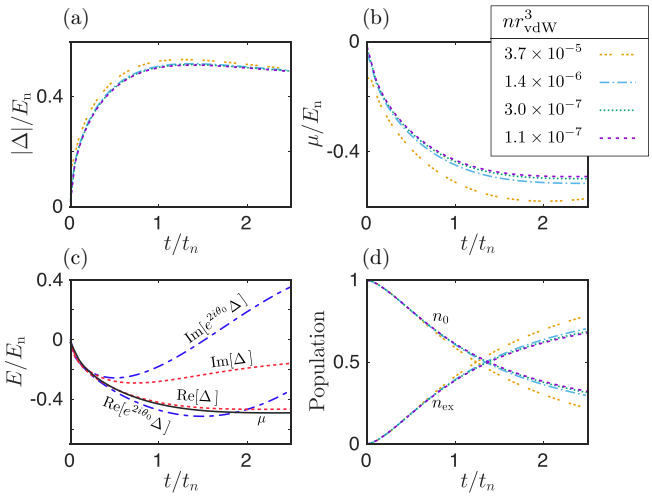

FIG. 1. Dynamics of (a)–(c) energy scales and (d) populations for different values of the van der Waals diluteness parameter within the doublet model. The asymptotic values of the pairing field and phase derivative are roughly equal $\Delta \approx \mu \approx -0.5E_{\rm n}$, where the development of the real part and decay of the imaginary part of the pairing field in the laboratory ($\Delta \exp 2i\theta_0$) and condensate (Δ) frames are shown in (c) for density $nr_{\rm vdW}^3 = 1.1 \times 10^{-7}$.

with the two-body T matrix in Eqs. (52) and (56), which is dominated by the unitarity limit of the s-wave partial cross section on resonance [48]. Importantly, the reality of Δ at long times [68] is due to working in the frame of the condensate as shown in Fig. 1(c). In the laboratory-frame description of this steady state, the pairing field rotates as $\sim \exp(-2i\mu t/\hbar)$ characteristic of the behavior at true equilibrium. We understand the approximate equality of μ and Δ from the rapid growth of pairing correlations, which leads to dominance of the c-cumulant contributions in Eqs. (35) and (36) (see also Appendix B) such that $\mathrm{Re}\,\Delta \approx (g/V)\sum_{\mathbf{q}} \mathrm{Re}\, c_{\mathbf{q}} \approx \mu$. Even though these energies approach a steady state, other observables in the system remain far from equilibrium as we now discuss. In Fig. 2(a), the doublet model results for $n_{\mathbf{k}}$ are compared to the relevant experimental results [70] of Ref. [27]. This comparison is not made in the grey shaded region $k < 2\mu m^{-1} \approx 0.3k_{\rm n}$ where the experimental results are not quantitatively reliable due to initial cloud size and non-infinite time of flight [27]. Qualitatively, it is clear that the nodal pattern of the doublet model results is absent from the experimental data. To quantify these results, we follow Ref. [27] and fit the initial growth of $k_{\rm n}^3 n_{\mathbf{k}}^{(\rm expt)} = 3n_{\mathbf{k}}/4\pi$ for fixed k shown in Fig. 2(b) to a sigmoid $f(t) = a + b/(\exp(-c(t+d)) + 1)$, obtaining plateau value $\bar{n}_{\mathbf{k}} = a + b$ and halfway time $\tau_{\mathbf{k}}$ defined as $\bar{n}_{\mathbf{k}} = 2n_{\mathbf{k}}(\tau_{\mathbf{k}})$, finding generally good agreement [71], consistent with Refs. [34,35], as shown in Fig. 3.

1. Prethermal state

The equilibration of many-body observables in a quenched system while the microscopic degrees of freedom remain strongly out of equilibrium is characteristic of prethermalization [31]. To describe this stage of the doublet model in the universal limit ($nr_{\rm vdW}^3 \to 0$), we solve the doublet model using

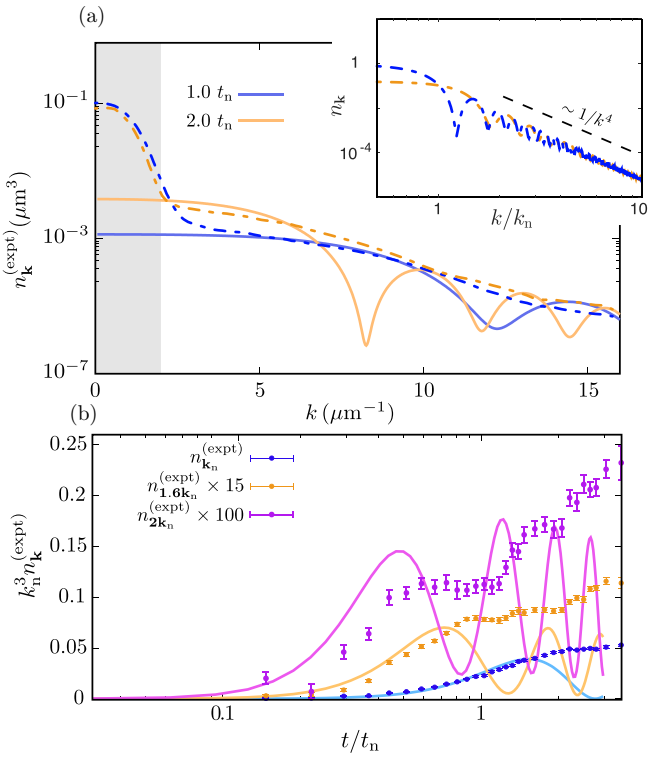

FIG. 2. Dynamics of the momentum distribution for $k_n = 6.7\mu m^{-1}$ with $t_n = 27\mu s$. We note that due to different normalizations, the experimental momentum distribution is related as $k_n^3 n_k^{(expt)} = 3n_k/4\pi$. The results of the doublet model simulation (solid lines) are compared against the experimental findings of Refs. [27,69] (dashed-dotted lines connecting ~200 raw data points each following the presentation in those works) at times $t = t_n$ (blue) and $t = 2t_n$ (orange). Experimental results in the shaded region are not quantitatively reliable (see the Methods section of Ref. [27]). The inset shows the $1/k^4$ power-law behavior of n_k at large-k. (b) Time dependence of the momentum distribution for at fixed k, comparing the results of the doublet model (solid lines) with the experimental data points of Refs. [27,69]. Each line has been multiplied by a numerical factor to increase visibility.

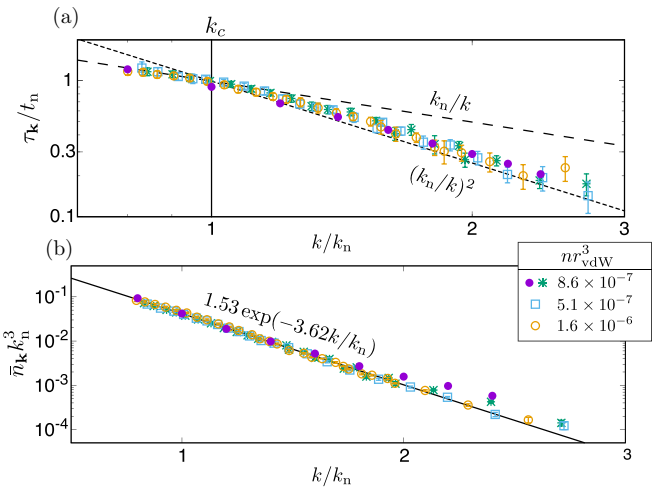

FIG. 3. (a) The momentum dependent half-way time τ_k (a) and the plateau value $\bar{n}_k$ (b) for three different densities considered in Refs. [27,69] compared against the results of the doublet model simulation (purple filled circles). In (a), the asymptotic behaviors $t_k = k_n/k$ and $t_k = (k_n/k)^2$ for the characteristic prethermal timescale t_k found in Sec. IVA1 are indicated by the dashed and dotted lines, respectively. The two asymptotes cross at $k_c = 2mc_{pth}/\hbar = \sqrt{2}/\xi_{pth} \approx k_n$ (vertical solid). In (b), we compare against the decaying exponential $1.53\exp(-3.62k/k_n)$ found experimentally, indicated by the solid line.

the asymptotic values for Δ and μ shown in Figs. 1(a) and 1(b) while the doublets n_k and c_k remain periodic in time [72],

$$n_k(t) = n_k(t_0) + \frac{\Delta \mathrm{Re}\,\alpha_k(t_0)}{2\omega_k^2}[1 - \cos(2\omega_k(t - t_0))] - \frac{\Delta \mathrm{Im}\,\alpha_k(t_0)}{2\xi_k\omega_k}\sin(2\omega_k(t - t_0)), \quad (61)$$

$$|c_k|^2 = n_k(1 + n_k), \quad (62)$$

in agreement with Ref. [34] [see in particular Eq. (S32) therein]. The eigenfrequency of these oscillations matches the HFB spectrum [73]

$$\omega_k = \sqrt{\xi_k^2 - \Delta^2}, \quad (63)$$

(with $\xi_k = \epsilon_k - \mu$ in the limit $nr_{vdW}^3 \to 0$ when $gn \ll \mu$) and the energy $\alpha_k(t_0) = \Delta[1 + 2n_k(t_0)] + 2\xi_k c_k(t_0)$ encodes the initial condition at t_0 (with $t > t_0 \gg t_n$). We note that $\alpha_k = 0$ gives the HFB ground state [74].

In the dilute limit where the van der Waals diluteness parameter nr_{vdW}^3 tends toward 0, the mean-field energy gn/E_n also vanishes relative to the Fermi energy (see Sec. III D) while Δ/E_n remains finite. According to Ref. [73], $\mu = gn + \Delta$, which implies $\mu = \Delta$ in the dilute strong-interacting limit. This matches the long-time, steady-state dynamics shown in Fig. 1. Remarkably, this condition $\mu = \Delta$ produces a *gapless* excitation spectrum ($\omega_0 = 0$), and the elementary excitations follow a Bogoliubov dispersion law $\omega_k = \sqrt{\epsilon_k(\epsilon_k + 2|\mu|)}$. We therefore find long-wavelength phonons with energy $\hbar ck$ and sound velocity $c_{pth} = \sqrt{|\mu|/m} \simeq 0.5\hbar k_n/m$ in the unitary regime. The smooth crossover to the particle-regime occurs for $\epsilon_k \sim mc_{pth}^2 \simeq 0.5E_n$, which allows us to define a characteristic healing length [1] in the prethermal state ($t \gg t_n$), $k = 1/\xi_{pth}$, such that $k_n\xi_{pth} \simeq \sqrt{2}$. This is to be contrasted against the usual Bogoliubov dispersion law at weak interactions $\omega_k^0 = \sqrt{\epsilon_k(\epsilon_k + 2U_0 n)}$ with $U_0 = 4\pi\hbar^2 a/m$, discussed in Sec. II A, and $a \gtrsim 0$ [1]. The dispersion laws ω_k and ω_k^0 are connected by replacing the usual mean-field energy $U_0 n$ by $E_n/2$, i.e. through a mapping of the form $a \to 1/k_n$. In Ref. [75], $U_0 n$ was replaced *ad hoc* by $4E_n/3\pi$, by assuming a universal Bogoliubov excitation spectrum. In the present paper, this replacement is not assumed *a priori*, rather a universal Bogoliubov spectrum *emerges* within the prethermal steady state at strong interactions. In a quasistationary picture, the mapping of quantities between vacuum and Fermi scales occurs smoothly as a result of the interplay between quantum depletion and few-body processes in the system [44].

From the inverse of the excitation energy, we obtain the characteristic timescale $t_k = \hbar/\omega_k$, behaving asymptotically as $t_k/t_n = k_n/k$ for $\xi_{pth}k \ll 1$ and $t_k/t_n = (k_n/k)^2$ for $\xi_{pth}k \gg 1$. In Fig. 3(a), these scalings (dashed and dotted lines) are

compared directly against the numerical and experimental results (symbols) for the half-way times $\tau_{\mathbf{k}}$ and are in excellent quantitative agreement without adjustment. This comparison assumes that the system has entered the prethermal stage on a timescale comparable to the range of $\tau_{\mathbf{k}}$ considered in Fig. 3(a). We address this assumption later in this section by defining a "prethermalization time" $t_{\rm pth}$ from the dynamics of the kinetic temperature following Ref. [31]. Qualitatively, the smooth crossover between sound and free-particle regimes takes place when $k \sim \hbar/\xi_{\rm pth}$, which is of order $O(k_{\rm n})$ consistent with the experimental findings of Ref. [27].

B. Dynamics of the two-body contact

Whereas the decaying exponential in Fig. 3(a) describes the full range of experimental data, the profile of $n_{\mathbf{k}}$ in the doublet model simulation transitions to a $1/k^4$ power-law tail, as can be seen in the inset of Fig. 2(a). We discuss this power-law behavior in the doublet model presently. In an ultracold quantum gases, typical momentum scales ($k_{\rm n}$, $\lambda_{\rm dB}^{-1}$, etc.) are such that $k/\Lambda \ll 1$, where Λ corresponds to the inverse range of the potential. In this regime, when two bosons separated by a distance $r = |\mathbf{r}_1 - \mathbf{r}_2|$ come together such that $\Lambda^{-1} \ll r \ll \{n^{-1/3}, |a|, \lambda_{\rm dB}\}$, their relative wave function is proportional to $\phi(r) = (1 - a/r)$, and the many-body wave function $|\Psi\rangle$ (normalized as $\langle\Psi|\Psi\rangle = N$) takes the form

$$\Psi(\mathbf{r}_1, \mathbf{r}_2, \ldots, \mathbf{r}_{\rm N}) \approx \phi(r)\mathcal{A}(\mathbf{c}_{12}, \mathbf{r}_3 \ldots, \mathbf{r}_{\rm N}), \qquad (64)$$

with center-of-mass coordinate $\mathbf{c}_{12} = (\mathbf{r_1} + \mathbf{r}_2)/2$. This microscopic behavior of the many-body wave function can be used to derive a set of important relationships between system properties, revolving around the extensive quantity $C_2 \underset{k\to\infty}{\equiv} Vk^4 n_{\mathbf{k}}$ known as the two-body contact that measures the probability for pairs of atoms to be close together [77–81]. The intensive counterpart $\mathcal{C}_2$ is the two-body contact density related to the (extensive) two-body contact as $V\mathcal{C}_2 = C_2$. The two-body contact is also related to the total interaction energy $U = \langle\hat{H}_{\rm int}\rangle$ as $C_2 = 2m^2gU/\hbar^4$, where $\hat{H}_{\rm int}$ is the interaction part of the many-body Hamiltonian [Eq. (2)]. Although these relations were derived for equilibrium states, they give consistent results for the dynamical two-body contact $\mathcal{C}_2(t)$ within the doublet model shown in Fig. 4(a). Additionally, these findings are consistent with previous studies, namely the universal early-time growth $n^{-4/3}\mathcal{C}_2(t) = 128\pi t/(6\pi^2)^{2/3}t_{\rm n}$ and asymptotic value $n^{-4/3}\mathcal{C}_2(t) \approx 12$ found in Refs. [33,46].

Although we have found consistent results for the dynamical two-body contact by blindly applying equilibrium relations within the doublet model, counterexamples from quenches in one-dimension [82] highlight that care should be taken when generalizing these relations to nonequilibrium scenarios. Therefore, we revisit the assumptions needed to derive the equilibrium contact relations. The simple form of the microscopic two-body wave function $\phi(r)$ [Eq. (64)] holds locally, regardless of whether the many-body system is in equilibrium or not, and one can define then the dynamical two-body contact $\mathcal{C}_2(t)$ density by integrating over the coordinates of the two-body regular part, $\mathcal{A}$, of the many-body wave function in Eq. (64) to obtain

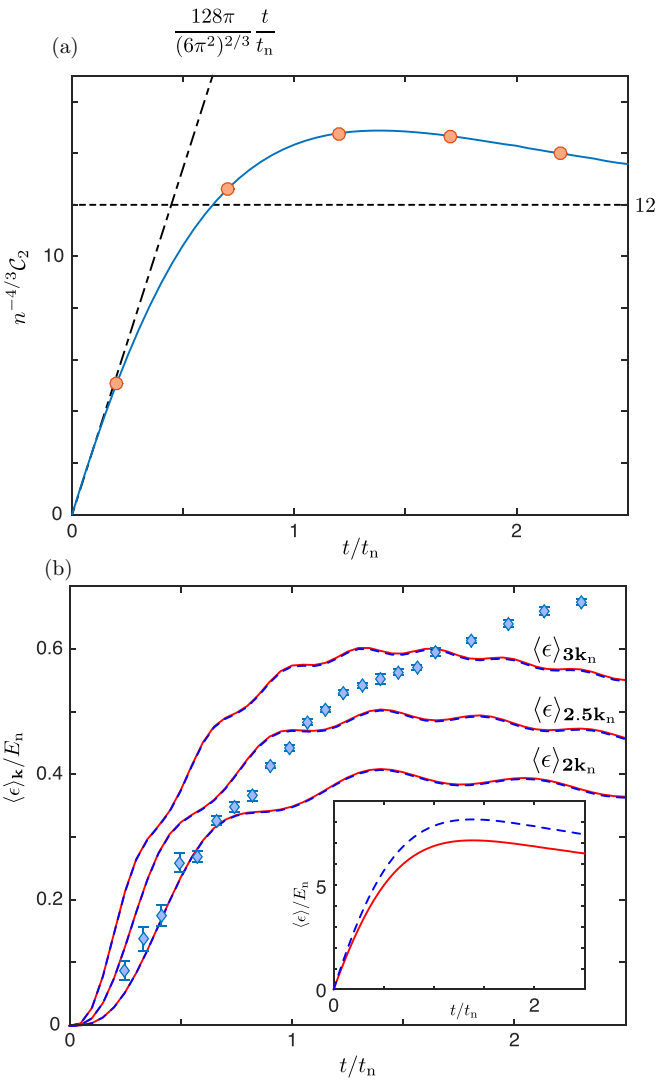

FIG. 4. (a) Universal two-body contact dynamics obtained via the k^{-4} power-law tail of $n_{\mathbf{k}}$ (solid blue) and from the interaction energy (circles) for $nr_{\rm vdW}^3 = 7.2 \times 10^{-8}$. We also compare with the universal early-time growth rate (dash-dotted) obtained in Ref. [46] and the asymptotic result (dotted) obtained in Ref. [33]. (b) Universal dynamics of the restricted kinetic energy per particle $\langle\epsilon\rangle_{\mathbf{k}=\{\mathbf{2k_n},\mathbf{2.5k_n},\mathbf{3k_n}\}}$ for $nr_{\rm vdW}^3 = 7.2 \times 10^{-8}$ (dashed blue) and $nr_{\rm vdW}^3 = 1.1 \times 10^{-7}$ (solid red) compared against the experimental data of Refs. [26,76] (blue diamonds). Inset: Nonuniversal dynamics of the full kinetic energy per particle $\langle\epsilon\rangle$ as predicted in the doublet model.

$$g^{(2)}(\mathbf{r}, t) \equiv \frac{\langle\hat{\psi}^\dagger(\mathbf{r})\hat{\psi}^\dagger(\mathbf{0})\hat{\psi}(\mathbf{0})\hat{\psi}(\mathbf{r})\rangle(t)}{n^2}, \qquad (65)$$

$$\underset{\mathbf{r}\to 0}{=} \frac{\mathcal{C}_2(t)}{16\pi^2 n^2 r^2} \qquad (66)$$

for the functional form of the pair correlation function in a uniform system. The interaction energy relation results then from balancing the divergence of $g^{(2)}(\mathbf{0}, t)$ by powers of the potential $V(\mathbf{0})$ and neglecting subleading finite-range corrections decaying as powers of $1/\Lambda$ [80,81,83]. To generalize

the k^{-4} power-law-tail equilibrium definition, in addition, one must consider the Fourier transform,

$$n_{\mathbf{k}}(t) = \frac{1}{V}\sum_i \int \left(\prod_{l\neq i} d^3 r_l\right) \times \left| \int d^3 r_i e^{-i\mathbf{k}\cdot\mathbf{r}_i} \Psi(\mathbf{r}_1, \mathbf{r}_2, \ldots, r_N, t)\right|^2, \quad (67)$$

where the sums are taken over all particles. When the short-distance divergent behavior in Eq. (64) dominates the large-k limit of Eq. (67), one obtains the power-law behavior $n_{\mathbf{k}} \propto 1/k^4$ and the equilibrium definition follows [80,83,84]. Although this argument holds in equilibrium, it is not guaranteed in a dynamical system due to the possibility of energetic nonlocal physics as shown in one dimension [82]. We note that this caveat also anticipates the difficulties encountered within the triplet model in the next section (Sec. V.)

C. Kinetic temperature

The two-body contact provides valuable insight into the dynamics of the interaction energy per particle $\langle u\rangle = U/N$ and the kinetic energy per particle $\langle\epsilon\rangle = \langle\hat{H}_{\rm kin}\rangle/N$, where $\hat{H}_{\rm kin}$ is the kinetic part of the many-body Hamiltonian [Eq. (2)]. Within the sudden approximation, the quench generates correlation waves out to arbitrarily large energies [82]. Finite-range effects cure this ultraviolet divergence by providing a natural short-range cutoff at the scale of Λ, calibrated to the scale of the van der Waals energy $E_{\rm vdW} = \hbar^2/mr_{\rm vdW}^2$ in our model (see Appendix A). Although the total energy per particle in the doublet model simulation $\langle e_{\rm tot}\rangle = \langle u\rangle + \langle\epsilon\rangle$ is negligible ($\langle e_{\rm tot}\rangle/E_{\rm n} \propto n^{1/3} r_{\rm vdW}$), both the interaction energy per particle $\langle u\rangle$ and kinetic energy per particle $\langle\epsilon\rangle$ diverge. This divergence can be understood by collecting powers of Λ in the contact relation $\langle u(t)\rangle = (\hbar^4/2gnm^2)\mathcal{C}_2(t)$. Whereas $\mathcal{C}_2$ scales universally with the density, the bare interaction scales as $g \propto 1/\Lambda$, and therefore $\langle u(t)\rangle$ scales linearly with Λ. In our model, this translates into a finite-range effect such that $\langle u(t)\rangle \propto r_{\rm vdW}^{-1}$. This behaviors applies analogously to $\langle\epsilon\rangle$ due to energy conservation $\langle\epsilon\rangle/E_{\rm n} = -\langle u\rangle/E_{\rm n} + O(n^{1/3} r_{\rm vdW})$. This explains the early-time linear growth, late-time asymptotics, and divergence with $r_{\rm vdW}^{-1}$ of $\langle\epsilon\rangle$ shown in the inset of Fig. 4(b).

The rapid equipartion of kinetic and potential energies with $\langle\epsilon\rangle/\langle u\rangle \approx -1$ provides the basis for discussing, in the far-from-equilibrium many-body system, a kinetic temperature proportional to $\langle\epsilon(t)\rangle$ [31]. In contrast to mode-specific quantities, $\langle\epsilon(t)\rangle$ provides a mode-averaged measure of the rate at which the system prethermalizes. Therefore, following in the spirit of the original treatment in Ref. [31], we define a prethermal time $t_{\rm tph}$ from the criterion $|\langle\epsilon(t_{\rm pth})\rangle - \langle\epsilon\rangle_{\rm as.}|/\langle\epsilon\rangle_{\rm as.} \lesssim 0.2$ for $t > t_{\rm pth}$ using the asymptotic estimate of $\mathcal{C}_2(t)$ [33] to obtain $\langle\epsilon\rangle_{\rm as.} \approx (-\hbar^4/gm^2)6n^{1/3}$. We find $t_{\rm pth} \simeq 0.4 - 0.5$, which is consistent with the saturation timescale estimate in Ref. [33] and the equilibration time of the largest momenta modes measured in Ref. [24]. Additionally, $\tau_{\mathbf{k}} > t_{\rm pth}$, for momenta in the crossover between sound and free-particle regimes shown in Fig. 3(a), clarifying the assumptions made in Sec. IVA1.

How can the dependence of $\langle\epsilon\rangle$ on the nonuniversal short-range scales be reconciled with the universal dynamics of the kinetic energy per particle observed in Ref. [26]? We understand this discrepancy then from the comparatively limited range of experimentally accessible momenta (cf. Figs. 2 and 3). To compare with experiment, we therefore define the *restricted* kinetic energy per particle $\langle\epsilon\rangle_{\mathbf{k}} = \int_0^k d^3k' n_{\mathbf{k}'}\epsilon_{\mathbf{k}'}/n$ and compare with the experiment as shown in Fig. 4(b). Here the doublet model simulation results are roughly consistent with the universal evolution of $\langle\epsilon\rangle_{\mathbf{2k}_{\rm n}}$ for early times $t \lesssim t_{\rm n}$. The oscillations of $\langle\epsilon\rangle_{\mathbf{k}}$ are due to the periodicities of the underlying $n_{\mathbf{k}}$ as discussed in Sec. IVA1. As the integration includes a larger range of modes, the oscillations dephase and are absent in $\langle\epsilon\rangle$. We note that the time range studied is, however, still less than the time $t \sim 4t_{\rm n}$ where the kinetic temperature of the experimental data begins to follow the power law $\langle\epsilon\rangle \propto t^{2/13}$ for recombinative heating in the thermal regime [85]. In the intermediate time $1 \lesssim t/t_{\rm n} \lesssim 4$, however, the effects of heating and lossless correlation dynamics are difficult to differentiate, requiring a theoretical investigation of each contribution individually.

D. Summary

In this section, the quenched unitary Bose gas was studied within the doublet model. This theory describes the universal prethermal state that rapidly forms as the condensate is depleted by pairing excitations. The signature of this prethermal state is the establishment of steady-state values for μ and Δ even while the momentum distribution dynamics remain far from equilibrium. Within this steady-state, one finds the emergence of a universal Bogoliubov dispersion law, which quantitively matches the prethermal timescales observed experimentally. This behavior at strong interactions is in stark contrast to quenches at weak interactions where the Bogoliubov dispersion law can be assumed [32]. Finding disagreement with the exponential tail of $n_{\mathbf{k}}$ found experimentally, we analyze the origin of the $1/k^4$ power-law tail observed in the doublet model by studying the dynamical two-body contact. In turn, the universal dynamics of the two-body contact were used to shed light on the nonuniversal growth of the kinetic temperature of the gas, which diverges for quenches treated within the sudden approximation. To connect with experiment, we consider the kinetic temperature one would obtain with access to only a restricted range of momentum modes, finding agreement at early times. In the next section (Sec. V), we go beyond the doublet model and also retain the triplet cumulants to understand the impact of three-body correlations on the prethermal state and to search for nonuniversal signatures of the Efimov effect.

V. TRIPLET MODEL OF THE QUENCHED UNITARY BOSE GAS

In this section, we study the quenched unitary Bose gas within the triplet model by neglecting all fourth-order cumulants in Sec. III such that only $n_{\mathbf{k}}$, $c_{\mathbf{k}}$, $M_{\mathbf{k},\mathbf{q}}$, and $R_{\mathbf{k},\mathbf{q}}$ remain. For consistency, we follow the same quench sequence as in Sec. IV, starting from an initially pure condensate. As the gas evolves in the unitary regime, the condensate is depleted

by both pairwise and three-body effects. However, the triplet model suffers from a violation of energy conservation as discussed in Sec. III B. This violation leads to unphysical behavior of the triplet model at long times (see Appendix B). We therefore limit our analysis to times $t \lesssim t_{\rm n}$ before these effects become significant. In this section, we focus on (i) departures from the prethermal state found in Sec. IVA1 due to the ergodic dynamics introduced by $\hat{H}_3$ and $\hat{H}_4^{\rm eff}$ and (ii) signatures of the Efimov effect in the system, motivated by few-body studies [28–30], the discussion in Sec. III D, and the experimental observation of a macroscopic population of Efimov trimers in Ref. [25].

Due to the limitations of the triplet model to times $t \lesssim t_{\rm n}$, we simulate only the dominant parts of the drive terms $\mathcal{M}^{H_4}_{\mathbf{k},\mathbf{q}}$ and $\mathcal{R}^{H_4}_{\mathbf{k},\mathbf{q}}$ [Eqs. (43) and (44)] so

$$\mathcal{M}^{H_4}_{\alpha,\beta} \approx -\frac{1}{V}\mathcal{S}_{\{\alpha,\beta\}}\left[\sum_{\mathbf{q}} V_{\mathbf{q}} \frac{1+n_\alpha+n_\beta}{2} M_{\gamma,\alpha-\mathbf{q}}\right], \tag{68}$$

$$\mathcal{R}^{H_4}_{\alpha,\beta} \approx \frac{1}{V}\mathcal{S}_{\{\alpha,\beta,\gamma'\}}\left[\sum_{\mathbf{q}} \frac{V_{\mathbf{q}}}{2}(1+n_\alpha+n_\beta) R_{\alpha-\mathbf{q},-\gamma'}\right]. \tag{69}$$

This contains the vacuum contribution (the 1 in $1+n+n$), which dominates at short times and ensures that few-body interactions at unitarity (see Sec. III D) are correctly described. Additionally, due to the increased computation resources required to simulating the triplet model, the results in this section are limited to densities $nr^3_{\rm vdW} \leqslant 6.9\times10^{-6}$, which includes a portion of the density range studied in Ref. [25] but is more dense than the range considered in Refs. [24,26,27]. We refer the interested reader to Appendix B3, where technical details related to convergence of the triplet model simulations and the computational hardware used are discussed.

A. Energy and number dynamics

We begin by revisiting the time dependence of the characteristic energies Δ and $\mu(t)$ in the triplet model as a function of the van der Waals diluteness parameter $nr^3_{\rm vdW}$ shown in Figs. 5(a)–5(c). Compared to the doublet model, $\mu(t)$ now has an additional contribution from the triplet M-cumulant [see Eq. (36)], whereas the expression for Δ [Eq. (35)] remains unchanged. This has the effect of introducing oscillations into the dynamics of $\mu(t)$, which can be see in Figs. 5(b) and 5(c). These oscillations, which are absent in the doublet model results, black dashed lines in Fig. 5, are signatures of Efimov states. The oscillation frequency is set by the three-body parameter $\kappa_* r_{\rm vdW} = 0.211$ (see Appendix A) and is therefore non-universal (density independent). This behavior is in contrast with the dynamics of Δ shown in Fig 5(a), with oscillations that are comparatively less visible and therefore weakly dependent on κ_*. By $t \sim t_{\rm n}$, we see that Δ seems to be converging to $\Delta \sim -0.4E_{\rm n}$ with decreasing imaginary component visible in Fig 5(c). The population dynamics shown in Fig. 5(d) also depend weakly on κ_*, and we see that the addition of three-body effects lead to more rapid depletion of the condensate than in the doublet model [compare with Fig. 1(d)]. Although not shown, the Hartree-Fock mean-field energies remain negligible as $nr^3_{\rm vdW}$ is decreased, which follows from the general conclusions in Sec. III D. As the

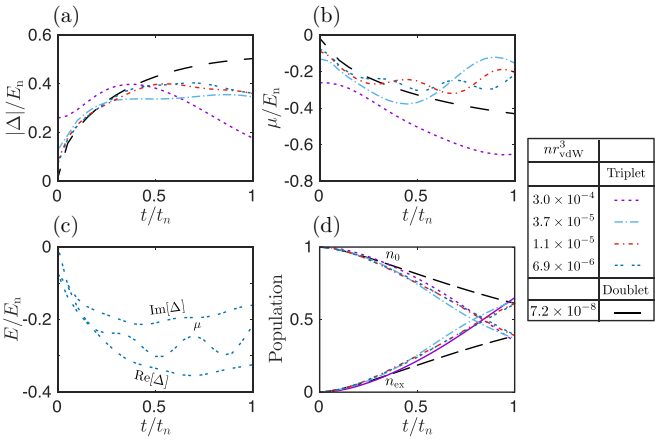

FIG. 5. Dynamics of (a)–(c) energy scales and (d) populations for different values of the van der Waals diluteness parameter within the triplet model. We compare with the doublet model results for density $nr^3_{\rm vdW} = 7.2\times10^{-8}$ (black dashed) in this section, which is sufficiently dilute to be universal. (c) The dynamics of the instantaneous chemical potential $\mu(t)$ and the real and imaginary parts of the pairing field shown for density $nr^3_{\rm vdW} = 6.9\times10^{-6}$.

energies Δ and μ begin to display steady-state and periodic behaviors, the dynamics of $n_{\mathbf{k}}$ remain far from equilibrium. The triplet and doublet model dynamics of $n_{\mathbf{k}}$ are shown in Fig. 6. By $t = 0.5t_{\rm n}$, we already see a departure in the large momentum behavior of $n_{\mathbf{k}}$ from the $1/k^4$ power-law tail toward a decaying exponential. The formation of a decaying exponential tail in $n_{\mathbf{k}}$ is a robust feature of the triplet model and can be found even at much later times (even though positivity of $n_{\mathbf{k}}$ becomes violated at low momenta due to violation of energy conservation.) Although the amplitude of the exponential tail grows in time, the decay rate remains roughly constant as $n_{\mathbf{k}} \propto \exp(-0.25k/k_{\rm n})$ for $nr^3_{\rm vdW} = 7.0\times10^{-6}$,

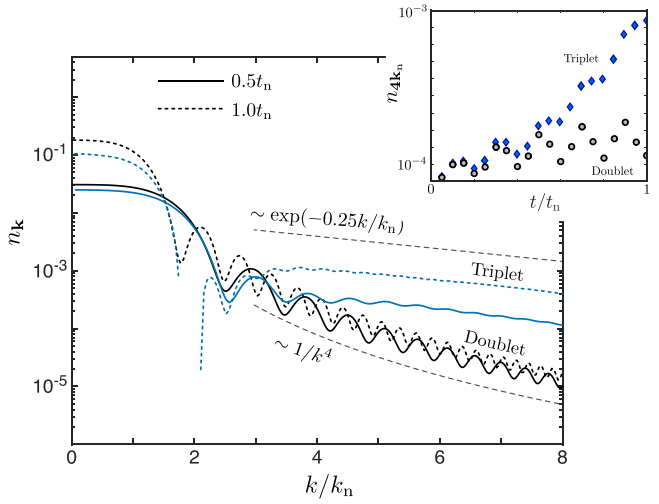

FIG. 6. Evolution of the single-particle momentum distribution within the triplet model at density $nr^3_{\rm vdW} = 6.9\times10^{-6}$ (blue) and the universal doublet model (black). Inset: Dynamics of $n_{\mathbf{k}}$ at fixed $k = 4k_{\rm n}$ from triplet and doublet models illustrating the transition out of the prethermal state.

which is more gradual than experimentally observed decay $n_{\mathbf{k}} \propto \exp(-3.62k/k_{\mathrm{n}})$ [27]. Although not shown, similar exponential decay of $n_{\mathbf{k}}$ at large momentum can be found over the full range of densities considered in this section. As noted in Ref. [27], the development of a decaying exponential tail at large momenta is not consistent with the power-law tail predictions from local short-range physics. Ultimately, due to its absence in the doublet model, the decaying exponential is necessarily due to three-body processes.

1. Departure from the prethermal state

Such deviations from the integrable doublet model dynamics also signal the departure from the prethermal state. Physically, this is expected due to the ergodic dynamics introduced by $\hat{H}_3$ and $\hat{H}_4^{\mathrm{eff}}$, which take the system toward true thermalization. For quenches in the weakly interacting regime, the timescales between the prethermal and thermal stages are separated by orders of magnitude [32] as nonintegrable Beliaev-Landau scatterings drive the system toward full thermalization. On resonance, this picture of distinct on-shell quasiparticle scatterings begins to breakdown, and one expects generically that all rates scale with the Fermi time so that distinct stages in the evolution of the gas may not be well-separated. Indeed, we see from Fig. 6 that the departure from the integrable doublet model dynamics occurs at a momentum-dependent rate evidenced by the widening gap between power-law and exponential tails at large momentum. This departure from the prethermal dynamics is shown explicitly in the inset of Fig. 6 in the dynamics of $n_{4k_{\mathrm{n}}}$ where the enhanced growth and damped oscillations in the triplet model are clearly visible at later times. We note that because the triplet model dynamics inherently violate energy conservation, the breaking of integrability removes the system from the initial phase-space manifold, which muddies the physical connection between the long-time dynamics and thermalization.

As the system shifts away from the prethermal state, the gradual decay in the occupation of large momentum modes leads to an increase in the average kinetic energy per particle $\langle\epsilon\rangle$ relative to the doublet model as shown in Fig. 7. To understand which modes are responsible for this growth, we examine in Fig. 7 how the dynamics of the restricted kinetic-energy per particle $\langle\epsilon\rangle_{\mathbf{k}}$ change as the large momentum modes transition into an exponentially decaying tail. First, we observe that the momentum-dependent departure of $n_{\mathbf{k}}$ from the prethermal doublet dynamics is also mirrored in $\langle\epsilon\rangle_{\mathbf{k}}$. Second, the kinetic energy per particle for modes $k \lesssim 0.3k_{\mathrm{n}}$ decreases relative to the doublet model dynamics, which illustrates the large pileup of kinetic energy in the decaying exponential tail and draining of kinetic energy from the low momentum modes. This accumulation of kinetic energy in the exponential tail is a signature of imbalanced three-body kinetics within the triplet model. Specifically, the three-body processes in the kinetic equation [Eq. (37)] require contributions from the quadruplet in order to satisfy the condition of detailed balance, which will be demonstrated in a forthcoming publication [86]. Because the total energy is not conserved, the rapid equipartition of energy observed in the doublet model (see Sec. IV C) is not observed distinctly in the triplet model, such that a kinetic

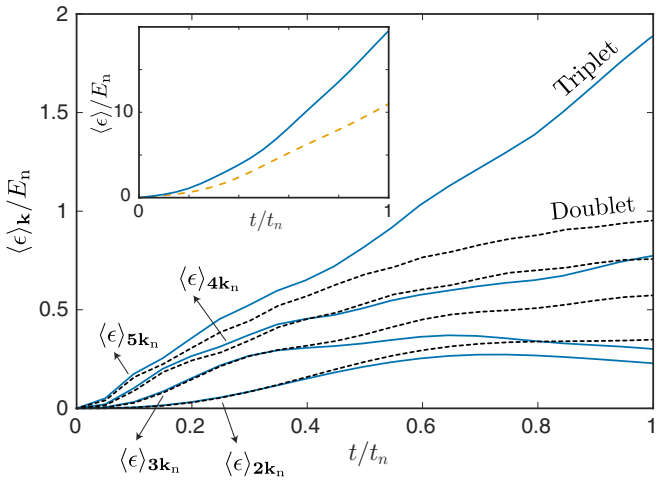

FIG. 7. Dynamics of the restricted kinetic energy per particle $\langle\epsilon\rangle_{\mathbf{k}=\{2\mathbf{k}_{\mathrm{n}},3\mathbf{k}_{\mathrm{n}},4\mathbf{k}_{\mathrm{n}},5\mathbf{k}_{\mathrm{n}}\}}$ for the triplet model with $nr_{\mathrm{vdW}}^3 = 6.9 \times 10^{-6}$ (solid blue) and the universal doublet model (dotted black). Inset: Nonuniversal dynamics of the full kinetic energy per particle $\langle\epsilon\rangle$ within the triplet model for $nr_{\mathrm{vdW}}^3 = 6.9 \times 10^{-6}$ (solid blue) and $nr_{\mathrm{vdW}}^3 = 1.9 \times 10^{-5}$ (dashed orange).

temperature cannot be so clearly defined as before. Here, the growth of the total kinetic energy results instead in an effective heating of the system. Due to this violation, the dynamics of $\langle\epsilon\rangle$ cannot be connected to the dynamical two-body contact $\mathcal{C}_2(t)$ as was done in Sec. IV, and we must turn to other methods as we discuss now.

B. Dynamics of the contacts

In addition to having pairs of correlated bosons close together, in the triplet model it is also possible to have triples of bosons clustered together, experiencing the attractive $1/R^2$ effective three-body potential in the Efimov channel. When three bosons in a configuration parameterized by hyperradius $R = \sqrt{(r^2+\rho^2)/2}$ and hyperangles $\Omega = \{\hat{\boldsymbol{\rho}}, \hat{\mathbf{r}}, \alpha = \arctan(r/\rho)\}$, with Jacobi coordinates $\mathbf{r} = \mathbf{r_1} - \mathbf{r_2}$ and $\boldsymbol{\rho} = (2\boldsymbol{r_3} - \boldsymbol{r_1} - \boldsymbol{r_2})/\sqrt{3}$ and spherical angles $\hat{\boldsymbol{\rho}}$ and $\hat{\boldsymbol{r}}$, come together $\Lambda^{-1} \ll R \ll \{n^{-1/3}, |a|, \lambda_{\mathrm{dB}}\})$ their relative wave function is proportional to [80]

$$\Phi(R, \mathbf{\Omega}) = \frac{1}{R^2} \sin\left(s_0 \ln \frac{R}{R_t}\right) \frac{\phi_{is_0}(\mathbf{\Omega})}{\sqrt{\langle\phi_{is_0}|\phi_{is_0}\rangle}}. \tag{70}$$

Here, R_t is related to the three-body parameter κ_* as $R_t = \sqrt{2}\exp(\mathrm{Im}\,\ln[\Gamma(1+is_0)]/s_0)/\kappa_*$ where $\Gamma(x)$ is the Gamma function and $s_0 = 1.006$. The hyperangular function describing s-wave pairwise scatterings is [87] $\phi_{s_0}(\mathbf{\Omega}) = (1 + \hat{P}_{13} + \hat{P}_{23})\varphi_{s_0}(\alpha)/\sin(2\alpha)\sqrt{4\pi}$ with $\varphi_s(\alpha) = \sin(s(\pi/2 - \alpha))$ where $\hat{P}_{ij}$ swaps particles i and j. When this occurs, the many-body wave function $|\Psi\rangle$ takes the form

$$\Psi(\mathbf{r}_1, \mathbf{r}_2, \mathbf{r}_3, \ldots, \mathbf{r}_{\mathrm{N}}) \approx \Phi(R, \mathbf{\Omega})\mathcal{B}(\mathbf{c}_{123}, \mathbf{r}_3 \ldots, \mathbf{r}_{\mathrm{N}}), \tag{71}$$

where $c_{123} = (\mathbf{r}_1 + \mathbf{r}_2 + \mathbf{r}_3)/3$ is the three-body center of mass, and $\mathcal{B}$ is the three-body regular part of the many-body wave function. The microscopic behaviors of the many-body wave function [Eqs. (64) and (71), respectively] can be used to derive a set of important relationships between system

properties extending the two-body contact relations discussed in Sec. IV B to when the Efimov effect arises,

$$V n_{\mathbf{k}} \to \frac{1}{k^4} C_2 + \frac{F(k)}{k^5} C_3, \tag{72}$$

$$\mathcal{C}_2 = \frac{m^2 g^2}{\hbar^4} \langle \hat{d}^\dagger \hat{d} \rangle - \frac{4 m^3 g^3}{\Lambda^2 \hbar^6} \left(H + \frac{J}{\pi} + \frac{J}{2a\Lambda} \right) \langle \hat{t}^\dagger \hat{t} \rangle, \tag{73}$$

$$\mathcal{C}_3 = -\frac{m^2 g^2}{2\hbar^4 \Lambda^2} \left(H' + \frac{J'}{a\Lambda} \right) \langle \hat{t}^\dagger \hat{t} \rangle, \tag{74}$$

where $\hat{d} = \hat{\psi}(\mathbf{0})\hat{\psi}(\mathbf{0})$ and $\hat{t} = \hat{\psi}(\mathbf{0})\hat{\psi}(\mathbf{0})\hat{\psi}(\mathbf{0})$ [80,81]. Here, the probability to measure such Efimovian triples is quantified by the (total) three-body contact C_3 and three-body contact density $\mathcal{C}_3$ related as $V\mathcal{C}_3 = C_3$. The quantities F, H, and J are log-periodic functions of k and Λ, given by

$$F(k) = A \sin(2 s_0 \ln(k/\kappa_*) + 2\phi), \tag{75}$$

$$H(\ln(\Lambda/\Lambda_*)) = h_0 \frac{C - s_0 S}{C + s_0 S}, \tag{76}$$

$$J(\ln(\Lambda/\Lambda_*)) = \frac{j_0 + j_1(2SC) + j_2(C^2 - S^2)}{(C + s_0 S)^2}, \tag{77}$$

where $C = \cos(s_0 \ln(\Lambda/\Lambda_*))$ and $S = \sin(s_0 \ln(\Lambda/\Lambda_*))$ and with universal constants $A = 89.262$, $\phi = -0.669$, $h_0 = 0.879$, $j_0 = -0.148$, $j_1 = -0.892$, $j_2 = -0.087$ and renormalization scale $s_0 \ln(\Lambda_*/\kappa_*) = 0.971 \bmod \pi$. The $'$ notation indicates a partial derivative with respect to $\ln(\Lambda/\Lambda_*)$. The log-periodic dependency in Eqs. (72)–(74) on the discrete scaling $e^{\pi/s_0} \approx 22.7$, reflects the infinite number of Efimov trimers which form at unitarity with binding energies scaling in the zero-range limit as $E_{3b}^{(n)} = -e^{-2n\pi/s_0} \hbar^2 \kappa_*^2/m$ for any integer n. For finite-range potentials, the Efimov trimer spectrum is bounded from below $n \geqslant 0$, and the three-body parameter κ_* sets the wavenumber of the ground Efimov trimer $E_{3b}^{(0)} = -\hbar^2 \kappa_*^2/m$ and, importantly, introduces a nonuniversal, finite length scale [18–20]. For the pairwise potential considered in this paper, the three-body parameter is $\kappa_* r_{\mathrm{vdW}} = 0.211$ (see discussion in Appendix A), which is in fair agreement with the universal result $\kappa_* r_{\mathrm{vdW}} \approx 0.226$ near the broad Feshbach resonances used experimentally [47,88,89].

Although the formal caveats in Sec. IV B were cautionary, Eq. (72) clearly fails when generalized to the triplet model of the quenched unitary Bose gas. It is necessary then to revisit the assumptions underlying Eqs. (72)–(74). Formally, Eqs. (73) and (74) follow directly from the forms of two- and three-body microscopic wave functions $\phi(r)$ and $\Phi(R, \mathbf{\Omega})$, respectively, that both hold locally, regardless of whether the many-body system is in equilibrium or not. One can then define the dynamical three-body contact density by integrating over the three-body regular part, $\mathcal{B}$, of the many-body wave function in Eq. (71) to obtain the relation [80]

$$g^{(3)}(\mathbf{0}, \mathbf{r}, \mathbf{r}', t) \equiv \frac{\langle \hat{\psi}^\dagger(\mathbf{r}) \hat{\psi}^\dagger(\mathbf{r}') \hat{\psi}^\dagger(\mathbf{0}) \hat{\psi}(\mathbf{0}) \hat{\psi}(\mathbf{r}') \hat{\psi}(\mathbf{r}) \rangle(t)}{n^3},$$

$$\underset{R \to 0}{=} |\Phi(R, \mathbf{\Omega})|^2 \frac{8}{n^3 s_0^2 \sqrt{3}} \mathcal{C}_3(t) \tag{78}$$

for the functional form of the triplet correlation function in the $R \to 0$ limit written here specifically for uniform systems.

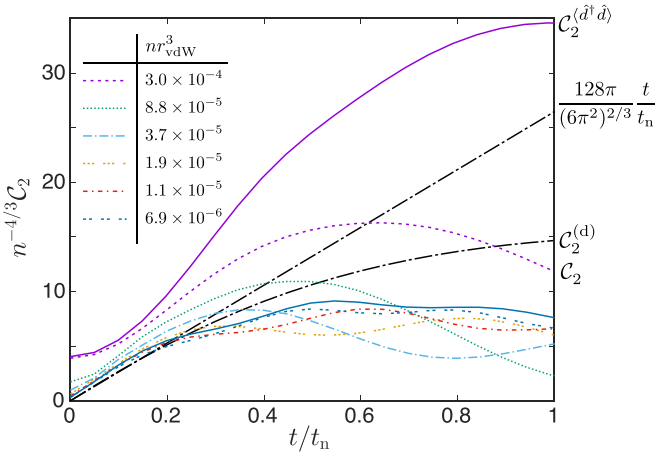

FIG. 8. Dynamics of the two-body contact [Eqs. (73)] over a range of densities and times up to $1.0t_{\mathrm{n}}$. Results for the dimensionless two-body contact density $n^{-4/3}\mathcal{C}_2$ from the triplet model over the range of densities indicated in the key. We also show the two-body contact density $\mathcal{C}_2^{\langle \hat{d}^\dagger \hat{d} \rangle}$ obtained from neglecting the term $\langle \hat{t}^\dagger \hat{t} \rangle$ in Eq. (73). This is shown only for the most and least dense cases as solid curves attached to the corresponding $n^{-4/3}\mathcal{C}_2$ results to illustrate the diminishing of this extra contribution in the zero-range limit. The universal doublet model results $\mathcal{C}_2^{(\mathrm{d})}$ along with the universal early-time growth rate obtained in Ref. [46] are indicated by the black dashed-dotted curves.

To obtain Eq. (72), one must make additional assumptions that the short-distance divergent behaviors Eqs. (64) and (71) dominate the large-k limit of the Fourier transform of the many-body wave function [Eq. (67)]. This clearly no longer holds for the dynamics of $n_{\mathbf{k}}$ in the triplet model, highlighting the nonlocal origin of the decaying exponential. Finally, we note the additional $\langle \hat{t}^\dagger \hat{t} \rangle$ dependence in Eq. (73) absent in the doublet model, following the convention of Ref. [81]. This extra contribution becomes negligible, scaling as $1/\Lambda$ and has been included here for completeness. We now discuss results for the dynamical two and three-body contacts using Eqs. (73) and (74), respectively.

1. $\mathcal{C}_2$ dynamics

In Fig. 8, the numerical results for the dynamical two-body contact in the triplet model are shown over a range of densities and times up to $t = 1.0t_{\mathrm{n}}$. Formally, we note that the cumulant decomposition of the dominant contribution $\langle \hat{d}^\dagger \hat{d} \rangle$ to $\mathcal{C}_2$ is the same as in Sec. IV B with the addition now of the triplet M-cumulant. Here we differentiate between $\mathcal{C}_2^{\langle \hat{d}^\dagger \hat{d} \rangle}(t)$ and $\mathcal{C}_2(t)$ defined without and with the $\langle \hat{t}^\dagger \hat{t} \rangle$ contribution, respectively, in Eq. (73) to demonstrate how this term becomes negligible as nr_{vdW}^3 is decreased. Comparing against the early-time doublet results, we find that linear early-time growth rate is approached as nr_{vdW}^3 is decreased. The early-time dynamics of $\mathcal{C}_2(t)$ are therefore insensitive to the Efimov effect, consistent with Ref. [30]. We note that the nonzero offset $\mathcal{C}_2(0) = g^2 n^2$ is a finite-range effect scaling as $1/\Lambda^2$. By $t \sim 0.2t_{\mathrm{n}}$, the triplet and doublet model results for $\mathcal{C}_2(t)$ begin to depart significantly after a period of universal growth. Echoing the findings of Ref. [30], we interpret this development as the timescale

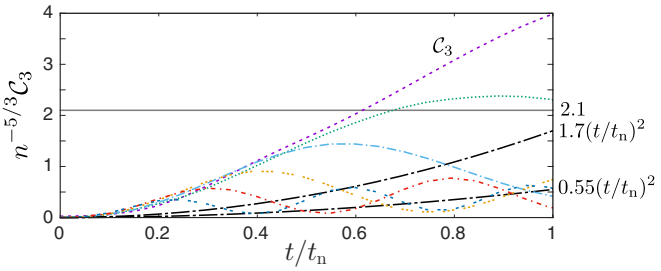

FIG. 9. Dynamics of the three-body contact [Eq. (74)] over a range of densities and times up to $1.0t_n$. Results for the dimensionless three-body contact density $n^{-5/3}\mathcal{C}_3$ (key same as Fig. 8) from the triplet model. For comparison, we show the range of quadratic early-time growths (dashed-dotted) found in Ref. [29]. For scale comparison, we also display the universal fit $n^{-5/3}\mathcal{C}_3 \approx 2.1$ [90] (grey solid) extracted from the experimental results of Ref. [24] under the assumption of a locally equilibrated metastable state.

when clustered pairs become sensitive to the surrounding "few-body medium" consisting of a third boson. This sensitivity leads to the secondary dependence of $\mathcal{C}_2(t)$ on the Efimov effect, as its dynamics display the characteristic nonuniversal beating phenomenon at the frequency of an Efimov trimer. At later times, the probability of finding pairs of atoms close together becomes less likely than in the doublet model. In the triplet model, there is now the competition between forming clustered pairs or triples, which develop more slowly as we find from the analysis of $\mathcal{C}_3(t)$ below.

2. $\mathcal{C}_3$ dynamics

So far, in the analysis of this section, we have assumed that the nonuniversal oscillations found in $\mu(t)$, $\mathcal{C}_2(t)$ and to a lesser extend $\Delta(t)$, which has no explicit dependence on triplet cumulants, are signatures of an Efimov state. Here, we analyze the triplet model results for $\mathcal{C}_3(t)$, which directly measures the probability to measure short-range Efimovian triples as correlations develop in the many-body system. In Fig. 9, the numerical results for the dynamical three-body contact are shown over a range of densities and times up to $t = 1.0t_n$. At all times, the dynamics are density dependent, and the nonuniversal oscillations in time become visible as nr_{vdW}^3 is decreased. To analyze these results, we first motivate why such oscillations should appear distinctly in $\mathcal{C}_3(t)$, then to make the discussion more quantitative, the triplet model results for $\mathcal{C}_3(t)$ are fit first for $t \leqslant 0.25t_n$ to obtain the relevant early-time scalings and then fit at later times $t < 0.5t_n$ to extract the oscillation frequencies, enabling a unambiguous identification of the Efimov state present in the many-body system.

Counting powers of Λ in the cumulant expansions in Eqs. (73) and (74) reveals that the dynamical two- and three-body contacts are dominated by the dynamics of the c and R cumulants, respectively. In Sec. III D, we discussed how the post-quench response of these cumulants [Eqs. (49) and (59)] is determined by the overlap between the few-body spectrum and the driving effect of the lower-order cumulants. For example, away from resonance, the dynamical two-body contact responds at the natural frequency of the universal dimer $-\hbar^2/ma^2$ as studied in Refs. [35,46]. At unitarity, the dimer energy is at threshold, however, the three-body contact can now respond at the frequency of any one of the infinity of three-body bound Efimov trimers. In practice, the Efimov trimer whose size $R_{3b}^{(j)} = \sqrt{2(1+s_0^2)/3}\exp(j\pi/s_0)/\kappa_*$ is comparable to the interparticle spacing $R_{3b}^{(j)} \sim k_n$ has the greatest overlap with the drive of the lower-order cumulants [see Eq. (59)]. Consequently, the infinity of trimers accumulating at threshold play a negligible role in the dynamics of the three-body contact as was found in Refs. [29,30]. For densities in the regime $|E_{3b}^{(j)}| \lesssim E_n$, the jth Efimov state is optimally embedded in the many-body configuration, and the mode-matching $|E_{3b}^{(j)}| \sim E_n$ signals maximally enhanced growth of the dynamical three-body contact at early times as found in Refs. [29,30]. When $|E_{3b}^{(j)}| \gtrsim E_n$, the Fermi and Efimovian timescales are distinct, and the frequency of the jth Efimov state is observable in the early-time dynamics of the three-body contact [29,30]. Finally, when $|E_{3b}^{(j)}| \gg E_n$, there is little overlap between density scales and the jth Efimov state, and therefore all deeply bound Efimov states relative to E_n play a negligible role in the dynamics. This behavior is then repeated over a full log-period (factor $\sim 22.7^3$) in the density.

Whereas $\mathcal{C}_2(t)$ displays a universal linear growth at early times, $\mathcal{C}_3(t)$ was shown to follow a range of gradual, density-dependent quadratic growth rates in Refs. [29,30]. In Fig. 9, we compare the triplet model results against the predictions of these few-body models, noting the absence of inelastic three-body losses in the present paper. To quantify this comparison, we fit the early-time ($t \lesssim 0.25t_n$) triplet model results for $n^{-5/3}\mathcal{C}_3(t)$ to the function $f_1(t) = a_1 t^{a_2}$ and extract the growth rates a_1 and power laws a_2. From averaging the fits given in Table II, we estimate a $a_2 = 2.3(2)$ scaling law. These fits are compared directly against the triplet model results in

TABLE II. Fits of the early-time triplet dynamics of $n^{-5/3}(\mathcal{C}_3(t) - \mathcal{C}_3(0))$ to power law $f_1(t) = a_1 t^{a_2}$ and oscillatory $f_2(t) = b_1 t^2 + b_2\sqrt{t}\sin^2(b_3 t/2\hbar - b_4)$ functions. For densities where $n^{-5/3}\mathcal{C}_3(t)$ does not display a full period of oscillation in the early-time dynamics, we fit to $f_1(t)$ in the window $t \lesssim 0.25t_n$ to obtain the growth rates and power laws. For densities where a full period is observable, we fit to $f_2(t)$ in the larger window $t \lesssim 0.5t_n$ to obtain growth rates and precise estimation of the oscillation frequency. We note that using $f_1(t)$ in this latter regime would result in an overestimation of the growth rates. The estimate of the ratio $|b_3/E_{3b}^{(0)}|$ is obtained by averaging over multiple fits in the window $0.4 \leqslant t/t_n \leqslant 0.6$ and the uncertainty is given simply by the standard deviation.

nr_{vdW}^3	$k_n R_{3b}^{(0)}$	a_1	a_2		
3.0×10^{-4}	1.42	15.06	2.65		
8.8×10^{-5}	0.95	9.31	2.19		
3.7×10^{-5}	0.71	9.54	2.17		
1.9×10^{-5}	0.57	10.10	2.11		
nr_{vdW}^3	$k_n R_{3b}^{(0)}$	b_1	b_2	$\lvert b_3/E_{3b}^{(0)}\rvert$	b_4
1.1×10^{-5}	0.48	0.25	1.02	0.97(3)	0.09
6.9×10^{-6}	0.41	0.43	0.71	1.01(2)	0.14

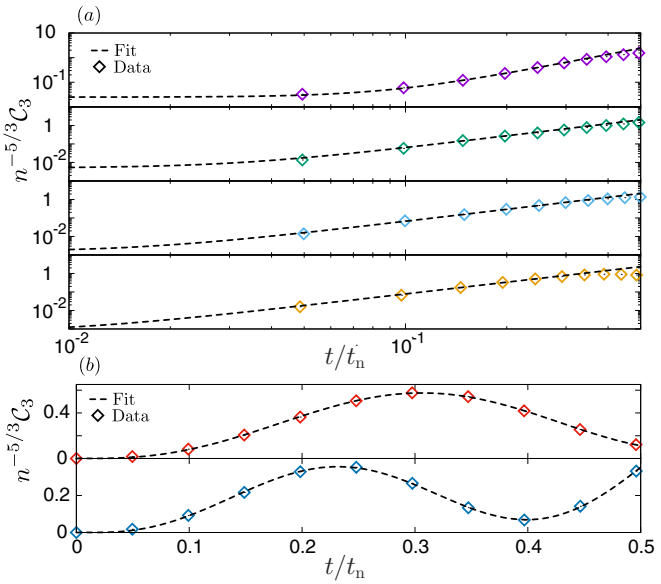

FIG. 10. Fits (dashed lines) of the early-time triplet model results (data points) for $n^{-5/3}\mathcal{C}_3(t)$ over a range of densities, corresponding in descending order to the key of Fig. 8. The results are fit to the functions (a) $f_1(t) = a_1 t^{a_2}$ and (b) $f_2(t) = b_1 t^2 + b_2\sqrt{t}\sin^2(b_3 t/2\hbar - b_4)$. The fit parameters are given in Table II.

Fig. 10(a), where the breakdown of the early-time power-law growth becomes apparent by $t \sim 0.5t_n$. Even though quadratic growth is approached for decreasing density, the rates remain larger than the predictions of Refs. [29,30] indicated by the black dashed-dotted lines in Fig. 9. At later times, however, we see that this growth is overestimated as dynamics become oscillatory, which indicates that a more sophisticated fitting function should be used for the lowest densities studied in this section as we address now.

For the lowest densities studied in the triplet model, the dynamical three-body contact displays oscillations with periods visible even at early times $t < 0.5t_n$. To quantify the frequency of this oscillation, we fit the dynamics of $n^{-5/3}\mathcal{C}_3(t)$ to $f_2(t) = b_1 t^2 + b_2\sqrt{t}\sin^2(b_3 t/2\hbar - b_4)$ to obtain the growth rates b_1 and b_2, the oscillation phase b_4, and the oscillation frequency b_3 reported in units of the nearby ground-state Efimov trimer binding energy $E_{3b}^{(0)}$ in Table II. The nonanalytic form of $f_2(t)$ was chosen as a combination of t^2 and $t^{5/2}$ power laws, motivated by the range of scalings found at larger densities. This provides an excellent fit of the data in the window $t \lesssim 0.5t_n$ as shown in Fig. 10(b) [91]. We note that the b_4 contribution to $f_2(t)$ adds an additional $\sqrt{t}$ scaling at early-times, which is generally negligible as the phase offset is typically small. From Table II, we find quadratic growth rates more comparable with the findings of Refs. [29,30] and, importantly, a *precise* identification of the oscillation frequency of the ground Efimov trimer to within an uncertainty of a few percent.

C. Summary

In this section, the quenched unitary Bose gas was studied within the triplet model, focusing on (i) how the doublet dynamics depart from the prethermal state and on (ii) signatures of the Efimov effect in the many-body observables of the system. Although the pairing field was found to approach a (roughly) universal steady-state, the dynamics of the instantaneous chemical potential did not, displaying visible non-universal oscillations at the frequency of the ground-state Efimov trimer. The momentum distribution $n_{\mathbf{k}}$ was found to depart from the $1/k^4$ power law toward an exponentially decaying tail at a momentum-dependent rate, although the violation of the total energy in the triplet model prevented any observation of the crossover to true thermalization. The development of the exponentially-decaying tail was shown to coincide with a large buildup of kinetic energy in the large-k modes and a corresponding draining of kinetic energy from the low-k modes relative to the doublet model results. The dynamics of the two-body contact were shown to depart nonuniversally from the doublet model results after a period of universal growth at early times, and to display the characteristic beating phenomenon at the frequency of the ground-state Efimov trimer at later times, consistent with the behavior found in the few-body studies [29,30]. The oscillatory dynamics of the three-body contact, which quantify the probability of measuring short-range Efimovian triples, were found to match quantitatively to the frequency of the ground-state Efimov trimer in vacuum, providing an important proof of the concept of the calibrated triplet model. We note that the sensitivity of the Efimov effect to the ultraviolet scales provides a stringent benchmark on the implementation of the numerics that are discussed further in Appendix B.

VI. CONCLUSION

We have illustrated that the cumulant expansion can be used to study the sequential buildup of correlations in a degenerate ultracold Bose gas quenched to the unitary regime. After outlining the cumulant theory of the many-body system, discussing its truncation, and identifying the few-body effects included at each level of the hierarchy, the quenched unitary Bose gas was then modeled at the doublet and triplet levels. In the doublet model, the gas was found to reach a universal prethermalized state after a period of rapid quantum depletion of the initially pure Bose-Einstein condensate. In this state, signatures of a universal Bogoliubov dispersion law emerge in the far-from-equilibrium dynamics of the occupation numbers. This can be understood from the proximal universal steady-states of the chemical potential and pairing fields in the prethermalized state. Using the dynamical two-body contact, we then analyzed the kinetic energy per particle and connected with the finite, universal kinetic temperatures measured over a restricted momentum range in Ref. [26]. In the triplet model, the introduction of nonintegrable three-particle processes caused the system to depart from the prethermal state at a momentum-dependent rate. This departure manifests in the large$-k$ occupation number dynamics as a transition away from the $1/k^4$ power law toward a decaying exponential $\exp(-\alpha k)$, coinciding with a large pileup of kinetic energy. Additionally, the many-body observables were found to display sensitivity to Efimovian length and time scales to varying degrees. By analyzing the dynamical three-body contact, we made a precise identification of this dynamical effect with Efimov states.

The Efimov effect is predicted not only to manifest dynamically but also as log-periodic violations of the continuous scaling of system observables with the atomic density [28–30,44]. Such a study may shed more light on the intriguing scenario $|E_{3b}^{(n)}| \approx E_n$ when an Efimov state becomes embedded in the medium. Simulating the triplet model over a factor $\sim 22.7^3$ in the density, however, remains a practical challenge due to the $\sim\Lambda^4$ scaling of the calculation time for the numerical implementation described in Appendix B.

More generally, this paper lays the groundwork for how a cumulant approach can be used to systematically include nonperturbative few-body effects in a description of strongly correlated, far-from-equilibrium many-body systems. This method provides a flexible tool for studying quenched quantum gases, regardless of their quantum statistics, with the flexibility of including, for instance, drive and loss terms to study open systems and out-of-equilibrium phase transitions. The range of possible extensions of this method highlights the importance of developing methods for truncating the hierarchy while preserving the underlying conservation laws. These topics, however, remain the subject of future study.

ACKNOWLEDGMENTS

We thank Murray Holland, José D'Incao, John Corson, Paul Mestrom, Thomas Secker, Jinglun Li, and Denise Braun for fruitful discussions. V.E.C., S.M., and S.J.J.M.F.K. acknowledge financial support by the Netherlands Organisation for Scientific Research (NWO) under Grant No. 680-47-623 and by the Foundation for Fundamental Research on Matter (FOM). H.K., M.V.R., and M.W. acknowledge support from the Flemish Research Foundation (FWO-Vl), Project No. FWO:G042915N. M.W. acknowledges additional support from project FWO:G016219N. H.K. acknowledges additional support from the European Union's Horizon 2020 research and innovation program under the Marie Skłodowska-Curie Grant Agreement No. 665501. M.V.R. gratefully acknowledges additional support from a BAEF postdoctoral fellowship.

APPENDIX A: FEW-BODY MODEL AT UNITARITY

In this Appendix, we detail the pairwise potential used to produce the numerical data analyzed in Secs. IV and V. Our choice of potentials is motivated by requirements to provide a good approximation of few-body scattering and bound-states on resonance while remaining computationally efficient.

1. Two-body calibration

The local potential introduced in Sec. II A can always be expanded as a sum of nonlocal separable potentials

$$\langle \mathbf{k}|\hat{V}|\mathbf{k}'\rangle = \sum_{j=1} g_j \langle \mathbf{k}|\zeta_j\rangle\langle\zeta_j|\mathbf{k}'\rangle, \tag{A1}$$

with form factors $|\zeta_j\rangle$ and interaction strengths g_j [92]. Using the separable expansion, the Lippman Schwinger equation for the T operator $\hat{T}(z) = \hat{V} + \hat{V}\hat{G}_{2B}^{(0)}(z)\hat{T}(z)$, with two-body free Green's function $\hat{G}_{2B}^{(0)}(z) = (z - 2\hat{\epsilon})^{-1}$ and one-body kinetic-energy operator $\hat{\epsilon}|\mathbf{k}\rangle = \hbar^2k^2/2m|\mathbf{k}\rangle$, can be solved for a closed expression of the T matrix $T(\mathbf{k}, \mathbf{k}', z) = \langle \mathbf{k}|\hat{T}(z)|\mathbf{k}'\rangle$ as

$$T(\mathbf{k}, \mathbf{k}', z) = \sum_{ij} g_j \langle \mathbf{k}|\zeta_i\rangle\langle\zeta_j|\mathbf{k}'\rangle[\Xi^{-1}(\mathbf{k}', z)]_{ij}, \tag{A2}$$

where

$$\Xi_{ij} = \frac{1}{g_j}\delta_{ij} + \int \frac{d^3k}{(2\pi)^3}\frac{\langle \mathbf{k}|\zeta_j\rangle\langle\zeta_i|\mathbf{k}'\rangle}{\hbar^2k^2/m - z}. \tag{A3}$$

In the limit where the binding energy of a shallow s-wave bound state nears threshold, referred to as a zero-energy resonance, the scattering length becomes large and the partial cross section approaches the unitarity limit [62]. In this case, one of the Ξ_{ii}'s will vanish for $z \to 0$, and the T matrix is dominated by the corresponding simple pole,

$$T(\mathbf{k}, \mathbf{k}', z) = \frac{\langle \mathbf{k}|\zeta\rangle\langle\zeta|\mathbf{k}'\rangle}{\Xi(z)}, \tag{A4}$$

known as the unitary pole approximation [93]. Within this approximation, the actual potential can be replaced by a nonlocal separable potential $\hat{V} = g|\zeta\rangle\langle\zeta|$, which reproduces Eq. (A4).

Following Refs. [44,45], we choose s-wave form factors $\langle \mathbf{k}|\zeta\rangle = \theta(\Lambda - |\mathbf{k}|)$ that are functions of the relative momentum. The function $\theta(x)$ is the Heaviside function defined such that $\theta(x \geqslant 0) = 1$ and $\theta(x < 0) = 0$. For a separable potential, the Lippmann-Schwinger equation for the two-body T operator $\hat{T}(z) = \hat{V} + \hat{V}\hat{G}_{2B}^{(0)}(z)\hat{T}(z)$ yields the closed expression

$$\hat{T}(z) = \frac{g|\zeta\rangle\langle\zeta|}{1 - g\langle\zeta|\hat{G}_{2B}^{(0)}(z)|\zeta\rangle}, \tag{A5}$$

$$= \begin{cases} \frac{g|\zeta\rangle\langle\zeta|}{1+g\frac{m}{2\pi\hbar^2}\left[\Lambda - k\tanh^{-1}\left(\frac{\Lambda}{k}\right) + \frac{i\pi k}{2}\right]} & \text{for } z = \frac{\hbar^2k^2}{m} \\ \frac{g|\zeta\rangle\langle\zeta|}{1+g\frac{m}{2\pi\hbar^2}\left[\Lambda - k\tan^{-1}\left(\frac{\Lambda}{k}\right)\right]} & \text{for } z = -\frac{\hbar^2k^2}{m}. \end{cases} \tag{A6}$$

The coupling constant g is determined by matching with the low-energy limit of the on-shell T matrix for s-wave scattering

$$\frac{4\pi\hbar^2}{m}a \underset{|\mathbf{k}|\to 0}{=} \langle \mathbf{k}, -\mathbf{k}|\hat{T}(\hbar^2k^2/m + i0)|\mathbf{k}', -\mathbf{k}'\rangle, \tag{A7}$$

$$= \left(\frac{1}{g} + \frac{m\Lambda}{2\pi^2\hbar^2}\right)^{-1}, \tag{A8}$$

which yields the expression $g = -2\pi^2\hbar^2/m\Lambda$ on resonance. The cutoff Λ is calibrated to reproduce finite-range corrections to the molecular binding energy $-\hbar^2/m(a - \bar{a})^2$ away from resonance, where $\bar{a} \approx 0.956 r_{vdW}$ is the mean-scattering length that is set by the van der Waals length r_{vdW} for a give atomic species [50]. For the ^{39}K experiments modeled in this paper, we take $r_{vdW} = 64.61a_0$ [47,94].

The simple pole of the T operator in Eq. (A5) gives the binding energy $E_D = -\hbar^2\kappa^2/m$ in the limit $\tilde{\kappa} = \kappa/\Lambda \ll 1$ as

$$\frac{\pi\tilde{\kappa}}{2} - \tilde{\kappa}^2 - \frac{\pi}{2a\Lambda} = O(\tilde{\kappa}^4). \tag{A9}$$

Ignoring quartic and higher-order contributions and equating with the molecular binding energy with finite range corrections [47,50] yields

$$\Lambda = \frac{2}{\pi\bar{a}(1-\bar{a}/a)} \approx \frac{2}{\pi\bar{a}}, \tag{A10}$$

which is expanded in the small parameter $\bar{a}/a$ valid in the strongly-interacting regime $a/r_{\rm vdW} \gg 1$. To understand the significance of this calibration, we compare the effective range approximation of the on-shell T matrix in the unitarity limit

$$\langle \mathbf{k}|\hat{T}(\hbar^2k^2/m + i0)|\mathbf{k}'\rangle \underset{k\to 0}{\approx} \frac{4\pi\hbar^2}{m}\frac{1}{ik - r_{\rm eff}k^2/2}, \tag{A11}$$

where $|\mathbf{k}| = |\mathbf{k}'|$, with the equivalent limit of Eq. (A5)

$$\langle \mathbf{k}|\hat{T}(\hbar^2k^2/m + i0)|\mathbf{k}'\rangle \underset{k\to 0}{\approx} \frac{4\pi\hbar^2}{m}\frac{1}{ik - 2k^2/\pi\Lambda}, \tag{A12}$$

which yields $r_{\rm eff} = 4\pi/\Lambda = 2\bar{a}$. We compare this with the result $r_{\rm eff} = 3\bar{a}$ for a Lorentzian form factor [95] and with the analytic result $r_{\rm eff} = \Gamma(1/4)^4\bar{a}/6\pi^2 \approx 2.92\bar{a}$ for the effective range of a pure $1/r^6$ van der Waals interaction at unitarity [50]. Taking the zero-range approximation yields the well-known $1/k^2$ scaling of the unitarity bounded partial cross section. It is instructive to also evaluate the equivalent zero-range expression for the retarded T operator [62] in the time domain

$$\begin{aligned}\hat{T}_+(\tau) &= \frac{1}{2\pi\hbar}\int_{-\infty}^{\infty} dE\, e^{-iE\tau/\hbar}\hat{T}(E+i0),\\ &= -\theta(\tau)\frac{|\zeta\rangle\langle\zeta|}{\sqrt{\tau}}\sqrt{\frac{16i\pi\hbar^5}{m^3}},\end{aligned} \tag{A13}$$

which can be obtained by analytic continuation of the Gaussian integral $I(z) = \int_0^\infty dk e^{-k^2z}$ in the half plane $\mathrm{Re}\,[z] > 0$. We contrast this gradual $\tau^{-1/2}$ decay with the sharply peaked Born approximation $\hat{T}_+(\tau) = g\delta(\tau)|\zeta\rangle\langle\zeta|$.

2. Efimov spectrum

The calibration scheme for the interaction parameters yields finite range corrections to two-body binding energies and scattering amplitudes due to the long-range van der Waals interactions remaining on resonance. On the two-body level, these corrections to the binding energy become less important near unitarity as the ratio $a/\bar{a}$ approaches infinity. However, on the three-body level, the spectrum of three-body bound Efimov states is set by finite-range effects. And so it is important to check that the calibration scheme produces a trimer spectrum which matches roughly what has been observed experimentally.

To solve the three-body problem in vacuum for our calibrated separable potential, we begin with the decomposition of the three-body wave function $|\Psi_{\rm 3B}\rangle = |\Psi^{(1)}\rangle + |\Psi^{(2)}\rangle + |\Psi^{(3)}\rangle$ into Faddeev components [92], satisfying the bound-state equation in momentum space

$$\Psi^{(1)}(\mathbf{q}_1,\mathbf{p}_1) = G_{\rm 3B}^{(0)}(q_1,p_1,E)\int\frac{d^3q'}{(2\pi)^3}\int\frac{d^3p'}{(2\pi)^3}\langle\mathbf{q}_1,\mathbf{p}_1|\hat{T}_{23}(E)|\mathbf{q}',\mathbf{p}'\rangle\langle\mathbf{q}',\mathbf{p}'|\hat{P}_+ + \hat{P}_-|\Psi^{(1)}\rangle, \tag{A14}$$

where $\hat{T}_{23}(z) = \hat{V}_{23} + \hat{V}_{23}\hat{G}_{\rm 3B}^{(0)}(E)\hat{T}_{23}(z)$, E is the binding energy, and $\hat{G}_{\rm 3B}^{(0)}(z) = (z - \sum_{i=1}^3\hat{\epsilon}_i)^{-1}$ is the vacuum three-body Green's function. In Eq. (A14), the three-body system with single-particle wave vectors $\mathbf{k}_1$, $\mathbf{k}_2$, and $\mathbf{k}_3$ is parametrized by Jacobi vectors $\mathbf{q}_1 = (\mathbf{k}_2 - \mathbf{k}_3)/2$ and $\mathbf{p}_1 = (2\mathbf{k}_1 - \mathbf{k_2} - \mathbf{k_3})/3$. Following the original formulation of Skorniakov and Ter-Martirosian [96], we make the ansatz $|\Psi^{(1)}\rangle = N\hat{G}_{\rm 3B}^{(0)}(E)(|\zeta\rangle\otimes|\mathcal{F}\rangle)$, where N is the normalization constant, and the tensor product is defined as $\langle\mathbf{q}_1,\mathbf{p}_1|(|\zeta\rangle\otimes|\mathcal{F}\rangle) = \zeta(2q_1)\mathcal{F}(p_1)$. Inserting this ansatz into Eq. (A14) yields the one-dimensional integral equation

$$\mathcal{F}(p_1) = 2g\tau\left(E - \frac{3\hbar^2p_1^2}{4m}\right)\int\frac{d^3p'}{(2\pi)^3}\frac{\zeta(|2\mathbf{p}_1+\mathbf{p}'|)\zeta(|2\mathbf{p}'+\mathbf{p}_1|)}{E - \frac{\hbar^2p_1^2}{m} - \frac{\hbar^2p'^2}{m} - \frac{\hbar^2\mathbf{p}_1\cdot\mathbf{p}'}{m}}\mathcal{F}(p'), \tag{A15}$$

where $\tau(z) = 1/(1 - g\langle\zeta|\hat{G}_{\rm 2B}^{(0)}(z)|\zeta\rangle)$. Nontrivial solutions of Eq. (A15) correspond to the Efimov trimer binding energies at unitarity [96]. For the calibrated separable potential introduced in Sec. A 1 and used in the many-body simulations, the resulting trimer spectrum is given in Table III. The wave number of the ground trimer $\kappa_* \equiv \kappa^{(0)} = 0.211/r_{\rm vdW}$ is the three-body parameter, which compares with the universal result $\kappa_* r_{\rm vdW} \approx 0.226$ for broad, open-channel dominated Feshbach resonances [47,88,89]. Additionally, the zero-range model predictions for the 22.7^2 geometric scaling between neighboring energies is recovered for the highly-excited Efimov trimers as is expected in a finite-ranged model [18–20]. Ultimately, we see that our calibrated separable potential, despite being tailored to corrections on the two-body level, captures the sensitive dependence of Efimov physics on finite-range effects on the three-body level.

APPENDIX B: NUMERICAL METHODS

In this section, the cumulant equations of motion of Sec. III are rewritten for the nonlocal separable potential discussed in Sec. A that is used in our numerics. We will see in Sec. B 2

TABLE III. Approximate values for the ground and first-excited Efimov trimer binding energies obtained from numerical solutions of Eq. (A15) using the calibrated separable pairwise potential. In practice, to obtain trimer binding energies from the integral equation (Eq. (A15)), we follow the Nystrom method and convert the integral equation into a summation over a Gauss-Legendre quadrature [97]. The resultant equation can be solved as an eigenvalue problem, with eigenvalues corresponding to trimer binding energies.

j	$E_{3b}^{(j)}/E_{vdW}$	$E_{3b}^{(j)}/E_{3b}^{(j+1)}$	$\kappa^{(j)}r_{vdW}$	$\kappa^{(j)}/\Lambda$
0	0.0446	24.2^2	0.211	0.317
1	7.62×10^{-5}	22.7^2	0.00873	0.0131

that the factorized form of the s-wave separable potential effectively reduces some integrations in the triplet cumulant equations of motions from 3D to 2D.

In Sec. B 1, we give this simulation form of the cumulant equations. Besides the different interaction potentials, these cumulant equations differ from those in Sec. III in that we ignore all quadruplets to yield a triplet model, and we simulate only a subset of the most dominant terms in $\mathcal{M}^{H_4}$ [Eq. (43)] and $\mathcal{R}^{H_4}$ [Eq. (44)] to simplify numerics. In Sec. B 2, we discuss our numerical methods for simulating the cumulant equations. In Sec. B 3, the convergence of our simulation with respect to grid parameters is analyzed for completeness.

1. Equations of motion

We begin by rewriting the many-body Hamiltonian [Eq. (2)] for the nonlocal separable potential

$$\hat{H} = \sum_{\mathbf{k}} \epsilon_{\mathbf{k}} \hat{a}_{\mathbf{k}}^\dagger \hat{a}_{\mathbf{k}} + \frac{g}{2V} \sum_{\mathbf{p},\mathbf{p}',\mathbf{q}} \zeta_{\mathbf{p}-\mathbf{p}'+2\mathbf{q}} \zeta_{\mathbf{p}-\mathbf{p}'} a_{\mathbf{p}+\mathbf{q}}^\dagger a_{\mathbf{p}'-\mathbf{q}}^\dagger \hat{a}_{\mathbf{p}} \hat{a}_{\mathbf{p}'}, \tag{B1}$$

where we have used the shorthand $\langle \mathbf{k},\mathbf{k}'|\hat{V}|\mathbf{k}'',\mathbf{k}'''\rangle = g\delta_{\mathbf{k}+\mathbf{k}',\mathbf{k}''+\mathbf{k}'''}\zeta_{\mathbf{k}-\mathbf{k}'}\zeta_{\mathbf{k}''-\mathbf{k}'''}$ with $\zeta_{\mathbf{k}-\mathbf{k}'} = \theta(\Lambda - |\mathbf{k}-\mathbf{k}'|/2)$ to take expectation values of the form factors in the laboratory frame. From the Gross-Pitaevskii equation

$$i\hbar\partial_t\psi_0 = g\left(\zeta_0^2 n_0 + \frac{2g}{V}\sum_{\mathbf{l}}\zeta_{\mathbf{l}}^2 n_{\mathbf{l}}\right)\psi_0 + \frac{g\psi_0^*}{V}\sum_{\mathbf{l}}\zeta_0\zeta_{2\mathbf{l}}c_{\mathbf{l}} + \frac{g}{V^{3/2}}\sum_{\mathbf{l},\mathbf{s}}\zeta_{\mathbf{l}}\zeta_{2\mathbf{s}-\mathbf{l}}M_{\mathbf{l},\mathbf{s}}^*, \tag{B2}$$

we extract the condensate phase derivative as in Eq. (11):

$$\hbar\frac{d\theta_0}{dt} = -\frac{1}{2n_0}\left(\psi_0^* i\hbar\frac{d\psi_0}{dt} - i\hbar\frac{d\psi_0^*}{dt}\psi_0\right), \tag{B3}$$

$$= -\left[g\zeta_0^2 n_0 + \frac{2g}{V}\sum_{\mathbf{l}}\zeta_{\mathbf{l}}^2 n_{\mathbf{l}} + \frac{g}{V}\sum_{\mathbf{l}}\zeta_0\zeta_{2\mathbf{l}}\mathrm{Re}\,c_{\mathbf{l}} + \frac{g}{\sqrt{n_0 V^3}}\sum_{\mathbf{l},\mathbf{s}}\zeta_{\mathbf{l}}\zeta_{2\mathbf{s}-\mathbf{l}}M_{\mathbf{l},\mathbf{s}}^*\right]. \tag{B4}$$

From the Heisenberg equation for the unrotated operators $\hat{b}_{\mathbf{k}}$ [see Eq. (8)], we obtain the form of the doublet equations of motion for the separable potential,

$$i\hbar\partial_t n_{\mathbf{k}} = 2i\,\mathrm{Im}\left[\Delta_{\mathbf{k}}c_{\mathbf{k}}^* + 2g\sqrt{\frac{n_0}{V}}\sum_{\mathbf{l}}\zeta_{2\mathbf{k}-\mathbf{l}}\zeta_{\mathbf{l}}M_{\mathbf{l},\mathbf{k}} + g\sqrt{\frac{n_0}{V}}\sum_{\mathbf{l}}\zeta_{\mathbf{k}}\zeta_{2\mathbf{l}-\mathbf{k}}M_{\mathbf{k},\mathbf{l}}^*\right], \tag{B5}$$

$$i\hbar\partial_t c_{\mathbf{k}} = 2E_{\mathbf{k}}c_{\mathbf{k}} + (1+2n_{\mathbf{k}})\Delta_{\mathbf{k}} + 4g\sqrt{\frac{n_0}{V}}\sum_{\mathbf{l}}\zeta_{\mathbf{l}+\mathbf{k}}\zeta_{\mathbf{l}-\mathbf{k}}M_{\mathbf{l},\mathbf{k}}^* + 2g\sqrt{\frac{n_0}{V}}\sum_{\mathbf{l}}\zeta_{\mathbf{k}}\zeta_{2\mathbf{l}-\mathbf{k}}R_{\mathbf{k},\mathbf{l}}, \tag{B6}$$

where we use the forms of the Hartree-Fock Hamiltonian [Eq. (34)] and pairing field [Eq. (35)] for a separable potential:

$$E_{\mathbf{k}} = \epsilon_{\mathbf{k}} + 2g\left[\zeta_{\mathbf{k}}^2 n_0 + \frac{1}{V}\sum_{\mathbf{l}}\zeta_{\mathbf{k}-\mathbf{l}}^2 n_{\mathbf{l}}\right] + \hbar\partial_t\theta_0, \tag{B7}$$

$$\Delta_{\mathbf{k}} = g\zeta_{2\mathbf{k}}\left[\zeta_0 n_0 + \frac{1}{V}\sum_{\mathbf{l}}\zeta_{2\mathbf{l}}c_{\mathbf{l}}\right]. \tag{B8}$$

For the triplet equations of motion, we obtain the forms of Eqs. (39) and (40) for a separable potential

$$i\hbar\partial_t M_{\mathbf{k},\mathbf{q}} = (E_{\mathbf{k}} - E_{\mathbf{q}} - E_{\mathbf{k}-\mathbf{q}})M_{\mathbf{k},\mathbf{q}} - \Delta_{\mathbf{k}-\mathbf{q}}^* M_{\mathbf{q},\mathbf{k}}^* - \Delta_{\mathbf{q}}^* M_{\mathbf{k}-\mathbf{q},\mathbf{k}}^* + \Delta_{\mathbf{k}}R_{\mathbf{k},\mathbf{q}}^* + \mathcal{M}_{\mathbf{k},\mathbf{q}}^{H_3} + \mathcal{M}_{\mathbf{k},\mathbf{q}}^{H_4}, \tag{B9}$$

$$i\hbar\partial_t R_{\mathbf{k},\mathbf{q}} = (E_{\mathbf{k}} + E_{\mathbf{q}} + E_{\mathbf{k}-\mathbf{q}})R_{\mathbf{k},\mathbf{q}} + \Delta_{\mathbf{k}}M_{\mathbf{k},\mathbf{q}}^* + \Delta_{\mathbf{q}}M_{\mathbf{q},\mathbf{k}}^* + \Delta_{\mathbf{k}-\mathbf{q}}M_{\mathbf{k}-\mathbf{q},\mathbf{k}}^* + \mathcal{R}_{\mathbf{k},\mathbf{q}}^{H_3} + \mathcal{R}_{\mathbf{k},\mathbf{q}}^{H_4}, \tag{B10}$$

where the doublet sources are the forms of Eqs. (41) and (42) for a separable potential

$$\frac{\mathcal{M}_{\mathbf{k},\mathbf{q}}^{H_3}}{\sqrt{n_0/V}} = 2g\left(\zeta_{2\mathbf{k}-\mathbf{q}}\zeta_{\mathbf{q}}c_{\mathbf{k}-\mathbf{q}}^* n_{\mathbf{q}} + \zeta_{\mathbf{k}+\mathbf{q}}\zeta_{\mathbf{k}-\mathbf{q}}n_{\mathbf{k}-\mathbf{q}}c_{\mathbf{q}}^* - n_{\mathbf{k}}(\zeta_{\mathbf{k}+\mathbf{q}}\zeta_{\mathbf{k}-\mathbf{q}}c_{\mathbf{q}}^* + \zeta_{\mathbf{q}}\zeta_{2\mathbf{k}-\mathbf{q}}c_{\mathbf{k}-\mathbf{q}}^*)\right)$$
$$+2g(\zeta_{2\mathbf{q}-\mathbf{k}}\zeta_{\mathbf{k}}n_{\mathbf{k}-\mathbf{q}}n_{\mathbf{q}} - \zeta_{2\mathbf{q}-\mathbf{k}}\zeta_{\mathbf{k}}n_{\mathbf{k}}(1+n_{\mathbf{q}}+n_{\mathbf{k}-\mathbf{q}}) - c_{\mathbf{k}}(\zeta_{2\mathbf{k}-\mathbf{q}}\zeta_{\mathbf{q}}c_{\mathbf{q}}^* + \zeta_{\mathbf{k}+\mathbf{q}}\zeta_{\mathbf{k}-\mathbf{q}}c_{\mathbf{k}-\mathbf{q}}^*)), \tag{B11}$$

$$\frac{\mathcal{R}^{H_3}_{\mathbf{k},\mathbf{q}}}{\sqrt{n_0/V}} = 2g(\zeta_{\mathbf{2q-k}}\zeta_{\mathbf{k}}c_{\mathbf{k}}(1+n_{\mathbf{q}}+n_{\mathbf{k-q}}) + \zeta_{\mathbf{2k-q}}\zeta_{\mathbf{q}}c_{\mathbf{q}}(1+n_{\mathbf{k}}+n_{\mathbf{k-q}}) + \zeta_{\mathbf{k+q}}\zeta_{\mathbf{k-q}}c_{\mathbf{k-q}}(1+n_{\mathbf{k}}+n_{\mathbf{q}}))$$
$$+2g(\zeta_{\mathbf{k-q}}\zeta_{\mathbf{k+q}}c_{\mathbf{k}}c_{\mathbf{q}} + \zeta_{\mathbf{q}}\zeta_{\mathbf{2k-q}}c_{\mathbf{k}}c_{\mathbf{k-q}} + \zeta_{\mathbf{k}}\zeta_{\mathbf{2q-k}}c_{\mathbf{q}}c_{\mathbf{k-q}}). \tag{B12}$$

We approximate the triplet terms $\mathcal{M}^{H_4}_{\mathbf{k},\mathbf{q}}$ and $\mathcal{R}^{H_4}_{\mathbf{k},\mathbf{q}}$ by calculating only their most dominant contributions:

$$\mathcal{M}^{H_4}_{\mathbf{k},\mathbf{q}} \approx -\frac{g}{V}\sum_{\mathbf{l}} \zeta_{\mathbf{2q-k}}\zeta_{\mathbf{2l-k}}M_{\mathbf{k},\mathbf{l}}\big(n_{\mathbf{k-q}}+n_{\mathbf{q}}+1\big), \tag{B13}$$

$$\mathcal{R}^{H_4}_{\mathbf{k},\mathbf{q}} \approx \frac{g}{V}\sum_{\mathbf{l}}\Big(\zeta_{\mathbf{2q-k}}\zeta_{\mathbf{2l-k}}R_{\mathbf{l},\mathbf{k}}\big(n_{\mathbf{q}}+n_{\mathbf{k-q}}+1\big) + \zeta_{\mathbf{2k-q}}\zeta_{\mathbf{2l-q}}R_{\mathbf{l},\mathbf{q}}\big(n_{\mathbf{k}}+n_{\mathbf{k-q}}+1\big)$$
$$+\zeta_{\mathbf{k+q}}\zeta_{\mathbf{k-q+2l}}R_{\mathbf{l},\mathbf{k-q}}\big(n_{\mathbf{k}}+n_{\mathbf{q}}+1\big)\Big). \tag{B14}$$

The $+1$ terms make the most dominant contributions to $\mathcal{M}^{H_4}$ and $\mathcal{R}^{H_4}$ at early times before quantum depletion becomes appreciable. This can be understood by simply counting the number of operator products, but is also something that we confirmed numerically. From Sec. III D, we also know that these terms are required to produce the correct form of the interacting few-body Hamiltonian. In addition to the these terms, we have included the subdominant Bose-enhancement factors of the form $1+n+n$ so scattering is described at the level of the many-body T matrix, consistent with the equation of motion for the c cumulant [Eq. (B6)]. We emphasize, however, that due to the restriction of our analysis of the triplet simulation to $t \lesssim t_{\mathrm{n}}$ before quantum depletion becomes significant, the difference between vacuum and many-body T matrices is minimal (cf. the discussion in Ref. [44]). Finally, the approximations in Eqs. (43) and (44) also have a practical purpose in significantly reducing the computational burden, which is addressed in the following subsection on implementation.

2. Implementation

Because we simulate a uniform Bose gas at rest in three dimensions, the doublets $n_{\mathbf{k}}$ and $c_{\mathbf{k}}$ are spherically symmetric and can be represented as a vector with index $k_i = |\mathbf{k}|_i$. For the triplets $M_{\mathbf{k},\mathbf{q}}$ and $R_{\mathbf{k},\mathbf{q}}$ the situation is a little bit more complicated. We have that they are encoded by two 3D momentum vectors and should therefore depend on six parameters. However, we first have an overall rotation symmetry of $\mathbf{k}$ and $\mathbf{q}$ simultaneously, which already excludes two angles, and then also a rotation symmetry of $\mathbf{q}$ with respect to $\mathbf{k}$, which excludes another rotation angle. Therefore, we are left with three independent parameters and we can parametrize $M_{\mathbf{k},\mathbf{q}} \equiv M(k, q, \cos\theta_{\mathbf{k},\mathbf{q}})$ as a 3D array on a grid $(k_i, q_i, \cos\theta|_i)$, where k_i are q_i are the vector norms and $\cos\theta_i$ is the discretized cosine of the polar angle between $\mathbf{k}$ and $\mathbf{q}$. Many operations in the cumulant equations of motion in Sec. B 1 are pointwise and can be evaluated directly within this parametrization.

For the implementation, we also need to evaluate objects with swapped and/or shifted indices, like the doublet $n_{\mathbf{k-q}}$ or the triplets $M_{\mathbf{q},\mathbf{k}}$ or $M_{\mathbf{k-q},\mathbf{k}}$. For the doublets, we can simply evaluate the vector norm $|\mathbf{k}-\mathbf{q}| = \sqrt{k^2+q^2-2kq\cos\theta_{\mathbf{k},\mathbf{q}}}$ and project the result to the nearest k_i in our predefined grid, so that now $n_{\mathbf{k-q}}$ becomes a 3D array after interpolation. If we have to swap two indices $\mathbf{k}$ and $\mathbf{q}$ of a triplet, we can simply swap the first two momentum indices of the 3D array, since $\cos\theta_{\mathbf{k},\mathbf{q}}$ is invariant under the exchange of the two momenta, i.e., $M_{\mathbf{q},\mathbf{k}} \equiv M(q, k, \cos\theta_{\mathbf{k},\mathbf{q}})$. To evaluate $M_{\mathbf{k-q},\mathbf{k}} \equiv M(|\mathbf{k}-\mathbf{q}|, k, \cos\theta_{\mathbf{k-q},\mathbf{k}})$, we also have to evaluate $\cos\theta_{\mathbf{k-q},\mathbf{k}} = (k - q\cos\theta_{\mathbf{k},\mathbf{q}})/|\mathbf{k}-\mathbf{q}|$ if we align $\mathbf{k}$ along the z axis, after which we can apply a zeroth-order interpolation in 3D, i.e., we select the 3D index $(k_i, q_i, \cos\theta|_i)$ that is closest to the point $(|\mathbf{k}-\mathbf{q}|, k, \cos\theta_{\mathbf{k-q},\mathbf{k}})$. We have numerically compared the zeroth-order interpolation with first order and even spline methods [97] but the result is indistinguishable when the grid spacing is chosen finely enough. Note that zeroth-order interpolation is essentially a map of indices and can be precomputed, making it much more efficient than higher-order interpolation schemes. The form factors $\zeta_{\mathbf{k}}$, $\zeta_{\mathbf{2q-k}}$ etc. can also be precomputed for our 3D grid $(k_i, q_i, \cos\theta|_i)$ and stored as logical 3D arrays for later use in the equations of motion.

Furthermore, we have to evaluate the summations in spherical coordinates. For example, in (B7), we encounter a spherically symmetric summation, which can be evaluated as follows:

$$\sum_{\mathbf{l}} \zeta_{2\mathbf{l}}c_{\mathbf{l}} \equiv \frac{V}{2\pi^2}\int_0^{k_{\max}} l^2 dl\, \zeta(2l)c(l) \approx \frac{V\Delta k}{2\pi^2}\sum_i k_i^2\zeta_{2i}c_i. \tag{B15}$$

Here Δk is the difference between two consecutive elements in the vector k_i (if uniform) and $k_{\max}$ is the numerical grid cutoff and we do a simple form of Riemann integration, where we use the spherically symmetric vectors $\zeta_i \equiv \zeta(k_i)$ and $c_i \equiv c(k_i)$. In principle, more involved algorithms can be implemented (like trapezoidal or Simpson's rule) but with a fine enough grid this turns out to be satisfactory.

Similarly, we also have integrals over a momentum index of a $(\mathbf{k}, \mathbf{q})$ object. Also, in (B7) we find the summation

$$\sum_{\mathbf{q}} \zeta^2_{\mathbf{k-q}}n_{\mathbf{q}} \equiv \frac{V}{4\pi^2}\int_0^{k_{\max}} q^2 dq \int_{-1}^{1} d\cos\theta\ \zeta_{\mathbf{k-q}}(k, q, \cos\theta)n(q)$$
$$\approx \frac{V\Delta k\,\Delta c}{4\pi^2}\sum_{j,m} k_j^2\zeta_{\mathbf{k-q};i,j,m}n_j \equiv \mathcal{H}_i, \tag{B16}$$

where Δc is the differential element of the $\cos\theta|_i$ and we have defined the 3D array $\zeta_{\mathbf{k}-\mathbf{q}}$ with indexing $\zeta_{\mathbf{k}-\mathbf{q};i,j,m} \equiv \zeta_{\mathbf{k}-\mathbf{q}}(k_i, q_j, \cos\theta|_m)$. The result $\mathcal{H}_i$ is again a spherically symmetric array. To summarize, we implement the summation over an index of a $(\mathbf{k}, \mathbf{q})$-object as a summation over two of the three indices of the corresponding 3D array, with the correct differential element for the Riemann integration. We note that using the seperable potential, any summation in (B5)–(B14) can be evaluated with one of the two ways described above, after construction of the right vector or 3D array as the integrand.

3. Convergence

In this section, we provide details related to the numerical convergence of the triplet simulation. We discuss the convergence of various simulation quantities with respect to the angular and momentum grid parameters. We also confirm that the violation of the total energy in the triplet simulation agrees with analytics, providing an additional convergence test. Finally, we detail the computing resources used to simulate the triplet equations of motion.

We choose a uniformly spaced momentum grid $\mathbf{k} = \{k_i\}_{i=1,\ldots \mathrm{nk}}$ extending from $k_i = \Delta k$ to $k_{\mathrm{nk}} = k_{\mathrm{max}}$, where the system volume V determines the grid spacing Δk through the usual relation $V = (2\pi/\Delta k)^3$. The numerical cutoff k_{max}, which is a truncation in the single-particle plane-wave basis, is distinct from the form factor cutoff Λ, which places an upper bound on both incoming and outgoing relative momentum involved in pairwise interactions. Therefore, the pairwise generation of excitations with zero center of mass momentum described by the c cumulant is inherently limited to single-particle momenta $k \leqslant \Lambda$. Setting $k_{\mathrm{max}} = \Lambda$ is therefore justified for the HFB simulation, and we have numerically confirmed that n_k vanishes for $k > \Lambda$. In the triplet simulation, however, the R and M cumulants describe interactions where the center of mass momentum of an interacting pair does not vanish. In fact, if this pairwise center of mass momentum does vanish, then the R and M cumulants are zero by construction. For the R cumulant the nonzero center of mass momentum of the interacting pair is offset by the third spectator atom. For the M cumulant, the nonzero center of mass momentum of the interacting pair corresponds to the momentum of the incoming atom, which has been defined in the rest frame of the condensate. Therefore, we have taken $k_{\mathrm{max}} > \Lambda$ in the triplet simulation to allow for the complete description of these processes.

The natural question then is what to choose for k_{max} in the triplet simulation given that the processes described by R and M can involve single-particle momenta larger than Λ. For example, consider the process described by $M_{\mathbf{k},\mathbf{q}}$ where the incoming excitation with momentum $\mathbf{k}$ decays into two excitations. The form factor for the incoming scattering will be of the form $\zeta_{\mathbf{k}} = \theta(\Lambda - |\mathbf{k}|/2)$, which is restricted to momentum $\mathbf{k} \leqslant 2\Lambda$. Conversely, this applies to the outgoing excitation of the process described by $M^*_{\mathbf{k},\mathbf{q}}$. The population of single-particle modes in the triplet model is described by $\dot{n}_{\mathbf{k}}$. Inspection of Eq. (B6) reveals the form factors $\zeta_{\mathbf{l}}$ and $\zeta_{\mathbf{k}}$, in the second and third terms, respectively, which act to restrict scattering into single-particle modes beyond 2Λ. In Fig. 11(a), we show how n_k remains nonzero for $1 < k/\Lambda < 2$ in the triplet model and confirm that $n_{\mathbf{k}}$ is numerically zero by $k = 2\Lambda$. We note that the choice of k_{max} also has consequences for the spectrum of bound states in the simulation because of the ultraviolet sensitivity of the three-body parameter discussed in Sec. A 2. The choice $k_{\mathrm{max}} = 2\Lambda$ of the numerical cutoff was used to produce the results of Sec. V, which also matches the expected frequency of the ground Efimov trimer in vacuum, serving as an additional consistency check. As a general rule, the chosen simulation time step, Δt, must be at least as fast as the frequency set by the largest energy in the simulation. In practice, we choose $\Delta t = m/2\hbar k^2_{\mathrm{max}}$ when the cutoff of the single-particle momentum sets the largest frequency in the simulation, which is generally the case. The simulation is then run up to $t \sim t_{\mathrm{n}}$, beyond which the positivity of n_k becomes violated typically for momentum in the vicinity of $k/k_{\mathrm{n}} \sim 2k_{\mathrm{n}}$

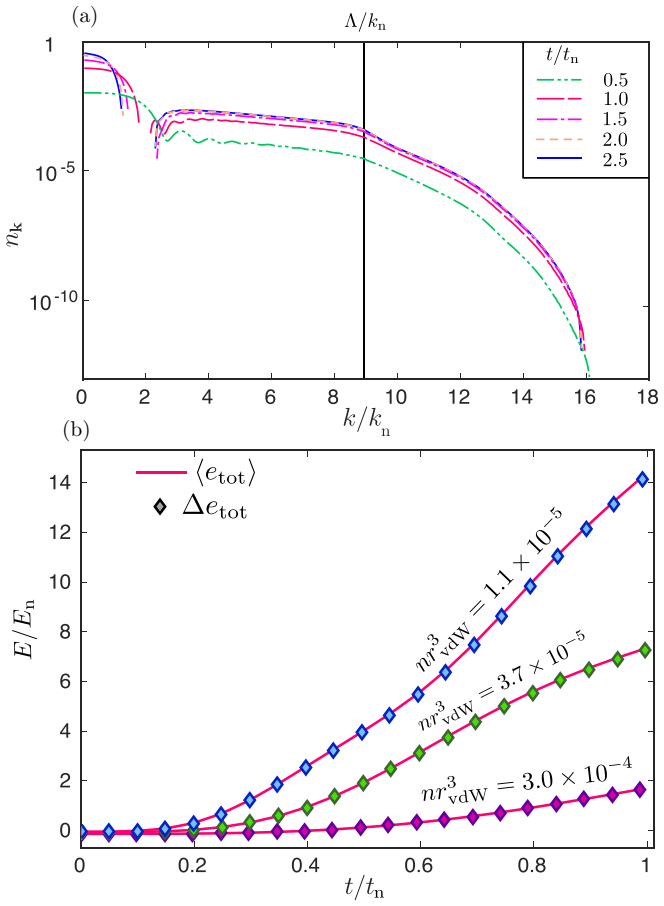

FIG. 11. (a) Time evolution of the momentum distribution for $nr^3_{\mathrm{vdW}} = 6.9 \times 10^{-6}$ up to time $t = 2.5t_{\mathrm{n}}$. The cutoff scale $\Lambda/k_{\mathrm{n}} \approx 9$ is indicated by the solid vertical line, and by $k/\Lambda = 2$ the momentum distribution remains vanishingly small for all times, demonstrating convergence with respect to the numerical cutoff k_{max}. The development and subsequent growth of the regime of negative n_k near k/k_{n} can be seen for $t/t_{\mathrm{n}} \gtrsim 1$. (b) Dynamics of Δe_{tot} (diamonds) versus $\langle e_{\mathrm{tot}} \rangle$ (solid red) for three different densities. The simulation parameters used to produce the data in (a) and (b) are $\mathrm{nc} = 150$, $\mathrm{nk} = 5k_{\mathrm{max}}/n^{1/3}$, $k_{\mathrm{max}} = 2\Lambda$, $\Delta t = m/2\hbar k^2_{\mathrm{max}}$, following the convergence guidelines in Sec. B 3.

[see Fig. 11(a)], which becomes a persistent feature at later times. Because this violation is not physical, in Sec. V we have restricted our analysis to results before this behavior occurs.

This violation is a symptom of the nonconservation of the total energy, which is inherent in the triplet cumulant theory as discussed in Sec. III B. Analytically, one can predict the extent to which the total energy $E_{\rm tot} = \langle \hat{H} \rangle$ will change by calculating its time derivative from the restricted source term [Eq. (B13)]:

$$\hbar \frac{dE_{\rm tot}}{dt} = \frac{2g^2}{V^{3/2}} \mathrm{Im}\left[\psi_0^* \sum_{\mathbf{q},\mathbf{k},\mathbf{l}} \zeta_{2\mathbf{q}-\mathbf{k}} \zeta_{2\mathbf{l}-\mathbf{k}} (1+n_{\mathbf{q}}) M^*_{\mathbf{k},\mathbf{l}} \right]. \quad \text{(B17)}$$

In Fig. 11(b), we compare the total energy per particle $\langle e_{\rm tot} \rangle = E_{\rm tot}/N$ with the quantity, $\Delta e_{\rm tot} = \int dt \ (d\langle e_{\rm tot}\rangle/dt)$, which is the result of simulating Eq. (B17) as an independent equation of motion supplied with an initial condition $\Delta e_{\rm tot}(t = 0) = \langle e_{\rm tot}(t=0)\rangle$. The excellent agreement between $\langle e_{\rm tot}\rangle$ and $\Delta e_{\rm tot}$ indicates that the observed violation of the total energy is inherent in the theory and *not* due to technical issues within the simulation itself. Although not shown, we find in general that the total number is conserved at all times within the triplet simulation as expected.

We now discuss the choice of the number of momentum and angular grid points and consequences for the convergence of simulation results. To study the convergence, we track the total energy per particle and the condensate fraction as a function of nk and nc at the latest times $t \sim t_{\rm n}$ analyzed in Sec. V. We fix $nr_{\rm vdW}^3 = 3.0 \times 10^{-4}$, $k_{\rm max} = 2\Lambda$, and $\Delta t = m/2\hbar k_{\rm max}^2$ and define the normalized variation of the slope

$$\delta e_{\rm tot}[x_i, x_{i-1}] = \left| \frac{1 - \langle e_{\rm tot}\rangle[x_{i-1}]/\langle e_{\rm tot}\rangle[x_i]}{x_i - x_{i-1}} \right|, \quad \text{(B18)}$$

$$\delta n_0[x_i, x_{i-1}] = \left| \frac{1 - n_0[x_{i-1}]/n_0[x_i]}{x_i - x_{i-1}} \right|, \quad \text{(B19)}$$

in terms of a vector of grid parameters $\underline{x} = \{x_1 \ldots x_{\rm f}\}$ as our measure of convergence. In Fig. 12, we have evaluated $\delta e_{\rm tot}$ and δn_0 using to different grid vectors $\underline{\rm nc} = \{25, 50, 100, 150, 200\}$ and $\underline{\rm nk} = \{j \times (k_{\rm max}/n^{1/3})\}_{j=1}^6$ rounded to the nearest integer. When evaluating convergence with respect to $\underline{\rm nc}$, we fix $\mathrm{nk} = 5k_{\rm max}/n^{1/3}$, and when evaluating with respect to $\underline{\rm nk}$, we fix $\mathrm{nc} = 150$. We find that the simulation results for $\langle e_{\rm tot}\rangle$ and n_0 are converged to the level of a percent or less when the normalized slope variations measured by $\delta e_{\rm tot}$ and δn_0, respectively, are on the order of 10^{-4}. Therefore, we have taken $\mathrm{nc} = 150$ and $\mathrm{nk} = 5k_{\rm max}/n^{1/3}$ as the standard grid parameters used to produce the data of Sec. V. Although we have not discussed the convergence of the HFB simulation, we follow the same guidelines for the grid parameters.

Finally, we note that the HFB and triplet simulations were run on an NVIDIA Tesla P100 GPGPU card which has 16 GB of memory and 3584 cores. Although GPGPUs greatly speed up pointwise arithmetic in the simulation, the limited amount of memory means that triplet simulations cannot be taken to large values of the numerical cutoff (beyond $k_{\rm max}/n^{1/3} \gtrsim 70$ in our case) while simultaneously fixing $\mathrm{nc} = 150$ and $\mathrm{nk} = 5k_{\rm max}/n^{1/3}$ to achieve convergence. This hardware restriction places a practical limit on the range of results presented in this paper. Additionally, we note that the calculation time for the numerical implementation scheme described in this section scales roughly as $\sim\Lambda^4$. In practice, the triplet simulations can be taken to larger values of $k_{\rm max}$ on workstations with a large number of CPUs and memory, although the slowdown compared to a GPGPU becomes significant.

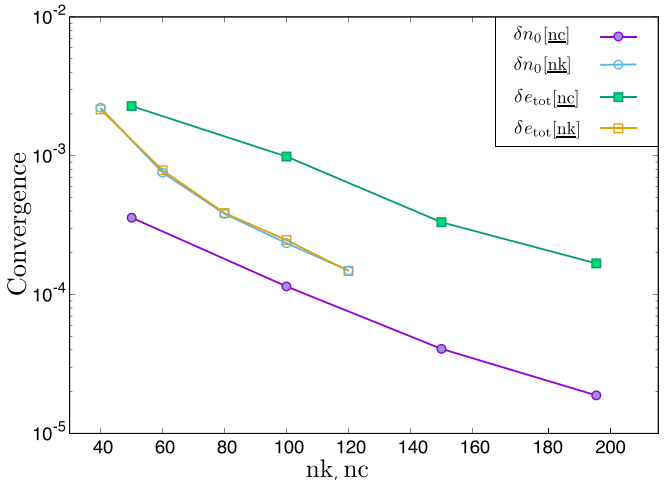

FIG. 12. Percent variation of the condensate fraction δn_0 [Eq. (B19)] and total energy $\delta e_{\rm tot}$ [Eq. (B18)] as a function of momentum space and angular grid vectors $\underline{\rm nc} = \{25, 50, 100, 150, 200\}$ and $\underline{\rm nk} = \{j \times (k_{\rm max}/n^{1/3})\}_{j=1}^6$, respectively. The simulation parameters that remained fixed to produce this data at density $nr_{\rm vdW}^3 = 3.0 \times 10^{-4}$ and time $t = t_{\rm n}$ are $k_{\rm max} = 2\Lambda$ and $\Delta t = m/2\hbar k_{\rm max}^2$, following the convergence guidelines in Sec. B 3.

APPENDIX C: QUADRUPLET CUMULANTS

To numerically simulate each of the quadruplets requires storing a six-dimensional complex array, which requires an enormous computational capacity and is beyond the present paper. Motivations of completeness aside, it is illustrative to discuss the explicit equations of motion for the quadruplets and to discuss their structure and formal solution in the early-time limit as we do in this section.

1. Equations of motion

Here, we give explicit expressions of the cubic $\langle[\hat{a}\hat{b}\hat{c}\hat{d}, \hat{H}_3]\rangle$ and quartic $\langle[\hat{a}\hat{b}\hat{c}\hat{d}, \hat{H}_4^{\rm eff}]\rangle$ contributions to the equations of motion for the quadruplets Eqs. (45)–(47). The contributions of the cubic Hamiltonian $\hat{H}_3$ are contractions of five-body operators, hence products of doublets and triplets:

$$\frac{\mathcal{Q}^{H_3}_{\alpha,\beta;\gamma}}{\sqrt{n_0/V}} = \mathcal{A}_{\{(\alpha,\beta),(\gamma,\delta)\}}\mathcal{S}_{\{\alpha,\beta\}}\mathcal{S}_{\{\gamma,\delta\}}\Bigg[\frac{V_\alpha}{2}(1+n_\alpha+n_\beta)M_{\gamma+\delta,\gamma} + \frac{V_\alpha+V_{\alpha+\beta}}{2}c_\alpha M_{\gamma+\delta,\gamma} + \frac{V_\beta+V_{\alpha+\beta}}{2}c_\alpha R^*_{\gamma,-\delta} + M^*_{\delta,\beta}\big\{(V_\gamma+V_{\alpha-\gamma})(n_\gamma-n_\alpha)+c^*_\gamma(V_\alpha+V_\gamma)\big\}\Bigg], \tag{C1}$$

$$\frac{\mathcal{P}^{H_3}_{\alpha,\beta,\gamma}}{\sqrt{n_0/V}} = \mathcal{S}_{\{\alpha,\beta,\gamma\}}\Bigg[V_\beta(1+n_\beta+n_\gamma)M^*_{\delta',\alpha} + \frac{V_\alpha+V_{\alpha-\delta'}}{2}(n_{\delta'}-n_\alpha)M^*_{\beta+\gamma,\beta} + \frac{V_{\delta'}+V_{\alpha-\delta'}}{2}(n_{\delta'}-n_\alpha)R_{\beta,-\gamma} + \frac{V_\alpha+V_{\delta'}}{2}(c^*_{\delta'}R_{\beta,-\gamma}-c_\alpha M^*_{\beta+\gamma,\beta}) + (V_\alpha+V_{\alpha+\beta})c_\alpha M^*_{\delta',\gamma} + (V_\beta+V_{\alpha+\beta})c_\alpha M_{\gamma,\delta'}\Bigg], \tag{C2}$$

$$\frac{\mathcal{T}^{H_3}_{\alpha,\beta,\gamma}}{\sqrt{n_0/V}} = \frac{\mathcal{S}_{\{\alpha,\beta,\gamma,\delta''\}}}{2}\Bigg[(V_\alpha+V_{\alpha+\beta})c_\alpha R_{\gamma,-\delta''} + (V_\alpha+V_\beta)\left(\frac{1}{2}+n_\alpha\right)R_{\gamma,-\delta''} + (V_\beta+V_{\alpha+\beta})c_\alpha M^*_{\gamma+\delta'',\gamma}\Bigg]. \tag{C3}$$

The contributions of the quartic Hamiltonian $\hat{H}_4^{\text{eff}}$ are the most difficult. Since they are contractions of six-body operators, they contain (i) products of (two or three) doublets, (ii) products of two triplets, and (iii) quadruplets eventually multiplied by a doublet. Separating those three contributions, we have

$$\mathcal{Q}^{H_4,\text{doub}}_{\alpha,\beta;\gamma} = \frac{1}{V}\mathcal{A}_{\{(\alpha,\beta),(\gamma,\delta)\}}\mathcal{S}_{\{\alpha,\beta\}}\mathcal{S}_{\{\gamma,\delta\}}\Bigg[V_{\gamma-\alpha}\left(\frac{1}{2}+n_\beta\right)n_\gamma n_\delta + (V_{\alpha+\beta}+V_{\alpha-\delta})c_\alpha c^*_\delta n_\gamma\Bigg], \tag{C4}$$

$$\mathcal{P}^{H_4,\text{doub}}_{\alpha,\beta,\gamma} = \frac{1}{V}\mathcal{S}_{\{\alpha,\beta,\gamma\}}[V_{\alpha+\gamma}(1+n_\alpha+n_\beta)c_\gamma n_{\delta'} + V_{\alpha+\beta}c_\alpha c_\gamma c^*_{\delta'} - V_{\alpha+\beta}c_\alpha n_\beta n_\gamma], \tag{C5}$$

$$\mathcal{T}^{H_4,\text{doub}}_{\alpha,\beta,\gamma} = \frac{1}{V}\mathcal{S}_{\{\alpha,\beta,\gamma,\delta''\}}\Bigg[V_{\alpha+\delta''}\left(\frac{1}{2}+n_\beta\right)c_\gamma c_{\delta''}\Bigg], \tag{C6}$$

$$\mathcal{Q}^{H_4,\text{tri}}_{\alpha,\beta;\gamma} = \frac{1}{V}\mathcal{A}_{\{(\alpha,\beta),(\gamma,\delta)\}}\mathcal{S}_{\{\alpha,\beta\}}\mathcal{S}_{\{\gamma,\delta\}}\sum_{\mathbf{q}}\Bigg[\frac{R^*_{\gamma,-\delta}}{2}V_{\mathbf{q}}R_{\alpha+\mathbf{q},-\beta} + \frac{M_{\gamma+\delta,\gamma}}{2}(V_\beta+V_{\mathbf{q}-\alpha})M^*_{\beta+\mathbf{q},\beta} + M_{\beta,\gamma}V_{\mathbf{q}}M^*_{\delta,\alpha+\mathbf{q}} + M^*_{\gamma,\beta}(V_\delta+V_{\mathbf{q}+\delta-\alpha})M_{\delta+\mathbf{q},\delta}\Bigg], \tag{C7}$$

$$\mathcal{P}^{H_4,\text{tri}}_{\alpha,\beta,\gamma} = \frac{1}{V}\mathcal{S}_{\{\alpha,\beta,\gamma\}}\sum_{\mathbf{q}}\Bigg[\frac{R_{\beta,-\gamma}}{2}(V_{\delta'}+V_{\mathbf{q}+\beta+\gamma})M_{\delta'+\mathbf{q},\delta'} + M^*_{\delta',\beta}(V_\alpha+V_{\mathbf{q}-\gamma})M^*_{\alpha+\mathbf{q},\alpha} + M^*_{\beta+\gamma,\beta}\frac{V_{\mathbf{q}}}{2}M^*_{\delta',\alpha-\mathbf{q}} + M_{\beta,\delta'}V_{\mathbf{q}}R_{\alpha,-\gamma-\mathbf{q}} - R_{\beta,-\gamma}\frac{V_{\mathbf{q}}}{2}M_{\alpha,\delta'-\mathbf{q}} - M^*_{\beta+\gamma,\beta}\frac{V_\alpha+V_{\mathbf{q}-\beta-\gamma}}{2}M^*_{\alpha+\mathbf{q},\alpha}\Bigg], \tag{C8}$$

$$\mathcal{T}^{H_4,\text{tri}}_{\alpha,\beta,\gamma} = \frac{1}{2V}\mathcal{S}_{\{\alpha,\beta,\gamma,\delta''\}}\sum_{\mathbf{q}}\big[M^*_{\gamma+\delta'',\gamma}V_{\mathbf{q}}R_{\alpha+\mathbf{q},-\beta} + R_{\gamma,-\delta''}(V_\beta+V_{\mathbf{q}-\alpha})M^*_{\beta+\mathbf{q},\beta}\big], \tag{C9}$$

$$\mathcal{Q}^{H_4,\text{quad}}_{\alpha,\beta,\gamma} = \frac{1}{V}\mathcal{A}_{\{(\alpha,\beta),(\gamma,\delta)\}}\mathcal{S}_{\{\alpha,\beta\}}\mathcal{S}_{\{\gamma,\delta\}}\sum_{\mathbf{q}}\Bigg[V_{\mathbf{q}}\frac{1+n_\alpha+n_\beta}{4}Q_{\alpha+\mathbf{q},\beta-\mathbf{q};\gamma} + (V_{\alpha-\gamma}+V_{\alpha-\mathbf{q}})\frac{n_\gamma-n_\alpha}{2}Q_{\beta,\mathbf{q};\delta} + V_{\mathbf{q}}c^*_\gamma P_{\alpha+\mathbf{q},\beta,-\gamma-\mathbf{q}} + \frac{V_{\alpha+\beta}+V_{\mathbf{q}+\beta}}{2}c_\beta P^*_{\gamma,\delta,\mathbf{q}}\Bigg], \tag{C10}$$

$$\mathcal{P}^{H_4,\text{quad}}_{\alpha,\beta,\gamma} = \frac{1}{2V}\mathcal{S}_{\{\alpha,\beta,\gamma\}}\sum_{\mathbf{q}}[V_{\mathbf{q}}(1+n_\alpha+n_\beta)P_{\alpha+\mathbf{q},\beta-\mathbf{q},\gamma} + (V_{\alpha-\delta'}+V_{\alpha-\mathbf{q}})(n_{\delta'}-n_\alpha)P_{\beta,\gamma,\mathbf{q}} + V_{\mathbf{q}}c_{\delta'}{}^*T_{\alpha+\mathbf{q},\beta,\gamma} + 2(V_{\alpha+\beta}+V_{\mathbf{q}-\beta})c_\alpha Q_{\gamma,\mathbf{q};\delta'} - V_{\mathbf{q}}c_\alpha Q_{\beta,\gamma;\delta'-\mathbf{q}}\Bigg], \tag{C11}$$

$$\mathcal{T}^{H_4,\text{quad}}_{\alpha,\beta,\gamma} = \frac{1}{2V}\mathcal{S}_{\{\alpha,\beta,\gamma,\delta''\}}\sum_{\mathbf{q}}\Bigg[V_{\mathbf{q}}\left(n_\beta+\frac{1}{2}\right)T_{\alpha+\mathbf{q},\gamma,\delta''} + (V_{\gamma+\delta''}+V_{\alpha-\mathbf{q}})c_\beta P_{\mathbf{q},\gamma,\delta''}\Bigg]. \tag{C12}$$

Here the replacements of $\delta \to \alpha+\beta-\gamma$, $\delta' \to \alpha+\beta+\gamma$, and $\delta'' \to -\alpha-\beta-\gamma$ should be done after acting with the symmetrizer and antisymetrizer.

2. Solution

The length expressions in Eqs. (C4)–(C12) hide the underlying structure of the quadruplet equations of motion as coupled few-body Schrödinger equations with nonlinear and drive terms. In this section, we follow Sec. III D and reduce these equations to their early-time form to make this structure explicit and to illustrate how one-, two-, three-, and four-body physics are encoded in the formal solutions.

First, we begin by reduced the equation of motion for the Q cumulant [Eq. (45)] to the early-time form

$$i\hbar\partial_t|Q_t,Q_t\rangle\langle Q_t,Q_t| = \hat{H}_{12}(t)|Q_t,Q_t\rangle\langle Q_t,Q_t| - |Q_t,Q_t\rangle\langle Q_t,Q_t|\hat{H}_{12}(t) + (1+\hat{P}_{12})\hat{V}[|\psi_t,M_t\rangle\langle M_t,M_t| + |n_{1,t},n_{2,t}\rangle\langle n_{2,t},n_{1,t}|]$$
$$- [|M_t,M_t\rangle\langle M_t,\psi_{0,t}| + |n_{1,t},n_{2,t}\rangle\langle n_{2,t},n_{1,t}|]\hat{V}(1+\hat{P}_{12}), \tag{C13}$$

where we have defined the rank (2,2) tensors $\langle\alpha,\beta|Q_t,Q_t\rangle\langle Q_t,Q_t|\gamma,\delta\rangle = VQ_{\alpha\beta;\gamma}(t)\delta_{\alpha+\beta,-\delta-\gamma}$ and

$$\langle\alpha,\beta|n_{1,t},n_{2,t}\rangle\langle n_{2,t},n_{1,t}|\delta,\gamma\rangle = n_\alpha(t)n_\beta(t)\delta_{\alpha,\gamma}\delta_{\beta,\delta}. \tag{C14}$$

Equation (C13) can be solved formally as

$$|Q_t,Q_t\rangle\langle Q_t,Q_t| = \hat{\mathcal{U}}_{12}(t-t_0)|Q_{t_0},Q_{t_0}\rangle\langle Q_{t_0},Q_{t_0}|\hat{\mathcal{U}}_{12}(t_0-t)$$
$$+\frac{1}{i\hbar}\int_{t_0}^{t}d\tau\hat{\mathcal{U}}_{12}(t-\tau)\hat{V}(1+\hat{P}_{12})[|\psi_{0,\tau},M_\tau\rangle\langle M_\tau,M_\tau| + |n_{1,\tau},n_{2,\tau}\rangle\langle n_{2,\tau},n_{1,\tau}|](\hat{\mathcal{U}}_{12}(\tau-t)$$
$$-\frac{1}{i\hbar}\int_{t_0}^{t}d\tau\hat{\mathcal{U}}_{12}(t-\tau)[|M_\tau,M_\tau\rangle\langle\psi_{0,\tau},M_\tau| + |n_{1,\tau},n_{2,\tau}\rangle\langle n_{2,\tau},n_{1,\tau}|](1+\hat{P}_{12})\hat{V}\hat{\mathcal{U}}_{12}(\tau-t). \tag{C15}$$

Here, we see that the $|n_{1,\tau},n_{2,\tau}\rangle\langle n_{2,\tau},n_{1,\tau}|$ parts of the memory kernel describes forward and backward Boltzmannian scattering in a classical dilute gas [37]. Including this contribution of Q in $\dot{n}_k$ it is possible to retrieve the Boltzmann equation describing two-body scattering as the level of the T matrix (cf. Ref. [98]).

Next, we reduce the equations of motion for the P cumulant [Eq. (46)] to the early time form

$$i\hbar\partial_t|P_t,P_t,P_t\rangle\langle P_t| = \hat{H}_{123}(t)|P_t,P_t,P_t\rangle\langle P_t| - |P_t,P_t,P_t\rangle\langle P_t|\hat{H}_1(t) + (1+\hat{P}_+ + \hat{P}_-)(\hat{V}_{12}+\hat{V}_{13})[|n_t,c_t,c_t\rangle\langle n_t|$$
$$+|\psi_{0,t},M_t,M_t\rangle\langle M_t|], \tag{C16}$$

where we have defined the rank (1,3) tensor $\langle\alpha,\beta,\gamma|P_t,P_t,P_t\rangle\langle P_t|\delta\rangle = VP_{\alpha,\beta,\gamma}(t)\delta_{\alpha+\beta+\gamma,\delta}$. Equation (C16) can be formally solved as

$$|P_t,P_t,P_t\rangle\langle P_t| = \hat{\mathcal{U}}_{123}(t-t_0)|P_{t_0},P_{t_0},P_{t_0}\rangle\langle P_{t_0}|\hat{\mathcal{U}}_1(t_0-t) + \frac{1}{i\hbar}\int_{t_0}^{t}d\tau\hat{\mathcal{U}}_{123}(t-\tau)(1+\hat{P}_+ + \hat{P}_-)(\hat{V}_{12}+\hat{V}_{13})[|n_\tau,c_\tau,c_\tau\rangle\langle n_\tau|$$
$$+|\psi_{0,\tau},M_\tau,M_\tau\rangle\langle M_\tau|]\hat{\mathcal{U}}_1(\tau-t). \tag{C17}$$

Finally, the T cumulant equation of motion reduces to the early-time form

$$i\hbar\partial_t|T_t,T_t,T_t,T_t\rangle = \hat{H}_{1234}(t)|T_t,T_t,T_t,T_t\rangle + (1+\hat{P}_{1234}+\hat{P}_{1324}+\hat{P}_{1423})\big(\hat{V}_{12}+\hat{V}_{13}+\hat{V}_{14}\big)|\psi_{0,t},R_t,R_t,R_t\rangle$$
$$+\big(1+\hat{P}_{234}+\hat{P}_{243}\big)\big(\hat{V}_{13}+\hat{V}_{14}+\hat{V}_{23}+\hat{V}_{24}\big)|c_{1,t},c_{1,t},c_{2,t},c_{2,t}\rangle, \tag{C18}$$

with $\hat{P}_{1234}|\alpha,\beta,\gamma,\delta\rangle = |\delta,\alpha,\beta,\gamma\rangle$, and where we have defined the range (0,4) tensor $\langle\alpha,\beta,\gamma,\delta|T_t,T_t,T_t,T_t\rangle = VT_{\alpha,\beta,\gamma}(t)\delta_{\alpha+\beta,-\gamma-\delta}$ and $\hat{H}_{1234} = \sum_{i<j}^{4}\hat{H}_{ij}(t)$ as the vacuum four-body Hamiltonian in the rotating frame of the condensate. Equation (C18) can be formally solved as

$$|T_t,T_t,T_t,T_t\rangle = \hat{\mathcal{U}}_{1234}(t-t_0)|T_{t_0},T_{t_0},T_{t_0},T_{t_0}\rangle$$
$$+\frac{1}{i\hbar}\int_{t_0}^{t}d\tau\hat{\mathcal{U}}_{1234}(t-\tau)(1+\hat{P}_{1234}+\hat{P}_{1324}+\hat{P}_{1423})\big(\hat{V}_{12}+\hat{V}_{13}+\hat{V}_{14}\big)|\psi_{0,\tau},R_\tau,R_\tau,R_\tau\rangle$$
$$+\frac{1}{i\hbar}\int_{t_0}^{t}d\tau\hat{\mathcal{U}}_{1234}(t-\tau)\big(1+\hat{P}_{234}+\hat{P}_{243}\big)\big(\hat{V}_{13}+\hat{V}_{14}+\hat{V}_{23}+\hat{V}_{24}\big)|c_{1,\tau},c_{1,\tau},c_{2,\tau},c_{2,\tau}\rangle, \tag{C19}$$

where $\hat{\mathcal{U}}_{1234}(t) = \exp[-i\int_{t_0}^{t}d\tau\hat{H}_{1234}(\tau)/\hbar]$ is the four-body evolution operator in the rotating frame of the condensate. Analogous the connection between Eq. (59) and the Faddeev equations [see Sec. III D and Refs. [44,63]), Eq. (C18)] yields generalized four-body T matrices satisfying the Yakubovsky equations [92]. To include the physics of the four-body bound states tied to Efimov states [18–20,99] in the cumulant theory of the unitary Bose gas, the hi-

erarchy must be taken then to at least the quadruplet level.

APPENDIX D: RELATION TO ALTERNATIVE APPROACHES

To construct the cumulant theory used in this paper, we make two main approximations. First, we describe Bose condensation in the $U(1)$-symmetry-breaking approach and, second, we truncate the cumulant hierarchy to consider cumulants only up to some finite order. In this Appendix, we first connect with the number-conserving description of Bose-condensation [100,101] in Sec. D 1. Second, we group many equivalent models of the quenched unitary Bose gas found in the literature [33–35,44–46] under the umbrella of the doublet model presented in the present paper in Sec. D 2. In Sec. III, the connection between the HFB theory and the doublet model was already established. We note that the Popov and bath theories of Refs. [75,102,103] both set the effective interaction strength g in an *ad hoc* fashion and ignored the c-cumulant dynamics. These works are not consistent with the unitarity limit of the s-wave cross section $\sigma \propto 1/k^2$ and therefore do not describe resonant scattering processes. We remark that the Hyperbolic Bloch equations, derived in Ref. [42] [see Eqs. (37) and (38)], have not been simulated to date as they require handling of the resource-intensive quadruplets. The triplet model studied in Sec. V represents the state of the art in this regard. Although these are mostly formal remarks, making distinctions and connections between approaches is instructive both for understanding the limitations of the present paper and for uniting equivalent lines of research on the quenched unitary Bose gas.

1. Number-conserving approach

In the number-conserving approach, one performs a quantum modulus-phase decomposition of the condensate operator $\hat{a}_0$:

$$\hat{a}_0 = e^{i\hat{\theta}_0}\sqrt{\hat{N}_0}. \tag{D1}$$

The phase $\hat{\theta}_0$ and population $\hat{N}_0$ of the condensate are canonically conjugated:

$$\left[\hat{\theta}_0, \hat{N}_0\right] = -i. \tag{D2}$$

They inherit this relation from the bosonic nature of $\hat{a}_0$. Note that this phase-modulus decomposition is possible only in the approximation that the condensate is never empty.

We then introduce the excitation field for $\mathbf{k} \neq 0$:

$$\hat{\Lambda}_{\mathbf{k}} = e^{-i\hat{\theta}_0}\hat{a}_{\mathbf{k}}. \tag{D3}$$

Conceptually, the advantage of using $\hat{\Lambda}_{\mathbf{k}}$ rather than $\hat{b}_{\mathbf{k}}$ as in the main text is that $\hat{\Lambda}_{\mathbf{k}}$ conserves the number of particles (it transfers one particle from the noncondensed fraction to the condensate). Thus, one can still have nonzero anomalous averages $\langle\hat{\Lambda}\hat{\Lambda}\rangle \neq 0$ even in states with a fixed number of particles. In terms of $\hat{\Lambda}$, $\hat{\Lambda}^\dagger$, and $\hat{N}_0$, the Hamiltonian reads

$$\hat{H}^{(\mathrm{NC})} = \frac{V_{\mathbf{0}}N^2}{2V} + \sum_{\mathbf{k}}\left(\left[\epsilon_{\mathbf{k}} + \frac{V_{\mathbf{k}}\hat{N}_0}{V}\right]\hat{\Lambda}^\dagger_{\mathbf{k}}\hat{\Lambda}_{\mathbf{k}} + \frac{V_{\mathbf{k}}\sqrt{\hat{N}_0(\hat{N}_0-1)}}{2V}[\hat{\Lambda}_{-\mathbf{k}}\hat{\Lambda}_{\mathbf{k}} + \hat{\Lambda}^\dagger_{\mathbf{k}}\hat{\Lambda}^\dagger_{-\mathbf{k}}]\right)$$
$$+\frac{\sqrt{\hat{N}_0}}{V}\sum_{\mathbf{k},\mathbf{q}} V_{\mathbf{q}}\left(\hat{\Lambda}^\dagger_{\mathbf{k}+\mathbf{q}}\hat{\Lambda}_{\mathbf{k}}\hat{\Lambda}_{\mathbf{q}} + \mathrm{H.c.}\right) + \frac{1}{2V}\sum_{\mathbf{k},\mathbf{k}',\mathbf{q}} V_{\mathbf{q}}\Lambda^\dagger_{\mathbf{k}'+\mathbf{q}}\hat{\Lambda}^\dagger_{\mathbf{k}-\mathbf{q}}\hat{\Lambda}_{\mathbf{k}}\hat{\Lambda}_{\mathbf{k}'}. \tag{D4}$$

To avoid cumbersome restrictions in the sums over $\mathbf{k}, \mathbf{k}'$ and $\mathbf{q}$, we set $\hat{\Lambda}_{\mathbf{0}} = 0$ by convention. Here, we collected the terms proportional to $V_{\mathbf{0}}$ in the constant first term using conservation of the total number of particles $N = \hat{N}_0 + \sum_{\mathbf{k}}\hat{\Lambda}^\dagger_{\mathbf{k}}\hat{\Lambda}_{\mathbf{k}}$. Although not done in the main text (Sec. II B), we note that such simplification is also possible in the symmetry-breaking picture. In Eq. (D4), we have kept the $O(1/\langle\hat{N}_0\rangle)$ corrections that come from the noncommutation of $\hat{\theta}_0$ and $\hat{N}_0$. In the thermodynamic limit, these corrections are negligible (as long as the condensate is macroscopically occupied).

We use the approach of Ref. [41] to identify all the terms that become negligible in the thermodynamic limit. We define $N_0(t) \equiv \langle\hat{N}_0\rangle$ and write $\hat{N}_0 = N_0(t) + \delta\hat{N}_0$, and similarly for the macroscopic sums of the noncondensed field, for example, $\sum_{\mathbf{k}}\hat{\Lambda}^\dagger_{\mathbf{k}}\hat{\Lambda}_{\mathbf{k}} = \sum_{\mathbf{k}}\langle\hat{\Lambda}^\dagger_{\mathbf{k}}\hat{\Lambda}_{\mathbf{k}}\rangle + \sum_{\mathbf{k}}\delta(\hat{\Lambda}^\dagger_{\mathbf{k}}\hat{\Lambda}_{\mathbf{k}})$. The product of fluctuations is of order $O(1/\sqrt{N})$ smaller than the leading (nonscalar) terms in the Hamiltonian, so it can be neglected. We then obtain

$$\hat{H}^{(\mathrm{NC})} \simeq \frac{V_{\mathbf{0}}Nn}{2} + \sum_{\mathbf{k}}\left([\epsilon_{\mathbf{k}} + V_{\mathbf{k}}n_0(t)]\hat{\Lambda}^\dagger_{\mathbf{k}}\hat{\Lambda}_{\mathbf{k}} + \frac{V_{\mathbf{k}}n_0(t)}{2}[\hat{\Lambda}_{-\mathbf{k}}\hat{\Lambda}_{\mathbf{k}} + \hat{\Lambda}^\dagger_{\mathbf{k}}\hat{\Lambda}^\dagger_{-\mathbf{k}}]\right)$$
$$+\sqrt{\frac{n_0(t)}{V}}\sum_{\mathbf{k},\mathbf{q}} V_{\mathbf{q}}\left(\hat{\Lambda}^\dagger_{\mathbf{k}+\mathbf{q}}\hat{\Lambda}_{\mathbf{k}}\hat{\Lambda}_{\mathbf{q}} + \mathrm{H.c.}\right) + \frac{1}{2V}\sum_{\mathbf{k},\mathbf{k}',\mathbf{q}} V_{\mathbf{q}}\Lambda^\dagger_{\mathbf{k}'+\mathbf{q}}\hat{\Lambda}^\dagger_{\mathbf{k}-\mathbf{q}}\hat{\Lambda}_{\mathbf{k}}\hat{\Lambda}_{\mathbf{k}'} - (\hat{N}_0 - N_0(t))\left\langle\hbar\frac{d\hat{\theta}_0}{dt}\right\rangle. \tag{D5}$$

This Hamiltonian is the same as $\hat{H}_b$ [Eq. (8)], the Hamiltonian found in the symmetry-breaking approach (up to the replacement $\hat{b} \to \hat{\Lambda}$, and the collection of the terms containing $V_{\mathbf{0}}$ discussed above). To show the complete equivalence of the two theories, we calculate the phase derivative in the number-conserving approach from the commutator of $\hat{N}_0$ with the exact expression (D4) of the Hamiltonian,

$$\left\langle \hbar \frac{d\hat{\theta}_0}{dt} \right\rangle = -\frac{1}{V}\sum_{\mathbf{k}} \left[V_{\mathbf{k}} \langle \hat{\Lambda}^\dagger_{\mathbf{k}} \hat{\Lambda}_{\mathbf{k}} \rangle + \frac{V_{\mathbf{k}}}{2} \left(\langle \hat{\Lambda}_{-\mathbf{k}} \hat{\Lambda}_{\mathbf{k}} \rangle + \text{cc.} \right) \right] - \frac{1}{2\sqrt{n_0 V^3}} \sum_{\mathbf{kq}} V_{\mathbf{q}} \left(\langle \hat{\Lambda}^\dagger_{\mathbf{k}+\mathbf{q}} \hat{\Lambda}_{\mathbf{k}} \hat{\Lambda}_{\mathbf{q}} \rangle + \text{cc.} \right), \tag{D6}$$

which is the same as (11), up to the constant rotation velocity $V_{\mathbf{0}} n$.

2. Nozières-Saint James approach

The time-dependent generalization of the NSJ approach [33–35,46,74] is based on the variational ansatz for the ground-state wave function,

$$|\Psi_{\text{NSJ}}(t)\rangle = \frac{1}{\mathcal{N}} \exp\left[\sqrt{V} \alpha_0(t) \hat{a}^\dagger_0 + \frac{1}{2} \sum_{\mathbf{k}} \beta_{\mathbf{k}}(t) \hat{a}^\dagger_{-\mathbf{k}} \hat{a}^\dagger_{\mathbf{k}} \right] |0\rangle, \tag{D7}$$

with normalization factor $\mathcal{N}$, variational parameters $\alpha_0(t)$ and $\beta_{\mathbf{k}}(t)$, and factor of $1/2$ in the summation to account for double counting of pairs $(\mathbf{k}, -\mathbf{k})$. The NSJ variational parameters are connected to the single and doublet cumulants as $\psi_0 = \alpha_0$, $\tilde{c}_{\mathbf{k}} = \beta_{\mathbf{k}}/(1-|\beta_{\mathbf{k}}|^2)$, and $n_{\mathbf{k}} = |\beta_{\mathbf{k}}|^2/(1-|\beta_{\mathbf{k}}|^2)$ with total number $N = |\alpha_0|^2 + \sum_{\mathbf{k}} |\beta_{\mathbf{k}}|^2/(1-|\beta_{\mathbf{k}}|^2)$. The equation of motion for $\alpha_0(t)$ corresponding to the Hamiltonian [Eq. (2)] is

$$i\hbar \frac{d\alpha_0}{dt} = n V_{\mathbf{0}} \alpha_0 + \alpha_0 \frac{1}{V} \sum_{\mathbf{k}} V_{\mathbf{k}} \frac{|\beta_{\mathbf{k}}|^2}{1-|\beta_{\mathbf{k}}|^2} + \alpha_0^* \frac{1}{V} \sum_{\mathbf{k}} V_{\mathbf{k}} \frac{\beta_{\mathbf{k}}}{1-|\beta_{\mathbf{k}}|^2}, \tag{D8}$$

where the term by term equivalence with the GPE [Eq. (5)] (for vanishing triplet contributions) is apparent. The corresponding equation of motion for $\beta_{\mathbf{k}}(t)$ is

$$i\hbar \frac{d\beta_{\mathbf{k}}}{dt} = 2(\epsilon_{\mathbf{k}} + V_{\mathbf{0}} n)\beta_{\mathbf{k}} + V_{\mathbf{k}} \left(\alpha_0^2 + (\alpha_0^*)^2 \beta_{\mathbf{k}}^2 + 2|\alpha_0|^2 \beta_{\mathbf{k}} \right) + \frac{1}{V} \sum_{\mathbf{q}} V_{\mathbf{k}-\mathbf{q}} \frac{2|\beta_{\mathbf{q}}|^2 \beta_{\mathbf{k}} + \beta_{\mathbf{q}} + \beta_{\mathbf{q}}^* \beta_{\mathbf{k}}^2}{1-|\beta_{\mathbf{q}}|^2}. \tag{D9}$$

To evaluate the equation of motion for the c cumulant, we consider the corresponding expression in the NSJ approach,

$$i\hbar \frac{d}{dt}\left(\frac{\beta_{\mathbf{k}}}{1-|\beta_{\mathbf{k}}|^2} \right) = i\hbar \frac{d\beta_{\mathbf{k}}}{dt} \frac{1}{(1-|\beta_{\mathbf{k}}|^2)^2} - \left(-i\hbar \frac{d\beta_{\mathbf{k}}^*}{dt} \right) \frac{\beta_{\mathbf{k}}^2}{(1-|\beta_{\mathbf{k}}|^2)^2}, \tag{D10}$$

$$= \left[2(\epsilon_{\mathbf{k}} + V_{\mathbf{0}} n) c_{\mathbf{k}} + 2\left(V_{\mathbf{k}} n_0 + \frac{1}{V} \sum_{\mathbf{q}} V_{\mathbf{k}-\mathbf{q}} n_{\mathbf{q}} \right) c_{\mathbf{k}} \right] \left[\frac{1}{1-|\beta_{\mathbf{k}}|^2} - \frac{|\beta_{\mathbf{k}}|^2}{1-|\beta_{\mathbf{k}}|^2} \right]$$

$$+ \left[V_{\mathbf{k}} \psi_0^2 + \frac{1}{V} \sum_{\mathbf{q}} V_{\mathbf{k}-\mathbf{q}} c_{\mathbf{q}} \right] \left[\frac{1}{(1-|\beta_{\mathbf{k}}|^2)^2} - \frac{|\beta_{\mathbf{k}}|^4}{(1-|\beta_{\mathbf{k}}|^2)^2} \right], \tag{D11}$$

where

$$\left[\frac{1}{(1-|\beta_{\mathbf{k}}|^2)^2} - \frac{|\beta_{\mathbf{k}}|^4}{(1-|\beta_{\mathbf{k}}|^2)^2} \right] = 1 + 2n_{\mathbf{k}}. \tag{D12}$$

From the relation $|c_{\mathbf{k}}|^2 = n_{\mathbf{k}}(n_{\mathbf{k}}+1)$, which is clear from the definitions of $\tilde{c}_{\mathbf{k}}$ and $n_{\mathbf{k}}$ in terms of the variational parameters, the equation of motion for $\dot{n}$ follows immediately. Finally setting $c_{\mathbf{k}} = e^{-2i\theta_0} \tilde{c}_{\mathbf{k}}$ to switch to the rotating frame of the condensate, we see then that the NSJ approach yields equations of motion that are identical to the doublet model [Eqs. (5), (37), and (38)] considered in this paper. Therefore, both the NSJ and HFB approaches are equivalent to each other, as also suggested in Ref. [46], and all correspond to a truncation of the cumulant hierarchy at the doublet level.

[1] L. Pitaevskii and S. Stringari, *Bose-Einstein Condensation and Superfluidity*, Vol. 164 (Oxford University Press, Clarendon, Oxford, 2016).

[2] M. Greiner, C. A. Regal, and D. S. Jin, Nature **426**, 537 (2003).

[3] M. W. Zwierlein, C. A. Stan, C. H. Schunck, S. M. F. Raupach, S. Gupta, Z. Hadzibabic, and W. Ketterle, Phys. Rev. Lett. **91**, 250401 (2003).

[4] S. Jochim, M. Bartenstein, A. Altmeyer, G. Hendl, S. Riedl, C. Chin, J. Hecker Denschlag, and R. Grimm, Science **302**, 2101 (2003).

[5] N. Navon, S. Nascimbène, F. Chevy, and C. Salomon, Science **328**, 729 (2010).

[6] M. Horikoshi, S. Nakajima, M. Ueda, and T. Mukaiyama, Science **327**, 442 (2010).

[7] M. J. H. Ku, A. T. Sommer, L. W. Cheuk, and M. W. Zwierlein, Science **335**, 563 (2012).

[8] W. Zwerger, *The BCS-BEC Crossover and the Unitary Fermi Gas*, Vol. 836 (Springer-Verlag, Berlin, Heidelberg, 2011).

[9] D. T. Son, Phys. Rev. Lett. **98**, 020604 (2007).

[10] C. Cao, E. Elliott, J. Joseph, H. Wu, J. Petricka, T. Schäfer, and J. E. Thomas, Science **331**, 58 (2011).

[11] T.-L. Ho and E. J. Mueller, Phys. Rev. Lett. **92**, 160404 (2004).

[12] M. L. Chiofalo, S. J. J. M. F. Kokkelmans, J. N. Milstein, and M. J. Holland, Phys. Rev. Lett. **88**, 090402 (2002).

[13] M. Holland, S. J. J. M. F. Kokkelmans, M. L. Chiofalo, and R. Walser, Phys. Rev. Lett. **87**, 120406 (2001).

[14] K. Van Houcke, F. Werner, E. Kozik, N. Prokof'ev, B. Svistunov, M. J. H. Ku, A. T. Sommer, L. W. Cheuk, A. Schirotzek, and M. W. Zwierlein, Nat. Phys. **8**, 366 (2012).

[15] J. Levinsen, P. Massignan, S. Endo, and M. M. Parish, J. Phys. B: At., Mol. Opt. Phys. **50**, 072001 (2017).

[16] V. Efimov, Sov. J. Nucl. Phys **12**, 101 (1971).

[17] V. Efimov, Sov. J. Nucl. Phys. **29**, 546 (1979).

[18] E. Braaten and H.-W. Hammer, Phys. Rep. **428**, 259 (2006).

[19] J. P. D'Incao, J. Phys. B: At., Mol. Opt. Phys. **51**, 043001 (2018).

[20] P. Naidon and S. Endo, Rep. Prog. Phys. **80**, 056001 (2017).

[21] C. H. Greene, P. Giannakeas, and J. Pérez-Ríos, Rev. Mod. Phys. **89**, 035006 (2017).

[22] Y. Nishida, Phys. Rev. Lett. **109**, 240401 (2012).

[23] H. Tajima and P. Naidon, New J. Phys. **21**, 073051 (2019).

[24] P. Makotyn, C. E. Klauss, D. L. Goldberger, E. Cornell, and D. S. Jin, Nat. Phys. **10**, 116 (2014).

[25] C. E. Klauss, X. Xie, C. Lopez-Abadia, J. P. D'Incao, Z. Hadzibabic, D. S. Jin, and E. A. Cornell, Phys. Rev. Lett. **119**, 143401 (2017).

[26] C. Eigen, J. A. P. Glidden, R. Lopes, N. Navon, Z. Hadzibabic, and R. P. Smith, Phys. Rev. Lett. **119**, 250404 (2017).

[27] C. Eigen, J. A. P. Glidden, R. Lopes, E. A. Cornell, R. P. Smith, and Z. Hadzibabic, Nature **556**, 221 (2018).

[28] J. P. D'Incao, J. Wang, and V. E. Colussi, Phys. Rev. Lett. **121**, 023401 (2018).

[29] V. E. Colussi, J. P. Corson, and J. P. D'Incao, Phys. Rev. Lett. **120**, 100401 (2018).

[30] V. E. Colussi, B. E. van Zwol, J. P. D'Incao, and S. J. J. M. F. Kokkelmans, Phys. Rev. A **99**, 043604 (2019).

[31] J. Berges, S. Borsányi, and C. Wetterich, Phys. Rev. Lett. **93**, 142002 (2004).

[32] M. Van Regemortel, H. Kurkjian, M. Wouters, and I. Carusotto, Phys. Rev. A **98**, 053612 (2018).

[33] A. G. Sykes, J. P. Corson, J. P. D'Incao, A. P. Koller, C. H. Greene, A. M. Rey, K. R. A. Hazzard, and J. L. Bohn, Phys. Rev. A **89**, 021601(R) (2014).

[34] C. Gao, M. Sun, P. Zhang, and H. Zhai, Phys. Rev. Lett. **124**, 040403 (2020).

[35] A. Muñoz de las Heras, M. M. Parish, and F. M. Marchetti, Phys. Rev. A **99**, 023623 (2019).

[36] E. A. Yuzbashyan, M. Dzero, V. Gurarie, and M. S. Foster, Phys. Rev. A **91**, 033628 (2015).

[37] K. Huang, *Statistical Mechanics* (Wiley, New York, 1987).

[38] J. Fricke, Ann. Phys. **252**, 479 (1996).

[39] T. Köhler and K. Burnett, Phys. Rev. A **65**, 033601 (2002).

[40] M. Kira and S. W. Koch, *Semiconductor Quantum Optics* (Cambridge University Press, Cambridge, 2011).

[41] M. Kira, Ann. Phys. **351**, 200 (2014).

[42] M. Kira, Ann. Phys. **356**, 185 (2015).

[43] M. Kira, Nat. Commun. **6**, 6624 (2015).

[44] V. E. Colussi, S. Musolino, and S. J. J. M. F. Kokkelmans, Phys. Rev. A **98**, 051601(R) (2018).

[45] S. Musolino, V. E. Colussi, and S. J. J. M. F. Kokkelmans, Phys. Rev. A **100**, 013612 (2019).

[46] J. P. Corson and J. L. Bohn, Phys. Rev. A **91**, 013616 (2015).

[47] C. Chin, R. Grimm, P. Julienne, and E. Tiesinga, Rev. Mod. Phys. **82**, 1225 (2010).

[48] J. R. Taylor, *Scattering Theory: The Quantum Theory of Nonrelativistic Collisions* (Courier Corporation, North Chelmsford, 2006).

[49] T. Köhler, T. Gasenzer, and K. Burnett, Phys. Rev. A **67**, 013601 (2003).

[50] V. V. Flambaum, G. F. Gribakin, and C. Harabati, Phys. Rev. A **59**, 1998 (1999).

[51] In Appendix D1, we show that our symmetry-breaking approach is equivalent to a number-conserving one in the thermodynamic limit.

[52] To avoid restrictions on the summations, we use the convention $\hat{b}_{\mathbf{0}} = 0$.

[53] A. Sinatra, Y. Castin, and E. Witkowska, Phys. Rev. A **80**, 033614 (2009).

[54] H. Kurkjian, Y. Castin, and A. Sinatra, Comptes Rendus Physique **17**, 789 (2016).

[55] J.-P. Blaizot and G. Ripka, *Quantum Theory of Finite Systems* (MIT Press, Cambridge, MA, 1985).

[56] A partial contraction is the replacement $\hat{a}\hat{b}\hat{c}\hat{d} \to \langle\hat{a}\hat{b}\rangle\hat{c}\hat{d} + \hat{a}\hat{b}\langle\hat{c}\hat{d}\rangle + \langle\hat{a}\hat{c}\rangle\hat{b}\hat{d} + \ldots$.

[57] H. R. Glyde, R. T. Azuah, and W. G. Stirling, Phys. Rev. B **62**, 14337 (2000).

[58] In the formal equations of motion (24)–(26) and (28)–(30), the operators $\hat{a}, \hat{b}, \hat{c}, \hat{d} \in \{\hat{b}^\dagger_{\mathbf{k}}, \hat{b}_{\mathbf{k}}\}_{\mathbf{k}\neq 0}$ are normally ordered .

[59] The equation of motion of the cumulant $\langle\hat{a}\hat{b}\hat{c}\hat{d}\rangle_c$ is deduced from that of the moment Eq. (30) using $i\hbar\partial_t\langle\hat{a}\hat{b}\hat{c}\hat{d}\rangle - i\hbar\partial_t\langle\hat{a}\hat{b}\hat{c}\hat{d}\rangle_c = \langle[\langle\hat{a}\hat{b}\rangle\hat{c}\hat{d} + \langle\hat{c}\hat{d}\rangle\hat{a}\hat{b}, \hat{H}_b]\rangle + \langle[\langle\hat{a}\hat{c}\rangle\hat{b}\hat{d} + \langle\hat{b}\hat{d}\rangle\hat{a}\hat{c} + \langle\hat{a}\hat{d}\rangle\hat{b}\hat{c} + \langle\hat{b}\hat{c}\rangle\hat{a}\hat{d}, \hat{H}_b]\rangle$. In practice, this removes from (30) (i) the nonquadruplet part of $\langle[\hat{a}\hat{b}\hat{c}\hat{d}, \hat{H}_2^{\text{eff}}]\rangle$ and (ii) the "reducible" contractions in $\langle[\hat{a}\hat{b}\hat{c}\hat{d}, \hat{H}_3 + \hat{H}_4^{\text{eff}}]\rangle$, i.e., those where a doublet is formed from two elements in $\{\hat{a}, \hat{b}, \hat{c}, \hat{d}\}$.

[60] This program uses the SNEG package [104] for basic second quantization operations such as commutation relations and is available online at https://doi.org/10.4121/uuid:720f48bc-e64e-47e1-8910-09f6832a09bb.

[61] N. Proukakis and K. Burnett, J. Res. Natl. Inst. Stand. Technol. **101**, 457 (1996).

[62] R. G. Newton, *Scattering Theory of Waves and Particles* (Springer-Verlag, Berlin, Heidelberg, 2013).

[63] T. Köhler, Phys. Rev. Lett. **89**, 210404 (2002).

[64] P. M. A. Mestrom, V. E. Colussi, T. Secker, and S. J. J. M. F. Kokkelmans, Phys. Rev. A **100**, 050702(R) (2019).

[65] P. M. A. Mestrom, V. E. Colussi, T. Secker, G. P. Groeneveld, and S. J. J. M. F. Kokkelmans, Phys. Rev. Lett. **124**, 143401 (2020).

[66] S. Tan, Phys. Rev. A **78**, 013636 (2008).

[67] We have ignored the coupling between channels, which is generally weak at unitarity [105].

[68] For evidence that this oscillation frequency is time independent in the laboratory frame at very long times ($t \sim 100 t_{\rm n}$), we direct the reader to Fig. 1 in the Supplemental Material of Ref. [34].

[69] Z. Hadzibabic, C. Eigen, J. Glidden, R. Lopes, R. Smith, and E. Cornell (2018). Research data supporting "Universal Prethermal Dynamics of Bose Gases Quenched to Unitarity" [Dataset]. https://doi.org/10.17863/CAM.30242.

[70] We note that the experimental momentum distribution is normalized as $1 = \int d^3k n_{\mathbf{k}}^{(\rm exp)}$, which gives the conversion $k_{\rm n}^3 n_{\mathbf{k}}^{(\rm exp)} = 3n_{\mathbf{k}}/4$.

[71] Although we have followed the fitting routine used on the experimental data in Ref. [27], the dynamics of $n_{\mathbf{k}}$ in the doublet model oscillate in the prethermal state and do not plateau. Therefore, we expect the experimental comparison of the plateau value $\bar{n}_{\mathbf{k}}$ in the doublet model to be qualitative. We note recent quantitative predictions for the halfway time in the thermal regime in Ref. [106]. Further complicating matters is the absence of a clear steady-state plateau for $k/k_{\rm n} < 0.8$ in the experimental data of Ref. [27], which adds ambiguity to the fitting routine without making additional assumptions about the timescale separation between heating and prethermalization.

[72] In the limit $n r_{\rm vdW}^3 \to 0$, the doublet equations of motion simplify to their universal form: $i\hbar\partial_t c_{\mathbf{k}} = 2(\epsilon_{\mathbf{k}} - \mu(t))c_{\mathbf{k}} + \Delta(t)(1 + 2n_{\mathbf{k}})$, $i\hbar\partial_t n_{\mathbf{k}} = \Delta(t)c_{\mathbf{k}}^* - \text{c.c.}$ Assuming that μ and Δ are real, negative, and time independent (as observed numerically in Fig. 1), this linear system solves into Eq. (61).

[73] A. Griffin, Phys. Rev. B **53**, 9341 (1996).

[74] P. Nozières and D. Saint James, J. Phys. France **43**, 1133 (1982).

[75] X. Yin and L. Radzihovsky, Phys. Rev. A **93**, 033653 (2016).

[76] C. Eigen, J. Glidden, R. Lopes, N. Navon, Z. Hadzibabic, and R. Smith (2017), Supporting data for 'Universal Scaling Laws in the Dynamics of a Homogeneous Unitary Bose Gas' [Dataset]. https://doi.org/10.17863/CAM.16741.

[77] S. Tan, Ann. Phys. **323**, 2952 (2008).

[78] S. Tan, Ann. Phys. **323**, 2971 (2008).

[79] S. Tan, Ann. Phys. **323**, 2987 (2008).

[80] F. Werner and Y. Castin, Phys. Rev. A **86**, 053633 (2012).

[81] E. Braaten, D. Kang, and L. Platter, Phys. Rev. Lett. **106**, 153005 (2011).

[82] J. P. Corson and J. L. Bohn, Phys. Rev. A **94**, 023604 (2016).

[83] F. Werner and Y. Castin, Phys. Rev. A **86**, 013626 (2012).

[84] M. Olshanii and V. Dunjko, Phys. Rev. Lett. **91**, 090401 (2003).

[85] B. S. Rem, A. T. Grier, I. Ferrier-Barbut, U. Eismann, T. Langen, N. Navon, L. Khaykovich, F. Werner, D. S. Petrov, F. Chevy, and C. Salomon, Phys. Rev. Lett. **110**, 163202 (2013).

[86] V. E. Colussi (unpublished).

[87] The normalization constant is given by $\langle\phi_s|\phi_s\rangle \equiv \int d\mathbf{\Omega}|\phi_s(\mathbf{\Omega})|^2 = -\frac{12\pi}{s}\sin(\frac{s^*\pi}{2})[\cos(\frac{s\pi}{2}) - \frac{s\pi}{2}\sin(\frac{s\pi}{2}) - \frac{4\pi}{3\sqrt{3}}\cos(\frac{s\pi}{6})]$.

[88] J. Wang, J. P. D'Incao, B. D. Esry, and C. H. Greene, Phys. Rev. Lett. **108**, 263001 (2012).

[89] P. Naidon, S. Endo, and M. Ueda, Phys. Rev. A **90**, 022106 (2014).

[90] D. H. Smith, E. Braaten, D. Kang, and L. Platter, Phys. Rev. Lett. **112**, 110402 (2014).

[91] To perform reliable fits over the larger window $t \leqslant t_{\rm n}$, we expect that a more involved fitting routine is required.

[92] L. D. Faddeev and S. P. Merkuriev, *Quantum Scattering Theory for Several Particle Systems*, Vol. 11 (Springer Science & Business Media, Dordrecht, 2013).

[93] W. Glöckle, in *The Quantum Mechanical Few-Body Problem*, edited by W. Beiglböck (Springer, Berlin, 1983).

[94] C. D'Errico, M. Zaccanti, M. Fattori, G. Roati, M. Inguscio, G. Modugno, and A. Simoni, New J. Phys. **9**, 223 (2007).

[95] R. Schmidt, S. Rath, and W. Zwerger, Eur. Phys. J. B **85**, 386 (2012).

[96] G. V. Skorniakov and K. A. Ter-Martirosian, Zh. Eksp. Teor. Fiz. **31**, 775 (1956).

[97] W. H. Press, B. P. Flannery, S. A. Teukolsky, and W. T. Vetterling, *Numerical Recipes*, Vol. 3 (Cambridge University Press, Cambridge, 1989).

[98] D. Kremp, M. Bonitz, W. Kraeft, and M. Schlanges, Ann. Phys. **258**, 320 (1997).

[99] D. Blume, M. W. C. Sze, and J. L. Bohn, Phys. Rev. A **97**, 033621 (2018).

[100] Y. Castin and R. Dum, Phys. Rev. A **57**, 3008 (1998).

[101] C. W. Gardiner, Phys. Rev. A **56**, 1414 (1997).

[102] X. Yin and L. Radzihovsky, Phys. Rev. A **88**, 063611 (2013).

[103] A. Rançon and K. Levin, Phys. Rev. A **90**, 021602(R) (2014).

[104] R. Žitko, Comput. Phys. Commun. **182**, 2259 (2011).

[105] F. Werner and Y. Castin, Phys. Rev. Lett. **97**, 150401 (2006).

[106] M. Sun, P. Zhang, and H. Zhai, Phys. Rev. Lett. **125**, 110404 (2020).